NONLINEAR PROPAGATION OF SURFACE-PLASMON-POLARITONS IN CHALCOGENIDE GLASS

BY

RAKIBUL HASAN SAGOR

A Thesis Presented to the
DEANSHIP OF GRADUATE STUDIES

KING FAHD UNIVERSITY OF PETROLEUM & MINERALS
DHAHRAN, SAUDI ARABIA

In Partial Fulfillment of the
Requirements for the Degree of

MASTER OF SCIENCE
In
ELECTRICAL ENGINEERING

JUNE 2011

KING FAHD UNIVERSITY OF PETROLEUM & MINERALS

DHAHRAN 31261, SAUDI ARABIA

DEANSHIP OF GRADUATE STUDIES

This thesis written by **Rakibul Hasan Sagor** under the direction of his thesis advisor and approved by his thesis committee, has been presented to and accepted by the Dean of Graduate Studies, in partial fulfillment of the requirements for the degree of **MASTER OF SCIENCE IN ELECTRICAL ENGINEERING**.

Thesis Committee

Dr. Mohammad A. Alsunaidi (Advisor)

Dr. Hussain Ali Al-Jamid (Member)

Dr. Boon S. Ooi (Member)

Dr. Ali Ahmad Al-Shaikhi
Department Chairman

Dr. Salam A. Zummo
Dean of Graduate Studies

2/7/11
Date

My parents

They bore me, raised me, supported me, taught me and loved me.

To them I dedicate this thesis.

ACKNOWLEDGMENT

All Praise and gratitude be to Allah, the most beneficent, the most merciful. First I offer my sincerest thanks to my supervisor, Dr M A Alsunaidi, who has supported me with his enthusiasm, his inspiration and his great efforts to explain things clearly and simply. Throughout my thesis work, he provided encouragement, sound advice, good company, and lots of innovative ideas. I have truly learned a lot during my thesis.

I would like to thank my thesis committee members, Dr. Husain Ali Al-Jamid and Dr. Boon S Ooi for their valuable advices and support. The amount of time they gave for this thesis is really appreciable. Their comments and positive feedbacks helped me improve my thesis.

In my daily work I have been blessed with a friendly and cheerful group of fellow students. I would like to reach out to the group and convey my heartfelt thanks for their support and encouragement.

I am grateful to the Department of Electrical Engineering for providing me the support and high performance computer facilities.

Finally, I wish to thank my family for supporting me throughout all my studies at the University.

Table of Contents

List of Figures

List of Tables

THESIS ABSTRACT

Name: Rakibul Hasan Sagor

Title: Nonlinear Propagation of Surface Plasmon-Polaritons in Chalcogenide Glass

Major Field: Electrical Engineering

Date of Degree: June, 2011.

The field of plasmonics has attracted a lot of research in nano-photonics. Surface Plasmon Polaritons (SPPs) are believed to be strong candidates for nano-scale imaging and computing. SPPs are electromagnetic modes which arise from the coupling effect between photons and the free conduction electrons on the interface between a metal and a dielectric. In integrated optical devices based on SPPs, the light can be confined in sub-wavelength scale, and the resultant EM wave propagates along the metal interface. In this thesis, a time-domain simulation algorithm for the investigation of nonlinear propagation properties of SPPs in chalcogenide glasses is developed. Chalcogenide glasses have become attractive in ultrafast nonlinear devices due to their high material non-linearity. The frequency-dependent dispersion relations as well as third-order non-linearity of chalcogenide glass have been modeled using the general polarization algorithm incorporated in the auxiliary differential equation (ADE). The resulting time domain model has been solved numerically using the Finite Difference Time Domain method. The dynamics of SPP propagation in several plasmonic structures containing third-order nonlinearity have been studied. It was found that non-linear SPP propagation leads to significant changes in the spectrum of the propagated pulse. Such changes can be utilized in novel SPP-based switching and other photonic structures.

ملخّص بحث

درجة الماجستير

الاسم: رقيب الحسن ساغر محمد

العنوان : الإنتشار اللاخطي للبلازمونات الضوئية السطحية في زجاج الكالكوجينات

مجال التخصص : الهندسة الكهربائية

تاريخ الدرجة العلمية : 2011 يونيو

جذب مجال البلازمونات الضوئية الكثير من البحوث في حقل النانو-فوتون. و تبرز هذه البلازمونات الضوئية كمرشح قوي في مجالات مثل التصوير و نقل المعلومات و الحساب. البلازمونات الضوئية أنماط كهرومغناطيسية تنشأ من التأثر المزدوج بين الفوتونات و الالكترونات الموصلة الحرة عند التقاء المعدن بالعازل. وعن طريقها يمكن حصر الضوء في نطاق أصغر بكثير من الطول الموجي للضوء، و عندها تنتقل الموجة الكهرومغناطيسية الناتجة على طول واجهة المعدن. و في هذه الرسالة تم تطوير خوارزمية في المجال الزمني لدراسة خصائص الانتشار اللاخطي للبلازمونات في زجاج الكالكوجينات.

و يعود الاهتمام البالغ في زجاج الكالكوجينات الى خواصها غير الخطية فائقة السرعة. وقد تم تطوير نموذج لخواص هذه المادة الخطية (علاقة التشتت المعتمدة على التردد) و غير الخطية (الدرجة الثالثة) عن طريق مطابقة الخواص المعملية لها لنماذج رياضية قياسية. ثم تم استخدام خوارزمية الاستقطاب العامة المدمجة في طريقة المعادلة التكميلية للوصول إلى وصف رياضي (معادلات تفاضلية جزئية) لحركة البلازمونات. اعتمد الحل العددي لهذا النموذج الرياضي على طريقة الفروق المحدودة (FDTD). وقد تم البحث في ديناميكة انتشار البلازمونات في تراكيب مختلفة تحوي تكوينات زجاج الكالكوجينات فوجد أن الانتشار اللاخطي للبلازمونات يؤدي إلى تغيرات مهمة في طيف الموجة خلال انتقالها عبر التركيب الضوئي. و يمكن الانتفاع بمثل هذه التغيرات في تطوير مفاتيح ضوئية (optical switch) و تراكيب ضوئية أخرى.

CHAPTER 1

INTRODUCTION

The interactions between light and matter have been studied for thousands of years. Since the advent of modern science, research on light had been extended to beyond the visible range. Exploring the interaction between light and matter has enabled us to explore a vast variety of natural phenomena, from the nano-particle interactions to the birth of giant stars.

In modern technology, use of light in nano-scale electronics device has become a top research field due to the possibility to confine light to the nano-scale and also the possibility to tune dispersion relations. Efficient integration of photonics and electronics results in the miniaturization of electronic components resulting improved performance. For example, when the photonics is used in computer chips as optical interconnectors or as active photonic circuitry, this results in higher speeds and lower power dissipation compared to electronic connections. The efficient use of photonics in nano-scale optical devices has led to drastic growth of the field of plasmonic research. For the past decade, research in the field of plasmonics has grown considerably with great potential applications in communications, sensing, imaging and computing.

1.1 General Overview on Plasmonics

Surface plasmon polaritons are electromagnetic waves which propagate at the interface between a dielectric and a conductor, evanescently confined in the perpendicular direction[1]. When a metal is exposed to light in a certain way, the incident light excites the electrons on the surface of the metal which causes electron oscillation. Plasmon, the unit of plasma oscillation, can be excited inside the metal by incident light outside the metal. When plasmons and photon are coupled together (figure 1-1), the resulting hybridized excitation is known as Surface Plasmon-Polariton (SPP).

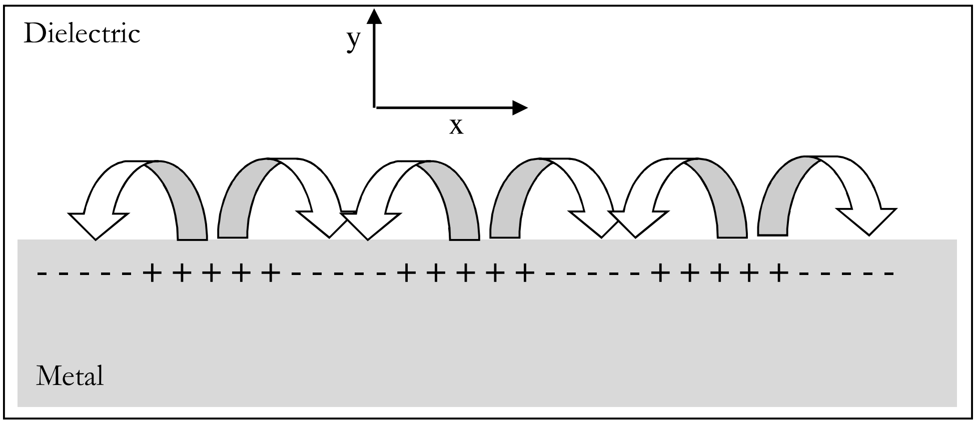

Figure 1-1: Surface Plasmon-polaritons propagation at the interface of metal and dielectric.

The surface excitations can be characterized in terms of their dispersion and spatial profile. The SPPs propagation along the surface of a metal continues until the energy is lost by absorption in the metal or by radiation. Considering a flat interface between a dielectric and metal having dielectric constants ε_d and ε_m respectively, SPPs are TM plane wave solution of Maxwell's equations which propagate along the metal-dielectric interface. Therefore, SPPs exist only in the vicinity of the interface that results in a nanoscale confinement of the optical waves. If the interface is normal to y axis and the propagation direction of SPPs is along the x direction, the SPP wave vector k_x can be related through the dispersion relation as[1],

$$k_{spp}(\omega) = k_o \sqrt{\frac{\varepsilon_d(\omega)\varepsilon_m(\omega)}{\varepsilon_d(\omega)+\varepsilon_m(\omega)}} \tag{1.1}$$

where $k_o = \frac{\omega}{c}$, is the free space wave number. In the presence of losses the wave vector is complex and can be represented as $k_{spp} = k'_{spp} + ik''_{spp}$. For a metal-dielectric single interface, the dispersion relation can be solved using Maxwell's equation and the boundary conditions, as described in chapter 2.

1.2 Nonlinear Optics

Nonlinear optics is the study which describes the change in optical behavior of a material by the presence of relatively intense light. The dielectric polarization P of the material responds nonlinearly to light. Typically, this nonlinearity is observed with high light intensity and only laser light is appropriately intense to change the optical properties of the material. The field of nonlinear optics started after the discovery of second harmonic generation by Fanken et al [2]. In order to describe more precisely the optical nonlinearity, we need to understand the internal behavior of material under the action of an electric field. In the case of electronic polarization, the electron cloud is displaced with respect to the nucleus and hence creates the dipole moment (Figure 1-2). The atom can be modeled as a spring-mass system in which the displacement of x of the electron from the nucleus can be compared to the extension or compression of the spring. The differential equation satisfied by the displacement $x(t)$ can be written as[3]

$$m_e\left[\frac{d^2x}{dt^2}+2\alpha\frac{dx}{dt}+\omega^{*2}x\right]=-eE_o cos\ \omega t \tag{1.2}$$

where *e* is the electronic charge, m_e is the mass of an electron, E_o is the amplitude of the applied electric field *E(t)* at the optical frequency ω, ω^* is the natural or resonant frequency of the oscillator and α represents the damping constant.

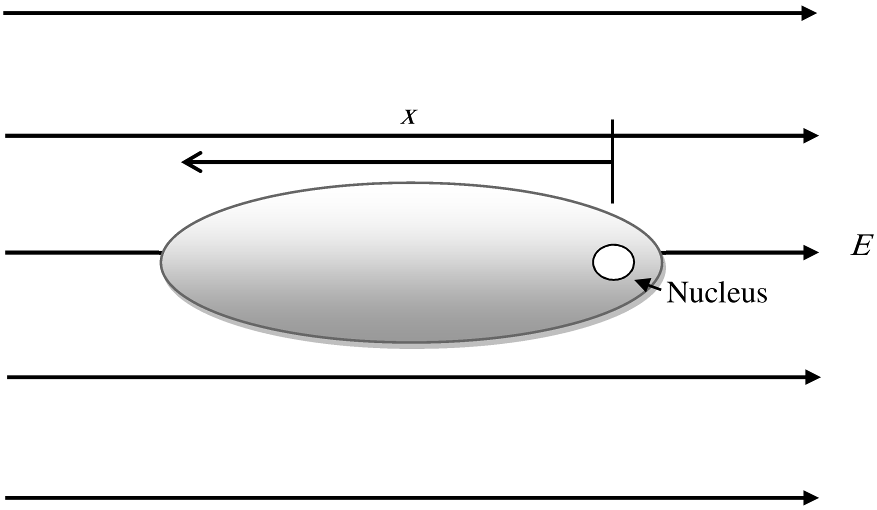

Figure 1-2: Distortion to an electron cloud in the presence of an applied optical field.

Equation (1.2) can be solved by taking *x(t)*=Re[*A* exp *jωt*] and then equating the coefficient of exp *jωt*. This results in $=-\left(\frac{eE_o}{m_e}\right)\frac{1}{\omega^{*2}+2j\alpha\omega-\omega^2}$, hence $x(t)$ becomes

$$x(t)=-\left(\frac{eE_o}{2m_e}\right)\frac{\exp j\omega t}{\omega^{*2}+2j\alpha\omega-\omega^2}+c.c \tag{1.3}$$

If there are *N* electrons per unit volume, the electron polarization $P(t)=-eNx(t)$ can be expressed as

$$P(t)=\frac{\varepsilon_o[\chi E_o \exp j\omega t+c.c]}{2} \tag{1.4}$$

$$\chi = \chi(\omega) = \left(\frac{Ne^2}{\varepsilon_o m_e}\right)\frac{1}{\omega^{*2} + 2j\alpha\omega - \omega^2} \tag{1.5}$$

When $\alpha = 0$, which means the absence of absorption, the polarization becomes $P = \varepsilon_o \chi E$, and χ becomes purely real. But for the case of nonlinear optics, this is no longer true. The mechanical restoring force on the electron, F_m, cannot be assumed to be a linear function of electron displacement. For larger values of x, F_m may be drastically non-linear with respect to x. Since F_m is nonlinear, equation (1.1) can be expressed as

$$m_e\left[\frac{d^2x}{dt^2} + \omega^{*2}x\right] - Bx^2 - Cx^3 = -eE(t) = -eE_o cos\ \omega t \tag{1.6}$$

considering the absence of absorption. Now, in order to obtain the natural solution of equation (1.6), which will formulate a general form for $x(t)$ and hence $P(t)$ in terms of $E(t)$, we need the natural response of the nonlinear system. To solve equation (1.6), $x = x_1 = a\cos\omega t$ is assumed in equation (1.6). This results in the following equation

$$\frac{3Ca^3}{4m_e\omega_o^2} = \left(1 - \frac{\omega^2}{\omega^{*2}}\right)a - \frac{E_o}{\omega^{*2}m_e}\,. \tag{1.7}$$

Equation (1.6) is a cubic equation where a determines the amplitude of oscillation. Now, using this solution x_1 as a second forcing term, solution of ODE for x, the second literate for the solution, x_2, is

$$x_2(t) = a\ cos\ \omega t - \left(\frac{Ca^3}{36m_e\omega^2}\right)\cos 3\omega t. \tag{1.8}$$

This approximation can be used in the nonlinear part of equation (1.6) to derive a third iterate and so on. The above derivation clearly shows that for a forced oscillation at frequency ω, the displacement x, hence the polarization P is a cubically non-linear system, which will have contributions from E and E^3. Similarly if we consider $C=0$, it can be shown that the response having contributions from E and E^2. So, in general, in the presence of non-linearity, the polarization P can be expressed as,

$$P = \varepsilon_o\left[\chi^{(1)}E + \chi^{(2)}E^2 + \chi^{(3)}E^3\right] + \cdots \tag{1.9}$$

where, $\chi^{(1)}$ is the linear susceptibility, and $\chi^{(2)}$ and $\chi^{(3)}$ are the second and third order nonlinear susceptibilities, respectively.

1.2.1 Chalcogenide Glasses

Chalcogenide glasses are based on one or more chalcogen elements of group IV (Sulphur,'S', Selenium, 'Se', and Tellurium, 'Te' but excluding oxygen), bonded to other elements such as As, Ge, Sb, Ga, Si or P[4]. Due to their excellent optical properties, chalcogenide glasses have been studied since the 1950s. The chalcogenide glasses have a high refractive index, high material nonlinearity combined with the strong confinement and dispersion characteristics which made these glasses attractive for the realization of ultrafast nonlinear devices. They also created significant interest due to their transparency in the mid-infrared region of the spectrum and photosensitivity to visible light. Research is ongoing to characterize the nonlinearity of chalcogenide glasses. Chalcogenide glasses with different compositions of chalcogenide materials provide a platform for fundamental research of light-mater interaction in nano structures. The non-linear index of sulfur based glass is over 100 times greater than that of silica and for tellurium based glass is more than 1000 time greater than in silica. The ultrafast high nonlinearity characteristics of chalcogenide glasses combined with metal can be used to propagate SPPs more efficiently which can be a significant contribution in the field of photonics[5].

1.3 Numerical Techniques

The experimental approach for any electromagnetic analysis needs a lot of efforts, cost and time. It is not economically viable to go for a particular experimental research by changing different parameters of the experimental setup, especially when the apparatus are very costly to manufacture. That is why simulation is becoming popular to most of the researchers, which gives almost exact output, if the system is modeled perfectly. This does not mean that experiments are not needed. It only means that accurate system simulation results fewer and more efficient experiments and thus results in important savings in costs and effort.

To evaluate electromagnetic quantities, there are two main categories: Analytical method and Numerical method. The most used analytical methods are: Separation of variables, series expansion and perturbation.

The analytical approaches may fail when the solution region is complex, the Partial Differential Equations (PDE) are not linear, or if there are time dependent boundary conditions. So to overcome these problems, numerical techniques are being used.

1.3.1 Overview

Numerical techniques include all methods which can reproduce the processes of a system numerically. Generally, in electromagnetics, numerical methods are used for solving differential equation. A lot of effort has been undertaken to find efficient and cost-effective numerical techniques. Scientists invented different methods which can solve the differential equations numerically. The performance of a particular numerical technique depends on how accurately it can solve the differential equations within the shortest possible time. There are various numerical methods which are currently being used by different researchers. Some well-known techniques are: the Finite Difference Time Domain (FDTD) method, the Method of Line (MOL), the Beam Propagation Method (BPM), the Finite Element Method (MEM), Transmission-line-matrix Method, Monte Carlo Methods, etc[6].

The method of lines (MOL) is one of the techniques for solving PDE. In this method the solution method consists of two parts: space-discretization and time-integration[7]. This method is used in linear and nonlinear parabolic boundary value problems with first boundary conditions. With the proper choice of the variable to discretize, the application of the MOL to the parabolic equation results in initial-value problems in the ordinary differential equations which may be easier to handle than the original boundary-value problem. One of the great advantages of MOL is that it uses standard general-purpose methods. However, the method has also some limitations. The resulting system of ODE often becomes difficult to solve accurately which causes the forced discretization of the other variable to find an approximate solution for the system of ODE[14]. Many papers have been published discussing the accuracy and stability of the MOL for different types of PDE. Also a good number of integration routines have been introduced in different programming languages.

The beam propagation method (BPM) is a widely used approximation technique for the simulation of light propagation in slowly varying optical waveguides. The BPM is a fast and simple method of solving for the field in integrated optical devices. This method is typically used in solving modes within shaped waveguide. These structures generally consist of isotropic optical materials. But the BPM is also being applied to simulate the light propagation in general anisotropic materials. The BPM computes both guided and radiation modes of linear z-variant devices without any special arrangement to account for radiation modes. The research work which is reported in this thesis is mainly based on the FDTD method. But the work can be simulated using other methods as well. The FDTD is discussed in more detail in the next section.

1.3.2 Finite Difference Time Domain (FDTD)

The Finite Difference Time Domain (FDTD) method is one of the most widely used methods in computational electromagnetics. Since this is a time-domain method, solutions can cover a wide frequency range with a single simulation run. The FDTD algorithm was first introduced by Yee in 1966[8] where he described the basis of the first space-grid time-domain technique for Maxwell's curl equation. The details of the space-grid time-domain are described in chapter 4. Taflove and Brodwin published the numerical stability principle for Yee's algorithm[9]. Since about 1990, various FDTD based techniques have emerged as primary means to model many scientific and engineering problems dealing with electromagnetic wave interactions with different material structures. Current FDTD modeling applications range from microwaves like, radar signature technology, antennas , wireless communications devices, digital interconnects, biomedical imaging or treatment to visible light, photonic crystals, nanoplasmonics, solitons and biophotonics[10].

Goorijan and Taflove used the FDTD to model the propagation of optical pulses in non-linear media in 1992[11]. Berenger introduced the Perfectly Matched Layer (PML) ABC for two dimensional FDTD grid in 1994[12]. The third-order non-linear cases and scalar continuous-wave (CW) are presented in a paper by Joseph and Taflove in 1997[13].

The FDTD method has become a popular numerical technique because it is more accurate and robust. FDTD treats non-linear behavior naturally. Due to these factors the FDTD methods will likely remain one of the dominant computational electrodynamics techniques.

1.4 Literature Review

A lot of research has been done separately on surface Plasmon polaritons and chalcogenide glasses. For the past decade SPP has become very attractive for researchers. The main focus of this literature review is towards the articles related to SPP simulation and the simulation of chalcogenide glasses using the FDTD numerical method. SPPs in thin films were first introduced in terms of electron energy loss spectroscopy in 1957 by R.H. Ritchie[15]. Then a major experimental work on SPPs was done by Otto[16], Kretschmann and Raether[17] in 1968. Here they reported the methods of surface plasmons excitation on metal films optically. In[18], Stefan A. Maier investigated the guiding EM energy at the visible and near-infrared frequencies using surface Plasmon (SP) excitations on metallic nanostructures. He took the geometry as metal/insulator/metal-gap to assess in terms of light confinement and the energy attenuation of the guided modes. He also presented a solution to the coupling problem of SPP modes in fiber accessible metal nanoparticles and experimentally showed a power transfer up to 75% for incident an wavelength of 1.5 micrometer. W.M. Saj[19] used the FDTD to simulate 2D plasmon waveguides on silver nanorods in a hexagonal lattice. The frequency dependent dielectric function of the metals was modeled by Drude model. In this paper W.M. Saj investigated energy transport and attenuation due to surface plasmon coupling for the visible range wavelengths from 400nm to 750nm. One of the main applications of localized surface plasmon, imaging, was studied by Richard J Blaikie et al [20, 21], both experimentally and numerically. The image of the tungsten grating was taken beyond the diffraction limit using silver as a planar lens. The experimental results were compared with the simulated results using the FDTD numerical method. The frequency dependent dielectric properties of silver were modeled by a two pole model of the form

$$\varepsilon(\omega) = \varepsilon' - j\varepsilon'' = \varepsilon_\infty + \frac{j\omega\beta + \gamma}{a\omega^2 + b\omega + c} \qquad (1.10)$$

where a, b, c, β and γ were taken from the experimental measurements. The results show that imaging beyond the diffraction limit is possible using a localized surface Plasmon. Propagation of surface plasmons along a micro scale metal strip was experimentally carried out by B. Lamprecht et al[22] and T. Onuki et [23] al. B. Lamprecht used 70 nm Au and Ag film deposited on the Al/SiO_2 substrate. On the other hand T. Onuki used a composite metallic film that consist of titanium (Ti) film and silver (Ag) film of different thickness and studied the propagation length of the SPPs. They did the experiments for 2 μm and 6 μm long nanowires for λ=532 nm and 830 nm. The results were compared with their numerical simulations using the FDTD which showed good agreement with the experimental one.

Chalcogenide glasses with different compositions of chalcogenide materials also provide a platform for fundamental research of light-mater interaction in nano structures. The optical properties of chalcogenide glasses were investigated since 1970. Most of these properties were measured experimentally for different compositions of chalcogen elements. References [24-27] report the optical properties of chalcogenide glasses. A. Zakery et al[28] presented the linear and non-linear optical properties of different chalcogenide glasses using different techniques such as absorption spectroscopy , degenerate four wave mixing (DFWM), Z-scan, third-harmonic generation (THG) and optical Kerr shutter (OKS). It has been observed here that As_2S_3 has one of the highest $\chi^{(3)}$values. J.S. Sanghera et al[29] related the non-linear index of the Chalcogenide glasses to the normalized photon energy. The fabrication of chalcogenide waveguides for nonlinear optical signal processing telecommunication wavelength was reported by Gai et al[30]. Suzuki and Baba[31] investigated the nonlinear light propagation in chalcogenide photonic crystal slow light waveguides based on Ag-As_2-Se_3. It was found that the waveguide exhibits negligible two-photon absorption and high efficiency self-phase modulation and four-wave mixing. Anu K Sharma et al[5] presented a theoretical model for a gas sensor based on chalcogenide prism and surface Plasmon resonance. The metal layer was based on an Ag-Au alloy and the chalcogenide prism was $Ge_{20}Ga_5Sb_{10}S_{65}$ which is also known as 2S2G. The wavelength dependent refractive index, (n_c) for 2S2G glass prism was taken as

$$n_c(\lambda) = 2.04047 + \frac{2.693\times10^{-2}}{\lambda^2} + \frac{8.08\times10^{-3}}{\lambda^4}$$

For dispersion in the metal layer, they used the Drude equation. The simulated result showed a very good sensitivity for change in the gaseous media refractive index in the IR region.

1.5 Thesis Objectives

The main thesis objective is to study the nonlinear propagation of SPP in chalcogenide glass. However, more particularly, the objectives include

- To study the properties of Chalcogenide glasses. This study includes thorough literature review, collection of data, etc.

- To develop a time-domain multidimensional simulator capable of presenting the propagation dynamics of SPP in Chalcogenide glass. This simulator is based on the FDTD method and the general dispersive algorithm.
- To formulate a frequency-dependent dispersion model for both linear as well as nonlinear responses for Chalcogenide glasses. This model will be used to study the non-linear behavior in the numerical simulator.
- To use the developed simulator to carry out some studies on SPP propagation including different plasmonic structures and material.
- To extract important conclusions regarding the nonlinear SPP propagation and their potential applications.

1.6 Thesis Organization

This thesis focuses on acquiring a fundamental understanding of the non-linear propagation of SPPs in chalcogenide glass.

- In **Chapter 2**, the basic theory of SPP propagation in general media has been described including SPPs propagation along a single interface. As SPPs are electromagnetic wave, some basics of the EM wave equation are also described.
- To have a realistic simulation output, it is important to model all the materials involved in the process of SPPs propagation. **Chapter 3** includes different models used widely to represent a metal. **Chapter 3** also describes the non-linear model of dispersive materials, where all the parameters affecting the non-linearity are also described.

- In **Chapter 4**, a time-domain two-dimensional simulator capable of representing the propagation dynamics of SPP in Chalcogenide glass is developed. This simulator is based on the FDTD method and the general dispersive algorithm. The third-order nonlinearity of the glass is also developed, which is basically a cubic equation and solved in the time domain.
- The verification of the Simulator is shown in **Chapter 5**. This was done by testing the simulator using published data and the theoretical equations. In this chapter, the non-linear material model and the dispersive material model were verified and tested.
- In **Chapter 6**, the detailed results of SPP propagation in a non-linear medium is described. In this chapter, only single interface plasmonic structure has been considered. The results were produced for different types and power levels of pumped signals, analyzed and discussed further.
- Similar observations were carried out for different multiple interface plasmonic structure in **Chapter 7**. Two structures were chosen to observe the SPPs effect on nonlinear media. The results are analyzed and important conclusions were made.
- In **Chapter 8**, some numerical considerations were discussed including numerical stability limit, computational time and some other techniques to make the simulation efficient.
- **Chapter 9** contains the conclusion of the thesis, where the brief summary of the results is given. Also the extension of this work is described at the end of this chapter.

CHAPTER 2

THEORY OF SPP PROPAGATION

In order to study the physical properties of surface plasmon polaritons (SPPs), understanding electromagnetic wave propagation is required. Basically, SPPs are electromagnetic excitations which propagate at the interface between a dielectric and a conductor, evanescently confined in the perpendicular direction. As EM wave propagation is described by Maxwell's equations, we need to apply Maxwell's equations to the flat interface between a conductor and a dielectric. To present the propagation behavior most clearly, it is advantageous to cast the equations first in a general form applicable to the guiding of electromagnetic waves.

Maxwell's equations can be described in the following form:

$$\nabla . D = \rho_{ext} \qquad (2.1)$$

$$\nabla . B = 0 \qquad (2.2)$$

$$\nabla \times E = -\frac{\partial B}{\partial t} \qquad (2.3)$$

$$\nabla \times H = J_{ext} + \frac{\partial D}{\partial t} \qquad (2.4)$$

where

E is the electric field vector in volt per meter

D is the electric flux density vector in coulombs per square meter

H is the magnetic field vector in amperes per meter

B is the magnetic flux density vector in Webbers per square meter

ρ_{ext} is the charge density

J_{ext} is the current density

The electric and magnetic fields are related to polarization *P* and magnetization *M*

$$D = \varepsilon_o E + P \tag{2.5}$$

$$H = \frac{1}{\mu_o} B - M \tag{2.6}$$

For linear, isotropic and nonmagnetic media the relation can be simplified to

$$D = \varepsilon_o \varepsilon_r E \tag{2.7}$$

$$B = \mu_o \mu_r H \tag{2.8}$$

where,

ε_o is the electric permittivity of vacuum in Farad per meter

μ_o is the magnetic permeability of vacuum in Henry per meter

ε_r is the relative permittivity

μ_r is the relative permeability

2.1 The EM Wave Equation

The EM wave equation is derived from Maxwell's equations. From Faraday's law we can change

$$\nabla \times \nabla \times E = -\mu_o \frac{\partial^2 D}{\partial t^2} \tag{2.9}$$

With the identities $\nabla \times \nabla \times E \equiv \nabla(\nabla . E) - \nabla^2 E$ and $\nabla .(\varepsilon E) \equiv E . \nabla\varepsilon + \varepsilon\nabla . E$ the above equation can be expressed as

$$\nabla\left(-\frac{1}{\varepsilon} E . \nabla\varepsilon\right) - \nabla^2 E = -\mu_o \varepsilon_o \varepsilon \frac{\partial^2 E}{\partial t^2} \tag{2.10}$$

If the variation of the dielectric profile ε is negligible over distance, equation (2.10) can be simplified to the following wave equation:

$$\nabla^2 E - \frac{\varepsilon}{c^2} \frac{\partial^2 E}{\partial t^2} = 0 \tag{2.11}$$

Equation (2.11) needs to be solved separately in regions of constant ε, and then the solutions are to be matched with appropriate boundary conditions. To have the solution in a suitable form we assume a harmonic time dependence of the electric field, namely $E(r,t)=E(r)e^{-j\omega t}$. Substituting E in (2.11), we get the Helmholtz equation

$$\nabla^2 E + k_o^2 \varepsilon E = 0 \tag{2.12}$$

where, the wave vector of the propagation = $k_o = \frac{\omega}{c}$, correspond to free space.

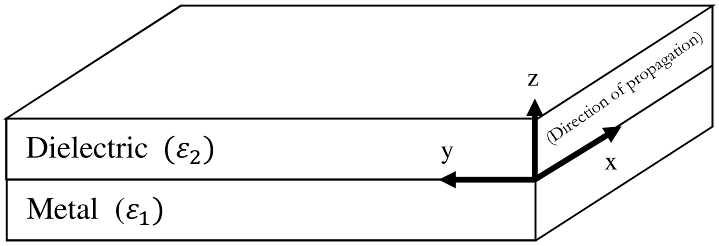

Figure 2-1: Typical planar waveguide geometry. The waves propagate along the x-direction in a cartesian coordinate system.

If the propagation wave is assumed to be along the x-direction of the Cartesian co-ordinate system, and no spatial variation in y direction (Figure 2-1) we can write $E(x,y,z)=E(z)e^{j\beta x}$, where $\beta=k_x$, which is called the propagation constant. Now inserting the value of E in equation (2.11) the wave equation takes the following form

$$\frac{\partial^2 E(z)}{\partial z^2} + (k_o^2\varepsilon - \beta^2)E = 0 \qquad (2.13)$$

A similar equation can be found for the magnetic field *H* as well. The field E and H can be decomposed in Cartesian coordinate system as

$$E = E_x.\overrightarrow{a_x} + E_y.\overrightarrow{a_y} + E_z.\overrightarrow{a_z} \qquad (2.14)$$

$$H = H_x.\overrightarrow{a_x} + H_y.\overrightarrow{a_y} + H_z.\overrightarrow{a_z} \qquad (2.15)$$

For harmonic time dependence $(\frac{\partial}{\partial t} = -j\omega)$, by solving Ampere's law and Faraday's law, the following set of coupled equations can be obtained

$$\frac{\partial E_z}{\partial y} - \frac{\partial E_y}{\partial z} = j\omega\mu_o H_x \qquad (2.16)$$

$$\frac{\partial E_x}{\partial z} - \frac{\partial E_z}{\partial x} = j\omega\mu_o H_y \qquad (2.17)$$

$$\frac{\partial E_y}{\partial x} - \frac{\partial E_x}{\partial y} = j\omega\mu_o H_z \tag{2.18}$$

$$\frac{\partial H_z}{\partial y} - \frac{\partial H_y}{\partial z} = -j\omega\varepsilon_o\varepsilon E_x \tag{2.19}$$

$$\frac{\partial H_x}{\partial z} - \frac{\partial H_z}{\partial x} = -j\omega\varepsilon_o\varepsilon E_y \tag{2.20}$$

$$\frac{\partial H_y}{\partial x} - \frac{\partial H_x}{\partial y} = -j\omega\varepsilon_o\varepsilon E_z \tag{2.21}$$

Because the propagation is assumed along x-direction in the form $e^{j\beta x}$, it then follows that $\frac{\partial}{\partial x} = -j\beta$. The homogeneity in the y-direction results in $\frac{\partial}{\partial y} = 0$. So the equations can be simplified to

$$-\frac{\partial E_y}{\partial z} = j\omega\mu_o H_x \tag{2.22}$$

$$\frac{\partial E_x}{\partial z} - j\beta E_z = j\omega\mu_o H_y \tag{2.23}$$

$$j\beta E_y = j\omega\mu_o H_z \tag{2.24}$$

$$\frac{\partial H_y}{\partial z} = j\omega\varepsilon_o\varepsilon E_x \tag{2.25}$$

$$\frac{\partial H_x}{\partial z} - j\beta H_z = -j\omega\varepsilon_o\varepsilon E_y \tag{2.26}$$

$$j\beta H_y = -j\omega\varepsilon_o\varepsilon E_z \tag{2.27}$$

There are two sets of independent solutions with different polarization properties: Transverse magnetic (TM) modes and Transverse electric (TE) modes. For the TM modes, the governing equations are

$$E_x = -j\,\frac{1}{\omega\varepsilon_o\varepsilon}\frac{\partial H_y}{\partial z} \qquad (2.28)$$

$$E_z = -\,\frac{\beta}{\omega\varepsilon_o\varepsilon}H_y \qquad (2.29)$$

The wave equation for TM polarized wave becomes

$$\frac{\partial^2 H_y}{\partial z^2} + (k_o^2\varepsilon - \beta^2)H_y = 0 \qquad (2.30)$$

Similarly for TE polarized the equation sets are

$$H_x = j\,\frac{1}{\omega\mu_o}\frac{\partial E_y}{\partial z} \qquad (2.31)$$

$$H_z = \frac{\beta}{\omega\mu_o}E_y \qquad (2.32)$$

The wave equation for TE waves becomes

$$\frac{\partial^2 E_y}{\partial z^2} + (k_o^2\varepsilon - \beta^2)E_y = 0 \qquad (2.33)$$

2.2 Surface Plasmon Polaritons at Single Interface

The simplest geometry to describe SPPs propagation is that of a single, flat interface (Figure 2-2) between a dielectric, with positive real dielectric constant ε_2 and a metal having a negative real part of the dielectric constant ε_1. For metals, this condition is fulfilled below the bulk Plasmon frequency ω_p. The evanescent decay occurs perpendicular to the z-direction (for the geometry shown in Figure 2-2)

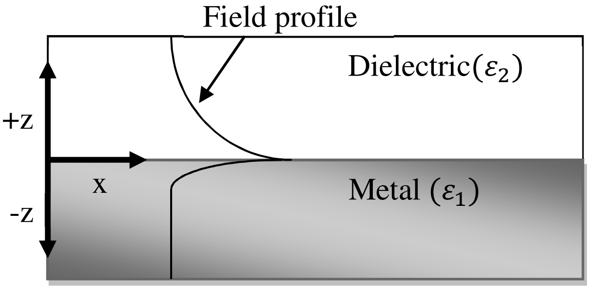

Figure 2-2: Fields profile of SPPs at the metal and dielectric interface.

For the TM solution, we can use equation (2.30) in both spaces: metal and dielectric. For z>0, one can write

$$H_y(z) = A_2 e^{j\beta x} e^{-k_2 z} \tag{2.34}$$

$$E_x(z) = jA_2 \frac{1}{\omega \varepsilon_o \varepsilon_2} k_2 e^{j\beta x} e^{-k_2 z} \tag{2.35}$$

$$E_z(z) = -A_1 \frac{\beta}{\omega \varepsilon_o \varepsilon_2} e^{j\beta x} e^{-k_2 z} \tag{2.36}$$

For and for z < 0 and

$$H_y(z) = A_1 e^{j\beta x} e^{k_1 z} \tag{2.37}$$

$$E_x(z) = -jA_1 \frac{1}{\omega \varepsilon_o \varepsilon_1} k_1 e^{j\beta x} e^{k_1 z} \tag{2.38}$$

$$E_z(z) = -A_1 \frac{\beta}{\omega \varepsilon_o \varepsilon_1} e^{j\beta x} e^{k_1 z} \tag{2.39}$$

where, $k_i \equiv k_{z,i} (i = 1,2)$ represents the component of the wave vector perpendicular to the interface of the two media.

Continuity of H_y and $\varepsilon_i E_z$ at the metal dielectric interface gives $A_1 = A_2$ and

$$\frac{k_2}{k_1} = -\frac{\varepsilon_2}{\varepsilon_1} \tag{2.40}$$

The surface wave exists at the interface between metal and dielectric with the opposite sign of their real dielectric permittivities. So one can write

$$k_1^2 \varepsilon = \beta^2 - k_o^2 \varepsilon_1 \tag{2.41}$$

$$k_2^2 \varepsilon = \beta^2 - k_o^2 \varepsilon_2 \tag{2.42}$$

So using (2.40) - (2.42) the dispersion relation of SPPs propagating in the interface between metal and dielectric can be found as

$$\beta = k_o \sqrt{\frac{\varepsilon_1 \varepsilon_2}{\varepsilon_1 + \varepsilon_2}} \tag{2.43}$$

Equation (2.43) is valid for both real and complex ε_1

The TE surface modes can be expressed as

$$E_y(z) = A_2 e^{j\beta x} e^{-k_2 z} \tag{2.44}$$

$$H_x(z) = -jA_2 \frac{1}{\omega \mu_o} k_2 e^{j\beta x} e^{-k_2 z} \tag{2.45}$$

$$H_z(z) = -A_2 \frac{\beta}{\omega \mu_o} e^{j\beta x} e^{-k_2 z} \tag{2.46}$$

for z > 0 and

$$E_y(z) = A_1 e^{j\beta x} e^{k_1 z} \tag{2.47}$$

$$H_x(z) = jA_1 \frac{1}{\omega \varepsilon_o \varepsilon_1} k_1 e^{j\beta x} e^{k_1 z} \tag{2.48}$$

$$H_z(z) = A_1 \frac{\beta}{\omega \varepsilon_o \varepsilon_1} e^{j\beta x} e^{k_1 z} \tag{2.49}$$

for z < 0. The continuity of E_y and H_x requires

$$A_1(k_1 + k_2) = 0 \tag{2.50}$$

Confinement to the surface requires that the real parts of k_1 and k_2 be greater than zero. This condition will be fulfilled if $A_1 = A_2 = 0$. So, there are no surface modes for the TE polarization. SPPs only exist for the TM polarization.

CHAPTER 3

MATERIAL MODELS

3.1 Modeling Metals

Metals behave as perfect conductors at low frequencies. They do not show any dispersive behavior. However, at high frequencies such as in the optical range, metals behave as dispersive materials. This behavior causes the existence of fields inside the metal at high frequency. Metals act as dielectrics at the frequencies higher than the optical range.

As metals play a vital role for SPPs propagation at the metal-dielectric interface, the behavior of the metals in the optical range should be studied first. In this chapter, the optical behavior of metals which supports SPPs will be studied.

In the presence of an external oscillating EM field, the behavior of any material can be determined from three vectors: D: the electrical flux density, E: the electric field intensity and P: the polarization density.

In the frequency domain, the following constitutive relation relates the above quantities:

$$D(\omega) = \varepsilon(\omega)E(\omega) \qquad (3.1)$$

$$P(\omega) = \varepsilon_o\chi(\omega)E(\omega) \qquad (3.2)$$

$$D(\omega) = \varepsilon_o E(\omega) + P(\omega) \qquad (3.3)$$

Combining (3.2) and (3.3), we have

$$D(\omega) = \varepsilon_o E(\omega)(1 + \chi(\omega)) \qquad (3.4)$$

where, χ is the electric susceptibility which is a measure of how easily the dielectric is polarized in response to an applied electric field.

Combining (3.1) and (3.4) we get

$$\varepsilon(\omega) = \varepsilon_o(1 + \chi(\omega)) \qquad (3.5)$$

So the relative permittivity can be written as

$$\varepsilon_r(\omega) = 1 + \chi(\omega) \qquad (3.6)$$

The above values become simple for a linear isotropic material which is mentioned in equation (2.7) and (2.8). But for a dispersive material, the frequency dependent permittivity and susceptibility are to be modeled perfectly in order to get the perfect response of the material for certain electromagnetic excitation. To model a dispersive material, different models such as the Drude model, Lorentz model, Debye model and Lorentz-Drude model are widely used. In the following subsections these models are briefly described.

3.1.1 The Drude Model

The Drude model of electrical conduction was first developed at the turn of the 20th century by Paul Drude[32],[33]. Drude published it a few years after J.J. Thompson revealed the electron in 1897. Here, Drude initialized a model where the metal is described as a volume filled with stationary positive ions; plunge in a gas of electron. These electrons are free to move inside the metal without any interaction with each other. The electrons in a metal are subjected to two forces; 1. Driving force F_d, 2. Damping force F_g. The driving force and the damping force can be expressed as

$$F_d = qE = -eE \tag{3.7}$$

$$F_g = -\Gamma \upsilon \tag{3.8}$$

They act opposite to each other, so the resultant force becomes

$$F = F_d - F_g \tag{3.9}$$

Using Newton's first law of motion,

$$mr^{''} = -eE + \Gamma \mathrm{r}' \tag{3.10}$$

where

m: mass of an electron.

Γ: damping constant in Newton second per meter.

r: displacement in meter.

υ: velocity of the electron.

q: electron's charge.

the prime indicates differentiation with respect to time.

the time harmonic electric field and displacement can be expressed as

$$E(t) = E_0 e^{-j\omega t} \Leftrightarrow E(\omega) \tag{3.11}$$

$$r(t) = R_0 e^{-j\omega t} \Leftrightarrow R(\omega) \tag{3.12}$$

The frequency domain form of equation (3.10) is

$$mR^{''}(\omega) - \Gamma m R'(\omega) + eE(\omega) = 0 \tag{3.13}$$

Writing the derivatives of the above equation in the frequency domain

$$-m\omega^2 R(\omega) + j\omega m \Gamma R(\omega) + eE(\omega) = 0 \tag{3.14}$$

Simplifying the above equation and solving for R gives

$$R(\omega) = \frac{-e}{m(j\Gamma\omega - \omega^2)} E(\omega) \qquad (3.15)$$

The polarization for *n* electrons can be expressed as

$$P(\omega) = -neR(\omega) \qquad (3.16)$$

So from (3.15) and (3.16) we can write

$$P(\omega) = \frac{ne^2}{m(j\Gamma\omega - \omega^2)} E(\omega) \qquad (3.17)$$

From the above equation an expression for the susceptibility can be obtained as

$$\frac{P(\omega)}{\varepsilon_0 E(\omega)} = \frac{ne^2}{\varepsilon_0 m(j\Gamma\omega - \omega^2)} = \chi(\omega) \qquad (3.18)$$

Substituting equation (3.18) in equation (3.6) yields

$$\varepsilon_r(\omega) = 1 + \frac{ne^2}{\varepsilon_0 m(j\Gamma\omega - \omega^2)} \qquad (3.19)$$

As the plasma frequency ω_p is given by $\omega_p^2 = \frac{ne^2}{\varepsilon_0 m}$, the above equation can be written as

$$\varepsilon_r(\omega) = (1 + \frac{\omega_p^2}{j\Gamma\omega - \omega^2}) \qquad (3.20)$$

So from equation (3.1) the frequency dependent electric flux density becomes

$$D(\omega) = \varepsilon_0 \left(1 + \frac{\omega_p^2}{j\Gamma\omega - \omega^2}\right) E(\omega) \qquad (3.21)$$

For low frequencies $\Gamma\omega \ll 1$. So equation (3.21) is reduced to

$$D(\omega) = \varepsilon_0 \left(1 - \frac{\omega_p^2}{\omega^2}\right) E(\omega) \qquad (3.22)$$

The above relationship is known as the Lorentz model.

3.1.2 The Lorentz Model

The Lorentz model gives a simpler picture of the atom. The model is a very useful tool to visualize atom-field interaction. In this model, Lorentz modeled an atom as a mass (nucleus) connected to another smaller mass (electron). So there is force acting between them which can be denoted as F_r. The force F_r can be written as

$$F_r = -kr \tag{3.23}$$

k: spring constant (N/m)

So equation (3.13) can be written as

$$mr'' + m\Gamma r' + mkr + eE = 0 \tag{3.24}$$

Expressing the above equation in the frequency domain, one gets

$$R(\omega)(m\omega_o^2 + j\omega m\Gamma - m\omega^2) = -eE(\omega) \tag{3.25}$$

where , $\omega_o = \sqrt{\frac{k}{m}}$

Equation (3.25) can be used to find $R(\omega)$ in terms of $E(\omega)$

$$R(\omega) = \frac{-e}{m(\omega_o^2 + j\Gamma\omega - \omega^2)} E(\omega) \tag{3.26}$$

Using (3.16) and (3.26) the susceptibility is found to be

$$\frac{P(\omega)}{\varepsilon_0 E(\omega)} = \frac{ne^2}{\varepsilon_0 m(\omega_o^2 + j\Gamma\omega - \omega^2)} = \chi(\omega) \tag{3.27}$$

Combining equation (3.1) and (3.6), the expression for *D* in the frequency domain becomes

$$D(\omega) = \varepsilon_0 \left(1 + \frac{\omega_P^2}{\omega_0^2 + j\Gamma\omega - \omega^2}\right) E(\omega) \qquad (3.28)$$

The above relationship is known as the Lorentz model.

3.1.3 The Lorentz-Drude Model

A classical theory was developed using Drude and Lorentz models to account for the complex index of refraction and dielectric constant of material and their variation with frequency. Usually for normal dispersion the dielectric constant increases slowly with frequency. However, in the vicinity of an atomic transition the material exhibits irregular dispersion, in which the dielectric constant decreases sharply with frequency, accompanied by absorption of light. The free electrons result in a permittivity that can be represented by a Drude model, and the bound electrons give a permittivity which is represented by the Lorentz model[34].

The permittivity of the more general Lorentz-Drude model can be expressed as

$$\varepsilon = \varepsilon_{free} + \varepsilon_{bound} \qquad (3.29)$$

The free electron permittivity is written as

$$\varepsilon_{free} = 1 + \frac{\omega_p}{j\Gamma\omega - \omega^2} \qquad (3.30)$$

and the bound electron permittivity as

$$\varepsilon_{bound} = \frac{\omega_p}{\omega_o + j\Gamma\omega - \omega^2} \qquad (3.31)$$

where, ω_p is the frequency of the pole pair.

So combining both, the electric field density in frequency domain becomes

$$D(\omega) = \varepsilon_o\left(1 + \frac{\omega_p}{j\Gamma\omega - \omega^2} + \frac{\omega_p}{\omega_o + j\Gamma\omega - \omega^2}\right)E(\omega) \qquad (3.32)$$

The above relation is known as the Lorentz-Drude model.

3.1.4 The Debye Model

The Debye model was first developed by Peter Debye in the year 1912. According to the Debye model, materials are assumed to have electric dipoles and when the electric field is applied, these dipoles follow the behavior of the field having some relaxation time. The polarization will have greater strength if the electric field oscillates at a slow frequency, whereas a fast oscillating field causes low polarization. Since metals have very short relaxation times, the polarization in metals is strong.

If a DC electric field is applied to a dielectric, the polarization takes some time to follow the electric field. The instantaneous polarization $P(t)$ is given by

$$P(t) = P_\infty\left(1 - e^{-t/\tau}\right) \qquad (3.33)$$

where

P_∞: Polarization in the DC steady state.

τ: Time constant.

The derivative of equation (3.33) is

$$\frac{dP(t)}{dt} = \frac{1}{\tau}P_\infty e^{-t/\tau} \qquad (3.34)$$

Combining (3.33) and (3.34) yields

$$P(t) = P_\infty - \tau\frac{dP(t)}{dt} \qquad (3.35)$$

As $P_\infty = \varepsilon_0(\varepsilon - 1)E(t)$ so equation (3.35) reduced to

$$P(t) = \varepsilon_0(\varepsilon - 1)E(t) - \tau\frac{dP(t)}{dt} \tag{3.36}$$

In the frequency domain equation (3.36) becomes

$$\varepsilon_0(\varepsilon - 1)\,E(\omega) = P(\omega) + j\omega\tau P(\omega) \tag{3.37}$$

The linear susceptibility is expressed as

$$\frac{\varepsilon - 1}{(1 + j\omega\tau\,)} = \frac{P(\omega)}{\varepsilon_0\,E(\omega)} = \chi(\omega) \tag{3.38}$$

From equation (3.6) the permittivity becomes

$$\varepsilon_r(\omega) = \chi(\omega) + 1 = \frac{\mathcal{E} - 1}{(1 + j\omega\tau\,)} + 1 \tag{3.39}$$

For the permittivity function to fit the range from zero frequency to infinite frequency, the boundary conditions are

$$\varepsilon_r(0) = \varepsilon_s \text{ and } \varepsilon_r(\infty) = \varepsilon_\infty$$

So the modified relation of the permittivity becomes

$$\varepsilon_r(\omega) = \varepsilon_\infty + \frac{\varepsilon_s - \varepsilon_\infty}{(1 + j\omega\tau\,)} \tag{3.40}$$

Another term related to the conductivity of metal is added to the above equation. Equation (3.40) can be expanded as

$$\varepsilon_r(\omega) = \varepsilon_\infty + \frac{\varepsilon_s - \varepsilon_\infty}{(1 + j\omega\tau\,)} - j\frac{\sigma}{\omega\varepsilon_0} \tag{3.41}$$

If the model is represented in terms of its real and imaginary parts, then,

$$\varepsilon_r(\omega) = \varepsilon'(\omega) - j\varepsilon''(\omega) \tag{3.42}$$

where the part of the permittivity, $\varepsilon'(\omega) = \varepsilon_\infty + \frac{\varepsilon_s - \varepsilon_\infty}{1 + \omega^2\tau^2}$ and the imaginary part of the permittivity, $\varepsilon''(\omega) = \frac{(\varepsilon_s - \varepsilon_\infty)\omega\tau}{1 + \omega^2\tau^2} + \frac{\sigma}{\omega\varepsilon_0}$.

3.2 Modeling Non-Linear Dispersive Glass (As_2S_3)

Most of the materials, by their nature, exhibit some form of frequency-dependent permittivity. So, to model the electromagnetic and optical phenomena of the material, frequency dependence behavior should be considered. Modeling non-linear optical behavior over a wide frequency range, on the other hand, demands inclusion of some form of dispersion in the model to get realistic outputs.

Accurate analytical modeling of non-linear characteristics of chalcogenide glass is complicated due to the presence of dispersion and non-linearity. This section considers the modeling of non-linear dispersive As_2S_3 chalcogenide glass. For the linear dispersive behavior, the Lorentz model is used and upgraded to the modeling of non-linear dispersive material. Both non-linear instantaneous Kerr and retarded Raman effects are analyzed as well.

3.2.1 Material Dispersion

Dispersion in general can be defined as the variation of the propagating wave's wavelength with frequency[10]. It is also sometimes defined as the variation of propagating wave's wave number $k = \frac{2\pi}{\lambda}$ with angular frequency $\omega = 2\pi f$. Consider the one dimensional scalar wave equation

$$\frac{\partial^2 u}{\partial t^2} = v^2 \frac{\partial^2 u}{\partial x^2} \tag{3.43}$$

where, $v^2 = \frac{1}{\mu\varepsilon}$

The continuous sinusoidal travelling wave solution of above equation, written in phasor form as

$$u(x,t) = e^{j(\omega t - kx)} \tag{3.44}$$

where the wave number $k = \frac{2\pi}{\lambda}$ and the angular frequency $\omega = 2\pi f$. Substitution in the wave equation yields

$$(j\omega)^2 e^{j(\omega t - kx)} = v^2(-jk)^2 e^{j(\omega t - kx)} \tag{3.45}$$

Factoring out the common factors from both side we get

$$k = \pm \frac{\omega}{v} \tag{3.46}$$

Equation (3.46) is the dispersion relation for the one dimensional scalar wave equation stated in (3.43). The '+' sign is for -x directed wave propagation and '-' sign is for +x directed wave propagation. The magnetic flux density and electric flux density for dispersive medium are

$$D(\omega) = \varepsilon(\omega)E \tag{3.47}$$

$$B(\omega) = \mu(\omega)H \tag{3.48}$$

Both $\varepsilon(\omega)$ and $\mu(\omega)$ are functions of frequency. A non-magnetic dielectric material has $\mu = \mu_o$ and thus μ is frequency independent.

3.2.2 Nonlinear Lorentz model of As_2S_3

The classical Lorentz model of dielectric dispersion is considered as an accurate description of material response for some media. To represent the dispersive non-linear properties of the material, the polarization is used. So equation (3.3) can be expanded to

$$D(\omega) = \varepsilon_o \varepsilon_\infty E(\omega) + P_{LN(1)}(\omega) + P_{NL(2)}(\omega) + P_{NL(3)}(\omega) \qquad (349)$$

Again the susceptibility in the frequency domain can be decomposed into

$$\chi(\omega) = \chi^{(1)}(\omega) + \chi^{(2)}(\omega)E(\omega) + \chi^{(3)}(\omega)E^2(\omega) \qquad (3.50)$$

where,

$P_{LN(1)}$ is the linear polarization.

$P_{NL(2)}$ is second-order non-linear polarization.

$P_{NL(3)}$ is third-order non-linear polarization.

ε_o is the permittivity of free space.

ε_∞ is the relative permittivity in the limit of infinite frequency.

$\chi^{(1)}$ is the linear susceptibility.

$\chi^{(2)}$ is second order non-linear susceptibility.

$\chi^{(3)}$ is third order non-linear susceptibility.

The work in this thesis will consider only third order nonlinear material and therefore second order non-linear part $\chi^{(2)}$ will be ignored. From equation (3.49) the linear polarization $P_{LN(1)}(\omega)$ can be expressed as

$$P_{LN(1)}(\omega) = \varepsilon_o \chi^{(1)}(\omega) E(\omega) \qquad (3.51)$$

Lorentz model for linear polarization can be written as a function of frequency as

$$P_{LN(1)}(\omega) = \left(\frac{a}{b + j\omega c - d\omega^2}\right) E(\omega) \qquad (3.52)$$

where

$a = \varepsilon_o(\varepsilon_s - \varepsilon_\infty){\omega_o}^2 \qquad b = {\omega_o}^2 \qquad c = 2\delta \qquad d = 1$

with

ε_s: The static value of the dielectric constant

ε_∞: Optical value of the dielectric constant

ω_o : Material resonance frequency (rad/s)

δ : Damping factor, (s^{-1}.)

So the linear susceptibility of the Lorentz dispersion can be expressed as

$$\chi^{(1)}(\omega) = \frac{a}{\varepsilon_o(b + j\omega c - d\omega^2)} \tag{3.53}$$

From equation (3.54) we can get

$$(b + j\omega c - d\omega^2)P_{LN(1)}(\omega) = aE(\omega) \tag{3.54}$$

Which can written in the time domain as

$$bP_{LN(1)}(t) + cP'_{LN(1)}(t) + dP''_{LN(1)}(t) = aE(t) \tag{3.55}$$

3.2.3 $\chi^{(3)}$ *Model for* As_2S_3

The third-order nonlinear polarization can be expressed as the time convolution between the third-order susceptibility function $\chi^{(3)}(t)$ and the electric field. For the simple model consisting of an electron and the core of the atoms, using Born-Oppenheimer approximation[35]

$$P_{NL}(t) = \varepsilon_o \chi_o^{(3)} E(t) \int_{-\infty}^{t} g(t-t') E^2(t') dt' \tag{3.56}$$

where $\chi_o^{(3)}$ is the strength of the third-order nonlinearity and the causal response function $g(t)$ is expressed as

$$g(t) = \alpha\delta(t) + (1-\alpha) g_R(t) \tag{3.57}$$

with

$$g_R(t) = \frac{\tau_1^2 + \tau_2^2}{\tau_1^2 \tau_2^2} \exp\left(-\frac{t}{\tau_2}\right) \sin\left(\frac{t}{\tau_1}\right) u(t) \tag{3.58}$$

The function $u(t)$ is normalized such that

$$\int_{-\infty}^{\infty} g(t) dt = 1 \tag{3.59}$$

So the third order non-linear part of equation (3.51) can be expressed in time domain as

$$P_{NL(3)}(t) = P_{NL(3)}^{k}(t) + P_{NL(3)}^{r}(t) \tag{3.60}$$

where

$\delta(t)$ represents the immediate response of the electrons.

$1/\tau_1$ is characteristic frequency of response function of damped oscillation.

τ_2 is damping constant.

α is the ratio of the Kerr intensity to the total Kerr and Raman nonlinearity.

$P_{NL(3)}^{k}$ is the polarization caused by instantaneous kerr non-linearity.

$P_{NL(3)}^{r}$ is the polarization caused by Raman effect .

1. **Instantaneous Kerr Nonlinearity:** The polarization of instantaneous kerr-nonlinearity is expressed as

$$P_{NL(3)}^{k}(t) = \varepsilon_o \chi_o^{(3)} E(t) \int_{-\infty}^{t} \alpha\delta(t-t') E^2(t') dt' = \alpha\varepsilon_o \chi_o^{(3)} E^3(t) \tag{3.61}$$

2. **Raman Nonlinearity:** The polarization due to Raman effect can be written as

$$P_{NL(3)}^{r}(t) = \varepsilon_o E(t) \int_0^t \chi_R^{(3)}(t-t')E^2(t')dt' = \varepsilon_o E(t)\left[\chi_R^{(3)}(t) * E^2(t)\right] \quad (3.62)$$

where

$$\chi_R^{(3)}(t) = (1-\alpha)\chi_o^{(3)} g_R(t) \quad (3.63)$$

Let us define

$$s(t) = \chi_R^{(3)}(t) * E^2(t) \quad (3.64)$$

Now, in the frequency domain, equation (3.66) becomes

$$s(\omega) = \chi_R^{(3)}(\omega).FT\{E^2(\omega)\} \quad (3.65)$$

Where *FT* represents the Fourier transform and '$*$' denotes convolution integral and $s(\omega)$ is the Fourier transform of $s(t)$.

$\chi_R^{(3)}(\omega)$ can be written as

$$\chi_R^{(3)}(\omega) = \frac{A{\omega_R}^2}{{\omega_R}^2 - 2j\omega\delta_R - \omega^2} \quad (3.66)$$

where,

$A = (1-\alpha)\,\chi_o^{(3)}$, damping factor $\delta_R = \frac{1}{\tau_2}$, and $\omega_R = \sqrt{\frac{{\tau_1}^2+{\tau_2}^2}{{\tau_1}^2{\tau_2}^2}}$.

CHAPTER 4

FDTD-BASED SOLUTION

4.1 Introduction to FDTD Method

The FDTD method is one of the most extensively used numerical methods for the solution of electromagnetic problems. Without requiring a complex mathematical formulation, it provides us with a simple way to discretize Maxwell's equations, and it does not need any symmetry in the structure being modeled. Moreover, it computes the solution in the time domain, from which the frequency behavior can be extracted over a wide range of frequencies. Since the introduction of the FDTD algorithm[8], it has undergone many modifications. As the computation costs continue to decline, this method is gaining even more popularity and a lot of FDTD-related research activities are being done.

To formulate FDTD in general we need to start with Maxwell's equations. For a non-dispersive linear isotropic material equation (2.3) and (2.4) can be expressed as

$$\frac{\partial H}{\partial t} = -\frac{1}{\mu}\nabla \times E \tag{4.1}$$

$$\frac{\partial E}{\partial t} = \frac{1}{\varepsilon}\nabla \times H \tag{4.2}$$

Assuming nonmagnetic media (i.e. $\mu = \mu_o$) expansion of the components of the curl operators of (4.1) and (4.2) yields the following six coupled scalar equations in Cartesian coordinates.

$$\frac{\partial E_z}{\partial y} - \frac{\partial E_y}{\partial z} = j\omega\mu_o H_x \tag{4.3}$$

$$\frac{\partial E_x}{\partial z} - \frac{\partial E_z}{\partial x} = j\omega\mu_o H_y \tag{4.4}$$

$$\frac{\partial E_y}{\partial x} - \frac{\partial E_x}{\partial y} = j\omega\mu_o H_z \tag{4.5}$$

$$\frac{\partial H_z}{\partial y} - \frac{\partial H_y}{\partial z} = -j\omega\varepsilon_r E_x \tag{4.6}$$

$$\frac{\partial H_x}{\partial z} - \frac{\partial H_z}{\partial x} = -j\omega\varepsilon_r E_y \tag{4.7}$$

$$\frac{\partial H_y}{\partial x} - \frac{\partial H_x}{\partial y} = -j\omega\varepsilon_r E_z \tag{4.8}$$

The system of six coupled partial differential equations (4.3)-(4.8) forms the beginning of the FDTD numerical algorithm for modeling electromagnetic wave interactions with arbitrary three-dimensional objects. The Yee algorithm[8] simultaneously deals with both the electric and magnetic fields in both time and space, rather than by solving the wave equation for either the electric field or the magnetic field alone.

Yee's FDTD scheme discretizes Maxwell's curl equations. It approximates the time and space first-order partial derivatives with central differences, and then solves the resulting equations by using a leapfrog scheme[36].

4.2 Yee's Orthogonal Mesh

Yee proposed a 3-D mesh having field components at different locations as shown in figure 4-1. *E* and *H* components are positioned at the centers of the grid lines and surfaces such that each component is surrounded by four components. This gives a simple picture of three-dimensional space being filled by interlinked arrays of Faraday's law and Ampere's law contours. Thus, it is possible to identify the *E* components related with the displacement current flux linking with the *H* loops and, correspondingly, the *H* components related with the magnetic flux are linked with the E loops, as shown in Figure 4-1.

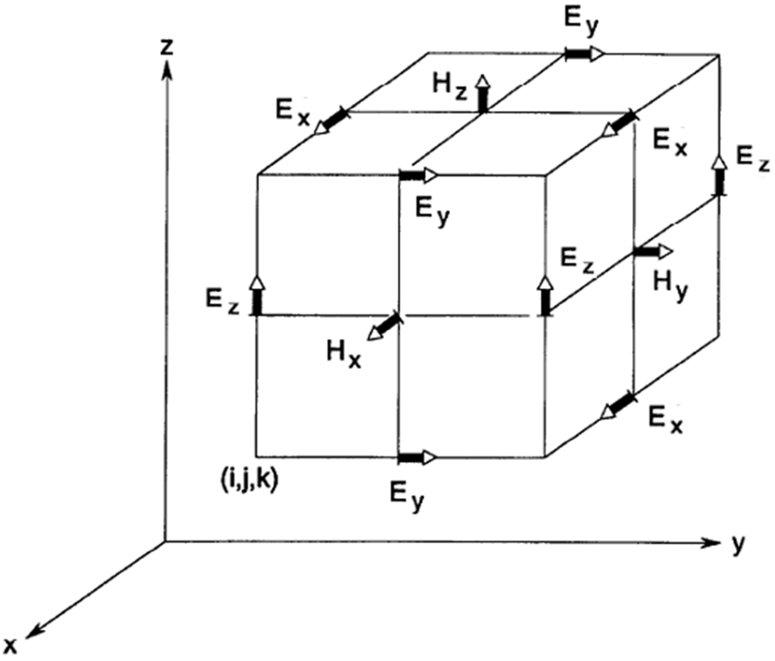

Figure 4-1: Yee's spatial grid.

If we consider only 2-dimensional space (i.e of x-y plane), and assuming no variation of the fields in the z-direction. Thus we have:

$$\frac{\partial Hy}{\partial z} = 0, \frac{\partial Hx}{\partial z} = 0, \frac{\partial Ey}{\partial z} = 0, \frac{\partial Ex}{\partial z} = 0$$

From equation (4.3)-(4.8), we can write two independent sets of coupled equations.

TM polarized field:

$$\frac{\partial Ex}{\partial t} = \frac{1}{\varepsilon}\frac{\partial Hz}{\partial y} \tag{4.9}$$

$$\frac{\partial Ey}{\partial t} = -\frac{1}{\varepsilon}\frac{\partial Hz}{\partial x} \tag{4.10}$$

$$\frac{\partial Hz}{\partial t} = \frac{1}{\mu}\left(\frac{\partial Ex}{\partial y} - \frac{\partial Ey}{\partial x}\right) \tag{4.11}$$

And TE polarized field:

$$\frac{\partial Hx}{\partial t} = -\frac{1}{\mu}\frac{\partial Ez}{\partial y} \tag{4.12}$$

$$\frac{\partial Hy}{\partial t} = \frac{1}{\mu}\frac{\partial Ez}{\partial x} \tag{4.13}$$

$$\frac{\partial Ez}{\partial t} = \frac{1}{\varepsilon}\left(\frac{\partial Hy}{\partial x} - \frac{\partial Hx}{\partial y}\right) \tag{4.14}$$

Utilizing Yee's spatial gridding scheme, the partial spatial derivatives in (4.9)-(4.11) can be approximated by a central difference approximation in space. For example, equations (4.9)-(4.11) respectively become

$$\frac{\partial E_x}{\partial t} = \frac{1}{\varepsilon}\frac{H_z(i,j) - H_z(i,j-1)}{\Delta y} \tag{4.15}$$

$$\frac{\partial E_y}{\partial t} = -\frac{1}{\varepsilon}\frac{H_z(i,j) - H_z(i-1,j)}{\Delta x} \tag{4.16}$$

$$\frac{\partial H_z}{\partial t} = \frac{1}{\mu}\left(\frac{E_x(i,j+1) - E_x(i,j)}{\Delta y} - \frac{E_y(i+1,j) - E_y(i,j)}{\Delta x}\right) \tag{4.17}$$

Yee's algorithm also utilizes central differencing in time for the *E* and *H* components. The *E* and *H* components are solved by using a leapfrog algorithm as shown in Figure 4-2. All of the *E* components in the modeled space are computed and stored in memory by using the previously computed values of *E* and the newly computed *H* field data. At the next step, *H* is recomputed based on the previously obtained *H* and the newly updated *E*. This process continues until the time-stepping is terminated.

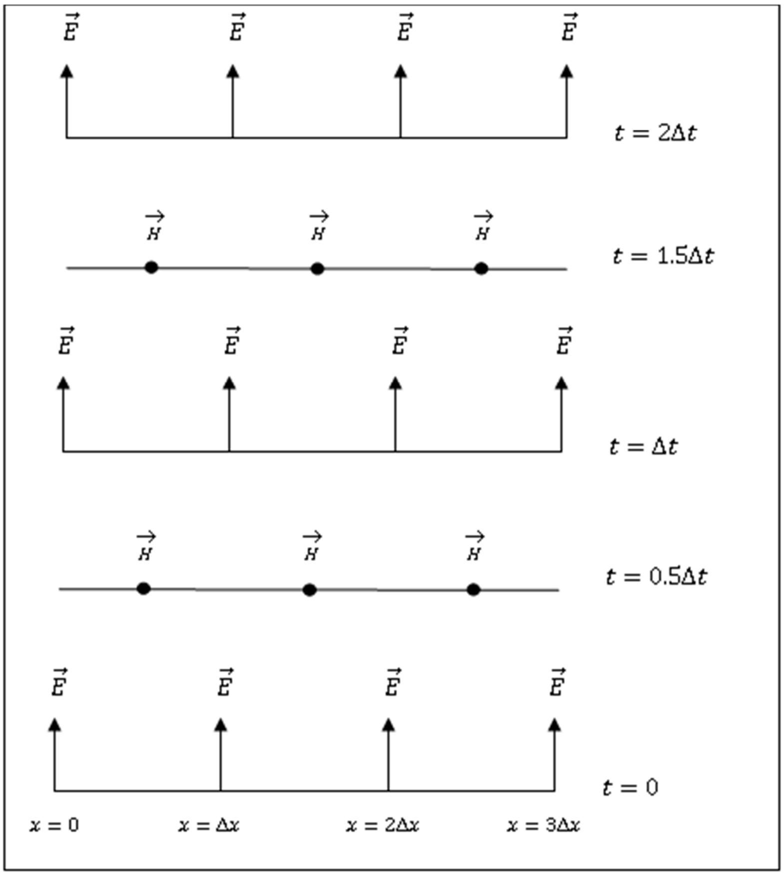

Figure 4-2: Leapfrog scheme: the temporal scheme of the FDTD method.

Applying central difference approximation equation (4.15)-(4.17) respectively, become

$$\frac{E_x^{n+1}\left(i+\frac{1}{2},j\right)-E_x^{n}(i+\frac{1}{2},j)}{\Delta t}=\frac{1}{\varepsilon}\frac{H_z^{n+\frac{1}{2}}\left(i+\frac{1}{2},j+\frac{1}{2}\right)-H_z^{n+\frac{1}{2}}\left(i+\frac{1}{2},j-\frac{1}{2}\right)}{\Delta y} \tag{4.18}$$

$$\frac{E_y^{n+1}\left(i,j+\frac{1}{2}\right)-E_y^{n}(i,j+\frac{1}{2})}{\Delta t}=-\frac{1}{\varepsilon}\frac{H_z^{n+\frac{1}{2}}\left(i+\frac{1}{2},j+\frac{1}{2}\right)-H_z^{n+\frac{1}{2}}\left(i-\frac{1}{2},j+\frac{1}{2}\right)}{\Delta y} \tag{4.19}$$

$$\frac{H_z^{n+\frac{1}{2}}\left(i+\frac{1}{2},j+\frac{1}{2}\right)-H_z^{n-\frac{1}{2}}(i+\frac{1}{2},j+\frac{1}{2})}{\Delta t}$$
$$=\frac{1}{\mu}\left(\frac{E_x^{n}\left(i+\frac{1}{2},j+1\right)-E_x^{n}\left(i+\frac{1}{2},j\right)}{\Delta y}-\frac{E_y^{n}\left(i+1,j+\frac{1}{2}\right)-E_y^{n}\left(i,j+\frac{1}{2}\right)}{\Delta x}\right) \tag{4.20}$$

To ensure the numerical stability of the Yee algorithm, it is required to set an upper bound of the time step, Δt, which is related with spatial increment Δx, Δy, and Δz in accordance with the Courant-Friedrich-Levy (CFL) stability condition[36]. In three dimensions, the CFL condition is

$$\Delta t \leq \Delta t_{max}=\frac{1}{c\sqrt{\frac{1}{\Delta x^2}+\frac{1}{\Delta y^2}+\frac{1}{\Delta z^2}}} \tag{4.21}$$

The upper bound on Δt in the above equation guarantees the stability of the algorithm, which is essential to guarantee its validity when applied to a wide variety of electromagnetic wave modeling problems.

4.3 Material Dispersion in FDTD

The FDTD method, which is a robust numerical modeling technique, has been commonly used for modeling electromagnetic wave interaction with complex materials. One of the most major developments in the FDTD method is its ability to model dispersive materials. As most of the dielectrics and metals are dispersive, modeling materials in FDTD requires the knowledge of modeling dispersive materials, which were discussed in chapter 3. There are three main methods to model dispersive materials in the FDTD:

1. The recursive convolution (RC) method.
2. The auxiliary differential equation (ADE) method.
3. The Z-transform method.

In this chapter, the ADE dispersive FDTD method will be discussed in detail and applied to model metals and dielectric materials.

4.3.1 The Auxiliary Differential Equation (ADE)

The auxiliary differential equation, first proposed by Taflove[10], was formulated to introduce dispersion relation in FDTD. The ADE method is widely used due to its high flexibility in fitting arbitrary permittivity functions and gives a more general representation of the dispersion relation[37]. Taflove's idea was to convert the dispersion relation from the frequency domain to the time domain through Fourier transform, where the new *E* field can be found from the previous value of *E* and *D*. To get a time domain relation between *D* and *E* in a dispersive medium, we can for instance start with the frequency domain relationship

$$D(\omega) = \varepsilon_o \frac{\sigma}{j\omega} E(\omega) \tag{4.22}$$

which can be simplified to

$$j\omega D(\omega) = \varepsilon_o \sigma E(\omega) \tag{4.23}$$

By applying inverse Fourier transform the above equation becomes

$$\frac{dD(t)}{dt} = \varepsilon_o \sigma E(t) \tag{4.24}$$

Discretizing the above relation using forward difference scheme

$$\frac{D^{n+1} - D^n}{\Delta t} = \varepsilon_o \sigma E^{n+1} \tag{4.25}$$

So the updated E will be

$$E^{n+1} = \frac{D^{n+1} - D^n}{\varepsilon_o \sigma \Delta t} \tag{4.26}$$

4.3.2 The General ADE-FDTD Algorithm for Ag Metal and As_2S_3 Glass

For a single-pole dispersion relation, the FDTD equation is simple to derive. But for a multi-pole dispersion relation, the FDTD equation becomes difficult to derive. For Lorentz-Drude six-pole dispersion, lengthy derivation and computation are required. Taflove proposed matrix inversion to solve for multi-poles which requires a large computational time and a large memory. However, Alsunaidi and Al-Jabr[37] proposed the general algorithm technique which solve these problems. Only one algorithm is required for any dispersion relation as a result of the ADE method. The dispersive relation has the general form as

$$D(\omega) = \varepsilon(\omega) E(\omega) \tag{4.27}$$

This can be expressed as the form of equation (3.3)

$$D(\omega) = \varepsilon_o \varepsilon_\infty E(\omega) + \sum_i^N P_i(\omega) \tag{4.28}$$

where, N is the number of poles. So applying the inverse Fourier transform, the discretized form of the equation (4.27) becomes

$$D^{n+1} = \varepsilon_o \varepsilon_\infty E^{n+1} + \sum_i^N P_i^{n+1} \tag{4.29}$$

Solving for *E* gives

$$E^{n+1} = \frac{D^{n+1} - \sum_i^N P_i^{n+1}}{\varepsilon_o \varepsilon_\infty} \tag{4.30}$$

The procedure for the evaluation of the time-domain polarization is as follows. For the general Lorentz formulation, the polarization in frequency domain can be expressed as

$$P(\omega) = \frac{a}{b + jc\omega - d\omega^2} E(\omega) \tag{4.31}$$

Taking the inverse Fourier transform, the following differential equation for time domain polarization is obtained

$$bP(t) + cP'(t) + dP''(t) = aE(t) \tag{4.32}$$

Now for any time instant *n* the updated equation of the polarization can be obtained by approximating the time derivatives in (4.31) and the resulting discretized equation is given by:

$$bP^n + c\frac{P^{n+1} - P^{n-1}}{2\Delta t} + d\frac{P^{n+1} - 2P^n + P^{n-1}}{\Delta t^2} = aE^n \tag{4.33}$$

which can be solved for P^{n+1} in terms of P^n, P^{n-1} and E^n

$$P^{n+1} = \frac{4d - 2b\Delta t^2}{2d + c\Delta t} P^n + \frac{-2d + c\Delta t}{2d + c\Delta t} P^{n-1} + \frac{2a\Delta t^2}{2d + c\Delta t} E^n \tag{4.34}$$

Equation (4.33) can be written compactly as:

$$P^{n+1} = C_1 P^n + C_2 P^{n-1} + C_3 E^n \tag{4.35}$$

where,

$$C_1 = \frac{4d - 2b\Delta t^2}{2d + c\Delta t}, \qquad C_2 = \frac{-2d + c\Delta t}{2d + c\Delta t}, \qquad C_3 = \frac{2a\Delta t^2}{2d + c\Delta t}$$

For the 6-pole Lorentz-Drude model the values of C_1, C_2 and C_3 are different for different materials. These constants can be found for any form of dispersion relation of *E* and *D*. In table 4-1 the general constants for some possible poles are given.

Table 4-1: Algorithm constant: C_1, C_2 and C_3 for different dispersion relation models [37]

Dispersion model	C_1	C_2	C_3
Lorentz Pole $P(\omega) = \frac{a}{b + jc\omega - d\omega^2}E(\omega)$	$\frac{4d - 2b\Delta t^2}{2d + c\Delta t}$	$\frac{-2d + c\Delta t}{2d + c\Delta t}$	$\frac{2a\Delta t^2}{2d + c\Delta t}$
Drude Pole $P(\omega) = \frac{a}{jc\omega - d\omega^2}E(\omega)$	$\frac{4d}{2d + c\Delta t}$	$\frac{-2d + c\Delta t}{2d + c\Delta t}$	$\frac{2a\Delta t^2}{2d + c\Delta t}$
Plasma frequency $P(\omega) = \frac{a}{\omega^2}E(\omega)$	2	-1	$2a\Delta t^2$
Debye $P(\omega) = \frac{a}{b + jc\omega}E(\omega)$	$-\frac{2b\Delta t}{c}$	1	$-\frac{2a\Delta t}{c}$
Conductivity term $P(\omega) = \frac{a}{jc\omega}E(\omega)$	0	1	$\frac{2a\Delta t}{c}$

The algorithm can be illustrated using the following flow chart:

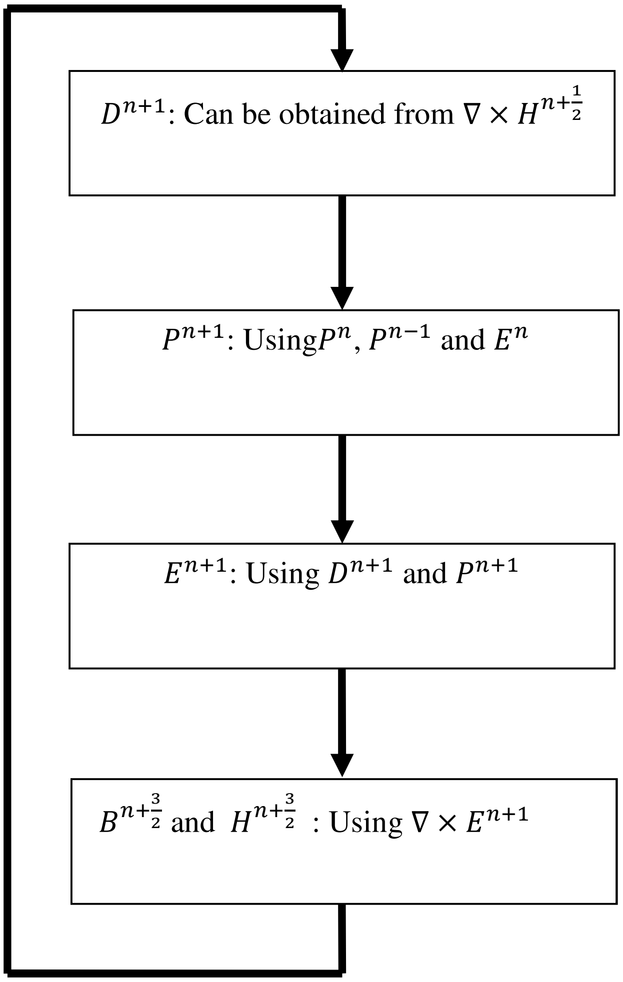

Figure 4-3: FDTD algorithm for linear dispersive case

4.4 Incorporating the Third-Order Nonlinear Susceptibility ($\chi^{(3)}$) into the FDTD Algorithm

This section elaborates the ADE-FDTD[37] method to model non-linear dispersive material, which is As_2S_3 chalcogenide glass in our case. The non-linearity is characterized by a multipole Lorentz model. This was described in chapter 3. From equation (3.67) and (3.68) we have

$$s(\omega) = \chi_R^{(3)}(\omega) FT\{E^2(t)\} \tag{4.36}$$

where *FT* represents the Fourier transform.

$\chi_R^{(3)}(\omega)$ can be written as

$$\chi_R^{(3)}(\omega) = \frac{A{\omega_R}^2}{{\omega_R}^2 - 2j\omega\delta_R - \omega^2} \tag{4.37}$$

Equation (4.35) can be written as

$$s(\omega) = \frac{A{\omega_R}^2}{{\omega_R}^2 - 2j\omega\delta_R - \omega^2} FT\{E^2(t)\} \tag{4.38}$$

This can be rewritten as

$$[{\omega_R}^2 - 2j\omega\delta_R + (j\omega)^2] s(\omega) = A{\omega_R}^2\, FT\{E^2(t)\} \tag{4.39}$$

In the time domain, the above equation takes the form

$${\omega_R}^2 s(t) - 2\delta_R \frac{ds(t)}{dt} + \frac{d^2 s(t)}{dt^2} = A{\omega_R}^2\, E^2(t) \tag{4.40}$$

Now for any time instant $n\Delta t$ the updated equation of *s* can be obtained by approximating the time derivatives in (4.38) and the update equation becomes

$$s^{n+1} = C_{11} S^n + C_{22} S^{n-1} + C_{33} {E^2}^n \tag{4.41}$$

where

$$C_{11} = \frac{4d - 2b\Delta t^2}{2d + c\Delta t}, \qquad C_{22} = \frac{-2d + c\Delta t}{2d + c\Delta t}, \qquad C_{33} = \frac{2a\Delta t^2}{2d + c\Delta t} E^n$$

$$a = (1-\alpha)\varepsilon_o \chi^{(3)}({\omega_R}^2), \qquad b = {\omega_R}^2, \qquad c = 2\delta_R, \qquad d = 1$$

Using equation (3.62) the update equation for polarization can be expressed as

$$P_{NL(3)}^{n+1} = \alpha_k (E^{n+1})^3 + s^{n+1}E^{n+1} \tag{4.42}$$

Then the updated value of the electric flux density is

$$D^{n+1} = \varepsilon_o \varepsilon_\infty E^{n+1} + P_{LN(1)}^{n+1} + \alpha_k (E^{n+1})^3 + s^{n+1}E^{n+1} \tag{4.43}$$

Solving for E^{n+1}, the following equation is obtained

$$A_k (E^{n+1})^3 + B_k \, (E^{n+1})^2 + C_k E^{n+1} + D_k = 0 \tag{4.44}$$

where,

$$A_k = 1, \qquad B_k = 0, \qquad C_k = \frac{(s^{n+1} + \varepsilon_o \varepsilon_\infty)}{\alpha \varepsilon_o \chi^{(3)}}, \qquad D_k = \frac{P_{LN(1)}^{n+1} - D^{n+1}}{\alpha \varepsilon_o \chi^{(3)}}$$

Equation (4.44) is a cubic equation in E^{n+1} with real solution given by

$$E^{n+1} = \left(-\frac{D_k}{2} + \sqrt{\left(\frac{C_k}{3}\right)^3 + \left(\frac{D_k}{2}\right)^2} \right)^{\frac{1}{3}} + \left(-\frac{D_k}{2} - \sqrt{\left(\frac{C_k}{3}\right)^3 + \left(\frac{D_k}{2}\right)^2} \right)^{\frac{1}{3}} \tag{4.45}$$

The algorithm to calculate the updated E and H can be illustrated using following flow chart.

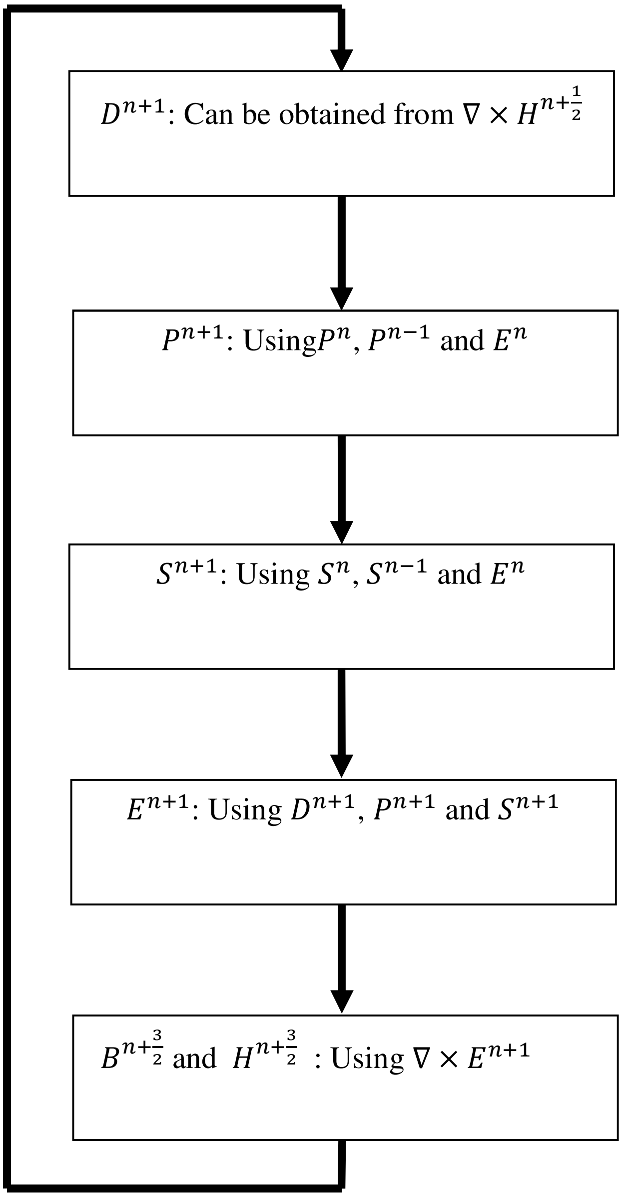

Figure 4-4: FDTD algorithm for nonlinear dispersive case.

CHAPTER 5

SIMULATOR VERIFICATION

The main purpose of the simulator is to produce accurate results of the simulated process. The accuracy of the simulator is extremely important to have a reliable and useful solution. Hence, before using any newly developed simulator, it is essential to verify the simulator with other methods such as, the analytical solutions or with the experimental results.

This chapter presents the verification of the simulator used to represent different materials. This is done by comparing the published results with the results of the developed simulator. As different types of material models have been used, the models are to be checked to minimize the error. Obviously, any numerical technique has its own limitations, but typically, when modeling conventional materials, it is assumed that the results are sufficiently accurate and that the effect of numerical material parameters is negligible.

In this thesis, the non-linear dispersive material: As_2S_3 chalcogenide glass is used to study the SPP propagation through a non-linear device. So, it is required to verify the simulator for non-linear dispersive material and the dispersion relation of the material for different wavelengths. The following sections give the results of simulation done using our developed simulator and comparison with some published results particular published cases.

5.1 Testing the Algorithm for Non-linear Dispersive Material

In order to test our algorithm for non-linear dispersive material, the one-dimensional temporal solitons was calculated using the data given by Taflove[10]. A 50-fs optical pulsed signal source was used at t=0 at the surface x=0. The material was considered to have a linear and non-linear susceptibility function $\chi^{(1)}$ and $\chi^{(3)}$ respectively.

Figure 5-1: 1-D structure to solve non-linear dispersive material of Taflove[10].

The linear susceptibility parameters used in the simulator is as follows

$$\chi^{(1)}: \quad \varepsilon_s = 5.25, \qquad \varepsilon_\infty = 2.24, \qquad \omega_o = 4 \times 10^{14} s^{-1}, \qquad \delta = 2 \times 10^9 s^{-1}$$

The non-linear susceptibility parameters are:

$\chi^{(3)}$: non-linear co-efficient, $\chi_o^{(3)} = 7 \times 10^{-2} (v/m)^{-2}$,

Lorentz relaxation times, $\tau_1 = 12.2\, fs$ and $\tau_2 = 32\, fs$

The *E* pump signal having unity amplitude (figure 5-2) was multiplied by a hyperbolic secant temporal envelope with a carrier frequency $f_c = 1.37 \times 10^{14}\ Hz$. The spatial step size Δx was set at 5 nm. The propagating pulse was graphed at 20,000 and 40,000 time steps which correspond to 55 μm and 126 μm at time 487 fs and 973 fs. The simulated results using our developed simulator, give a very good agreement with the published results[10]. Figure 5-2 is only for dispersive cases. In Figure 5-2, it is clearly seen that the pulse undergoes spatial broadening, which is due to material dispersion. Figure 5-3 corresponds the results for the nonlinear dispersive case showing the formation of solitons.

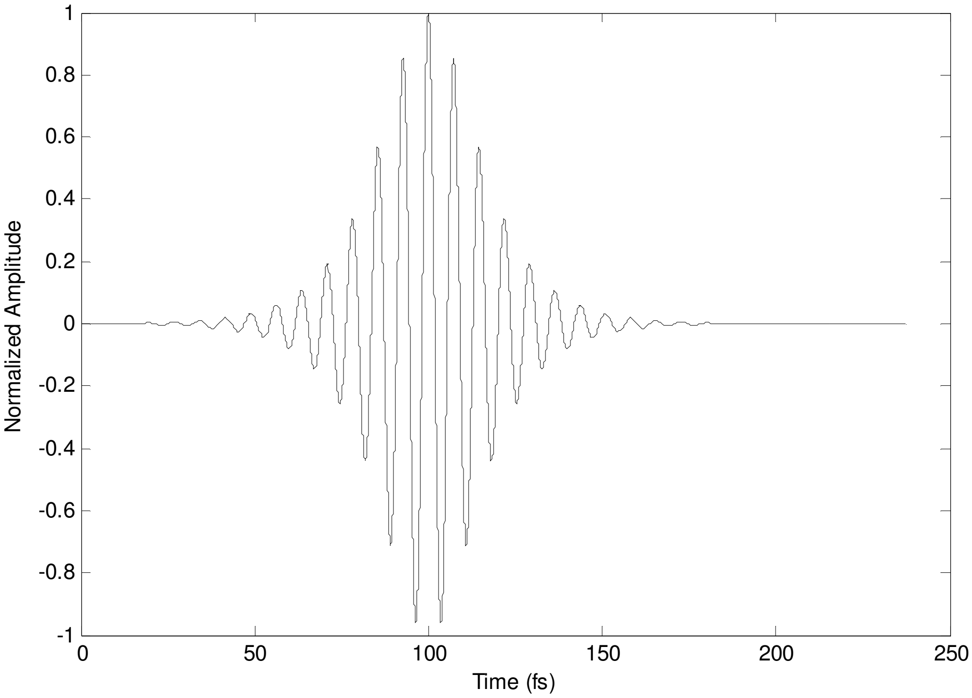

Figure 5- 2: Input pulse in the time domain.

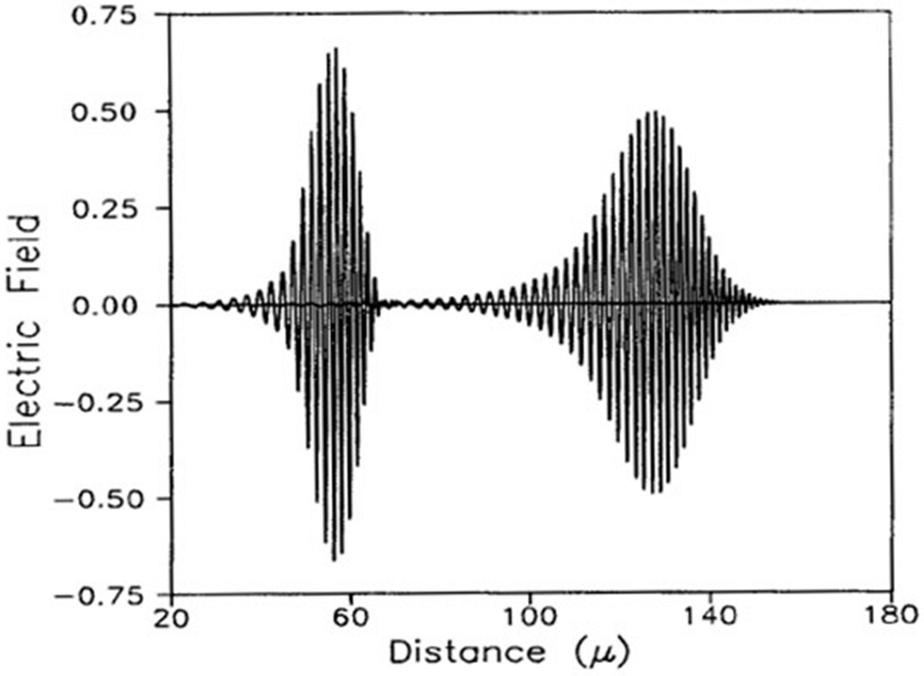

(a)

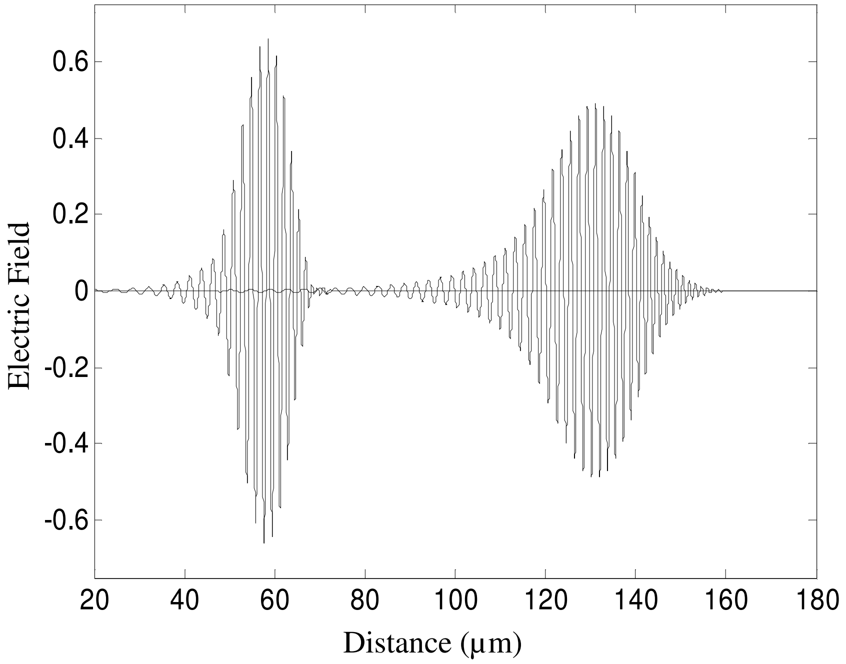

(b)

Figure 5-3: ADE-FDTD simulation result for linear Lorentz dispersive material at the time of 487fs and 973fs. (a) Published result[10] (b) Simulated result.

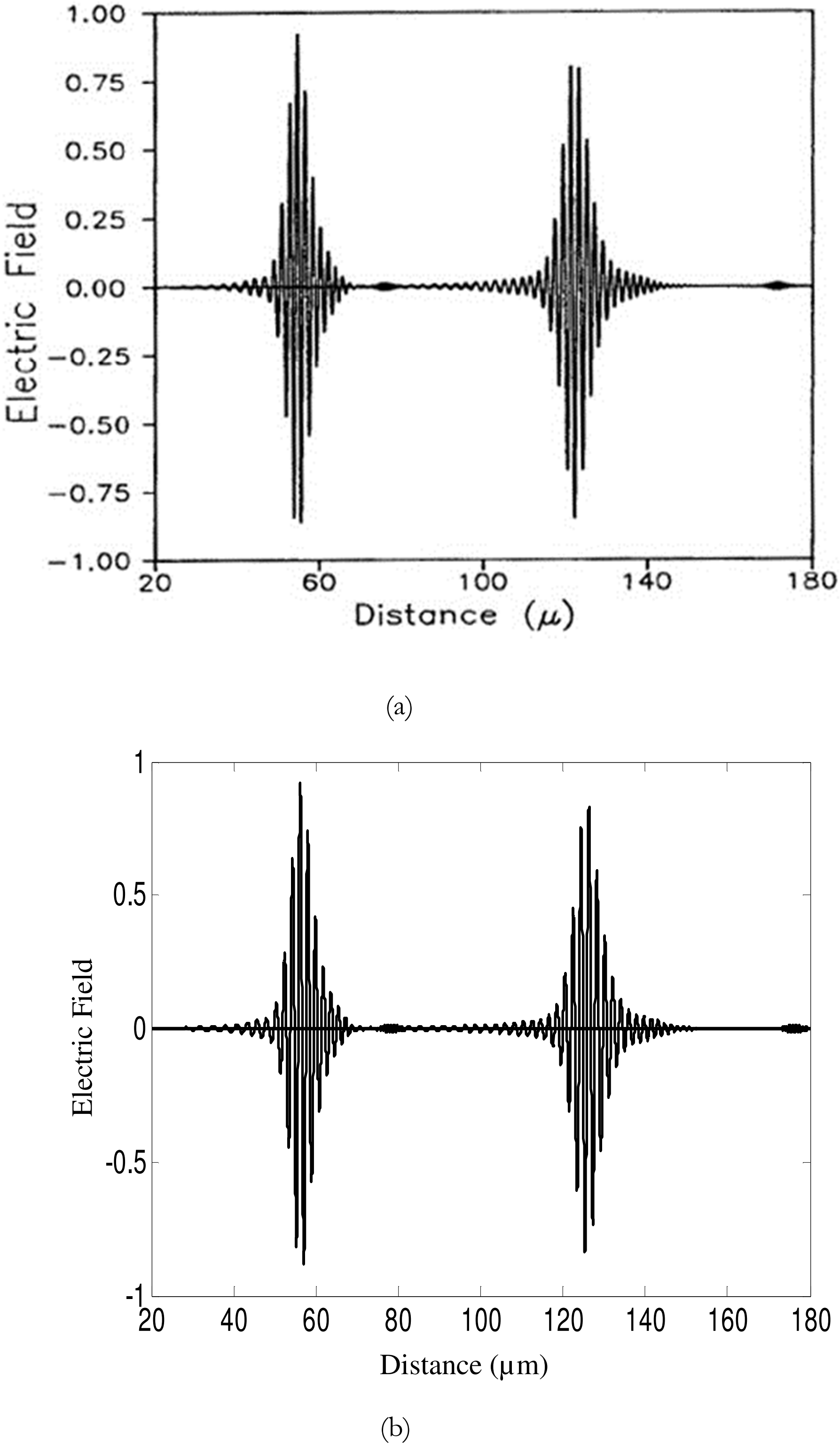

(a)

(b)

Figure 5-4: ADE-FDTD simulation result for non-linear dispersive material at the time of 487fs and 973fs. (a) Published result[10] (b) Simulated result.

5.2 Dispersion Relation of Chalcogenide Glass

The linear dispersion relation for chalcocogenide glass was modeled based the published experimental data by Zsolt L. Sámson et al[38]. The material is assumed to have the general Lorentz dispersion relation in the form of

$$\varepsilon_r(\omega) = \varepsilon_\infty + \frac{(\varepsilon_s - \varepsilon_\infty)\omega_o^2}{\omega_o^2 + 2j\omega\delta - \omega^2} \tag{5.1}$$

The parameters chosen for fitting are as follows

The static value of dielectric constant, $\varepsilon_s = (2.257)^2$

Optical value of dielectric constant, $\varepsilon_\infty = 2.7$

Material resonance frequency, ω_o=7×10^{15} rad/sec.

Damping factor, $\delta = 8 \times 10^{11}$rad/sec.

Figure 5-5 shows the dispersion relation for both fitting result and experimental result. Excellent agreement has been obtained for both real part and imaginary part of the frequency dependent dielectric constant. The range of wavelength has been taken from 400 nm to 1600 nm.

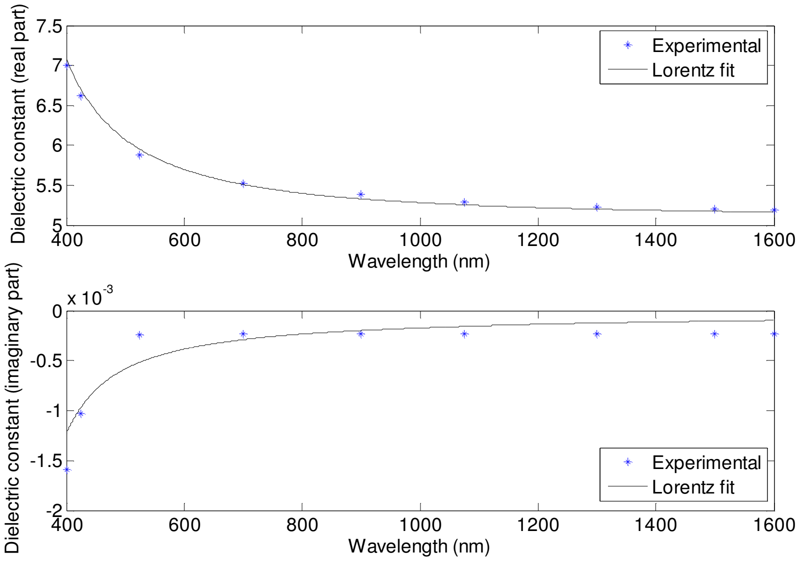

Figure 5-5: The dispersion relation of ChG glass.

5.3 Testing the Algorithm for Plasmonic Structure

The theory of SPPs is described in the literature. However, to test the algorithm in plasmonic structures, we will match our different simulated SPP parameters with the corresponding theoretical values. The basic structure that is used for the simulator verification is shown in figure 5-5. The following subsections demonstrate the verification of plasmonic algorithm for the simulator.

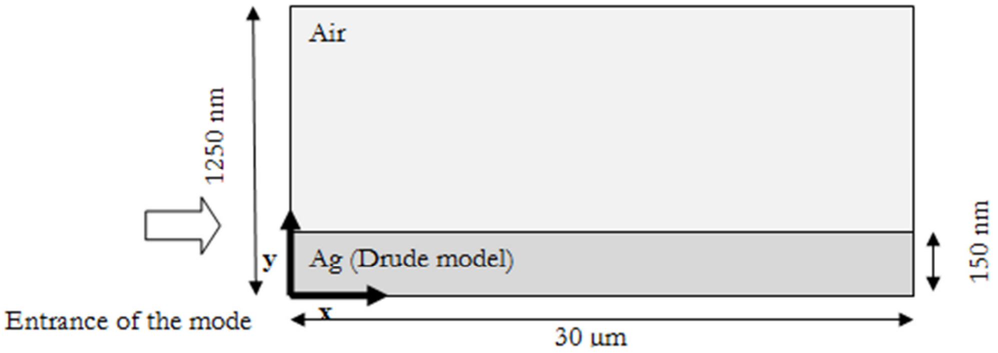

Figure 5-6: The dielectric metal structure considered for the simulator verification.

5.3.1 *The SPP wavelength*

The SPP wavelength, λ_{SPP} is given by [39]

$$\lambda_{SPP} = \lambda_o \sqrt{\frac{\varepsilon_d + \varepsilon_m'}{\varepsilon_d \varepsilon_m'}} \tag{5.2}$$

The normalized wavelength λ_{SPP}/λ_o is given by

$$\frac{\lambda_{SPP}}{\lambda_o} = \sqrt{\frac{\varepsilon_d + \varepsilon_m'}{\varepsilon_d \varepsilon_m'}} \tag{5.3}$$

where,

λ_o is the free space wavelength;

ε_d is the relative permittivity of the dielectric

ε'_m is the real part of the complex relative permittivity of the metal.

The normalized wavelength can be calculated by taking the distance between two consecutive peaks. The permittivity of both the dielectric and metal, are known. So, theoretical values of the normalized wavelength can be calculated using equation (5.3). This method is applied for our case and figure 5-6 shows an excellent agreement for theoretical and simulated results.

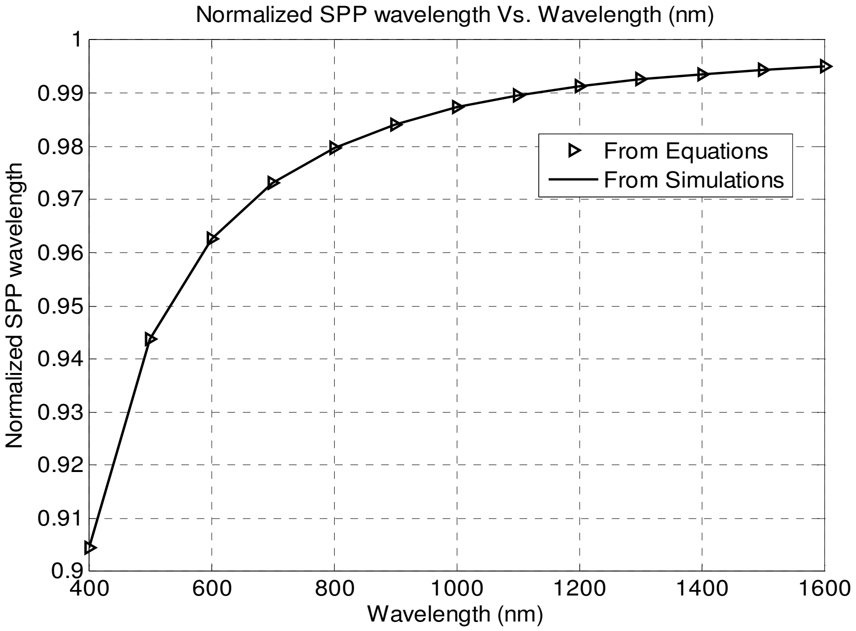

Figure 5-7: Normalized SPP wavelength at different free space wavelength.

5.3.2 The SPP field penetration depth

The penetration of the field into the materials bounding the interface can be expressed in terms of the relative permittivity of both metal and dielectric. The penetration depths into the dielectric, δ_d and metal, δ_m, are expressed as[39]

$$\delta_d = \frac{1}{k_o} \left| \frac{\varepsilon_d + \varepsilon_m'}{\varepsilon_d^2} \right|^{\frac{1}{2}} \tag{5.4}$$

$$\delta_m = \frac{1}{k_o} \left| \frac{\varepsilon_d + \varepsilon_m'}{\varepsilon_m^2} \right|^{\frac{1}{2}} \tag{5.5}$$

where,

k_o= wavevector for light in free space = $\frac{2\pi}{\lambda_o}$

This penetration depth of the SPP field can be verified using simulated result and using the equations above. The verification was done for the penetration depth in the dielectric and figure 5-7 shows a very good agreement for theoretical and simulated results.

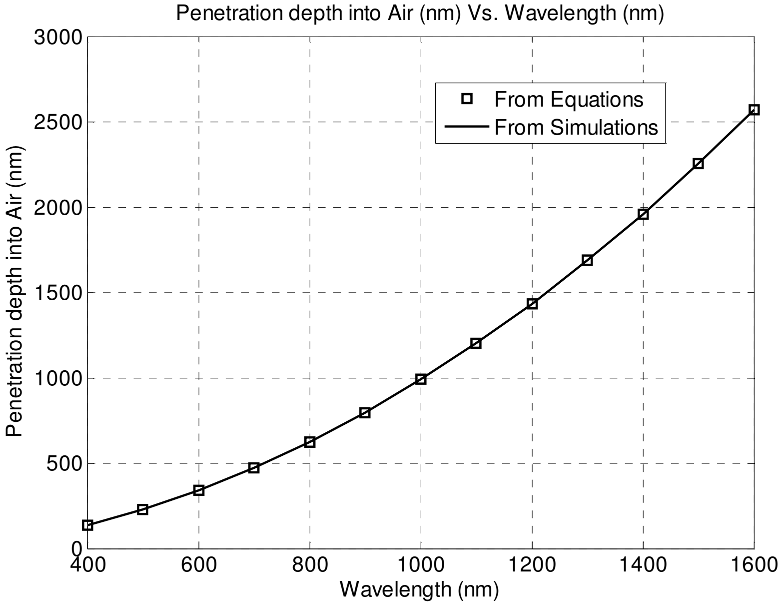

Figure 5-8: Penetration depth of SPP into air versus wavelength.

CHAPTER 6

SIMULATION RESULTS OF NON-LINEAR SPP PROPAGATION: SINGLE INTERFACE PLASMONIC STRUCTURE

The main observations of non-linear SPP propagations were done with a single interface plasmonic structure. In this chapter, simulation results of SPP propagation at the interface of metal and non-linear material is presented. We show that the instantaneous kerr non-linear behavior of the chalcogenide glass affects the plasmonic wave in a certain interesting way for high intensity of the input field. The non-linear propagation of SPP will be examined for different input intensities, different wavelengths and for different pulse durations.

6.1 SPPs Metal Surface Coated with Non-linear As_2S_3 Glass

The basic structure that is used for the simulation is shown in figure 6-1. The structure is excited by a TM polarized wave with temporal profile given by a hyperbolic secant pulse. The SPP propagation in the absence of non-linearity and in the presence of non-linearity is compared to observe the non-linear effect both in time-domain and frequency domain.

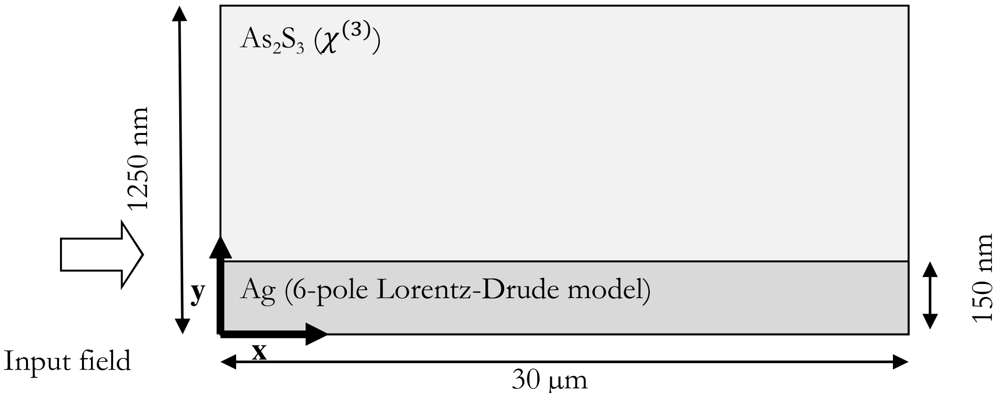

Figure 6-1: The non-linear dielectric metal structure considered for simulation.

6.2 Input Source

The normalized TM polarized wave that is pumped at x=0 distance is shown in figure 6-2.

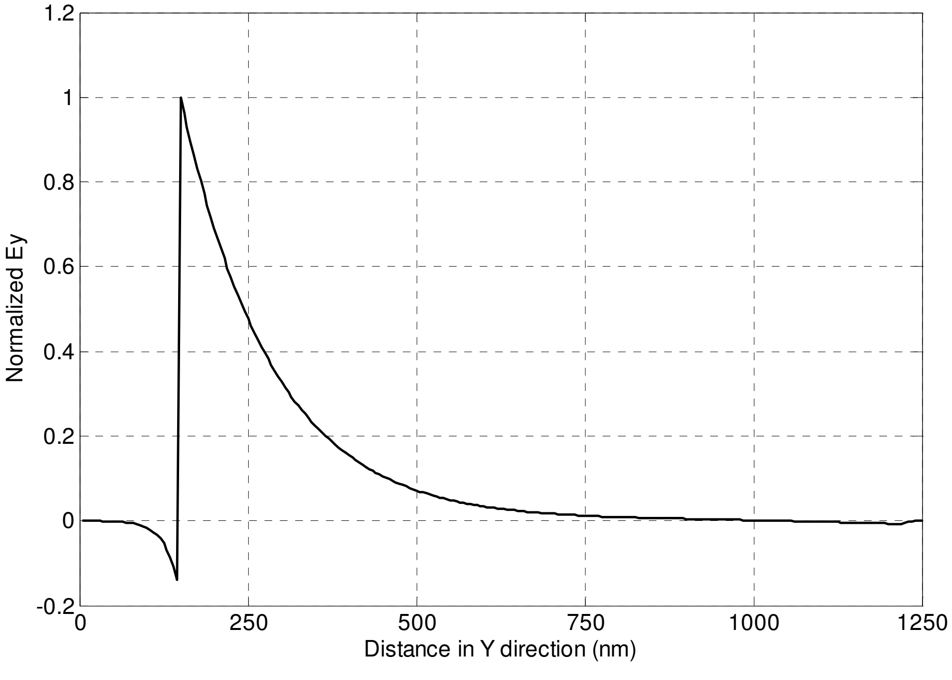

Figure 6-2: The normalized Ey field profile pumped in the device.

The Ey field is sent with a temporal profile of hyperbolic secant shape with a carrier wavelength of 1064 nm, which is the wavelength of YAG laser. The input source pulse was generated having unity amplitude; later the amplitude was increased in order to reach desired input intensity levels. Figure 6-3 and 6-4 show the source pulse in time domain and frequency domain respectively.

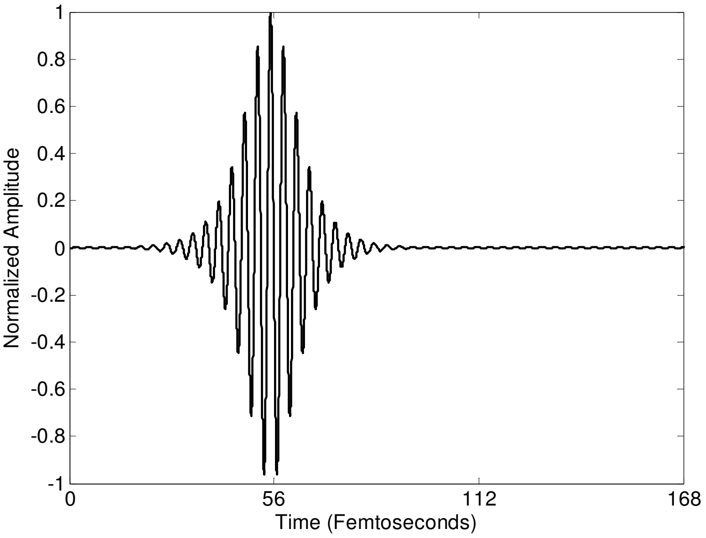

Figure 6-3: Input-Pulse in the time domain.

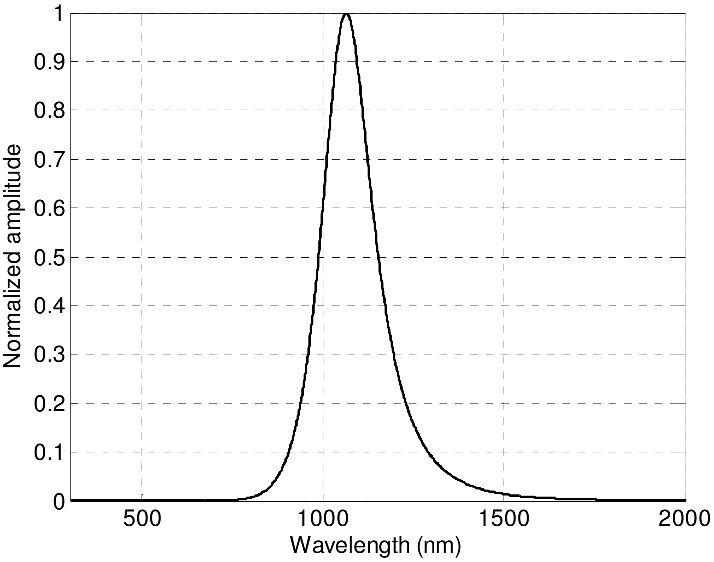

Figure 6-4: Input-Pulse in the frequency domain.

6.3 Inputs with Different Levels

Because non-linear effects are observed at high light intensities, it is desired to know the minimum input intensity that causes the nonlinear effect to manifest itself the non-linearity. This was done by pumping different intensities in the absence of non-linearity and in the presence of the non-linearity of the material. It is found that for Ey having peak amplitude more than 6×10^8 V/m, the non-linear effect starts to show up. Figures 6-7 to 6-11 describe the phenomena more elaborately.

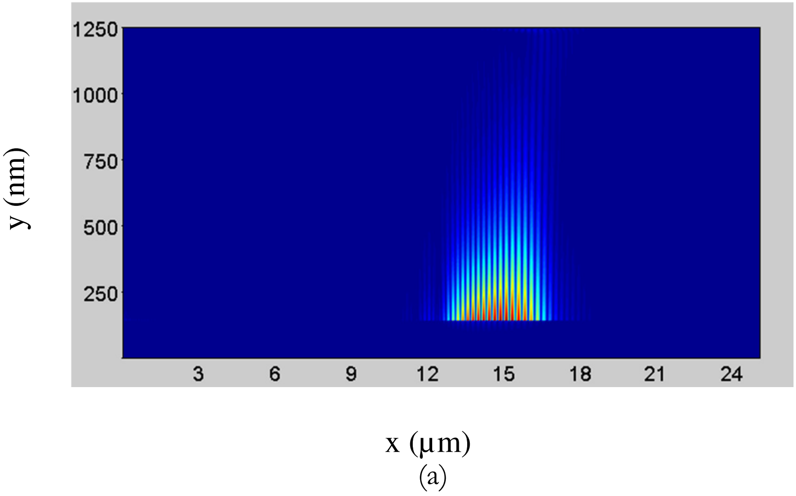

(a)

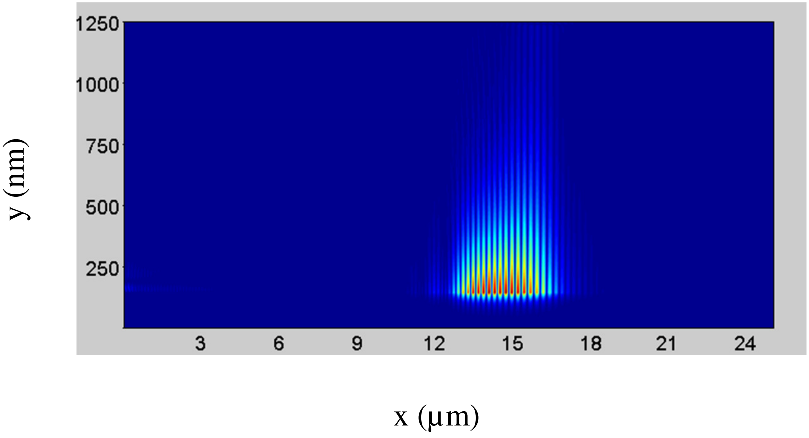

(b)

Figure 6-5: An SPP propagating on the interface between Ag and nonlinear As2S3 glass. (a) a snapshot of Ey (b) a snapshot of Ex

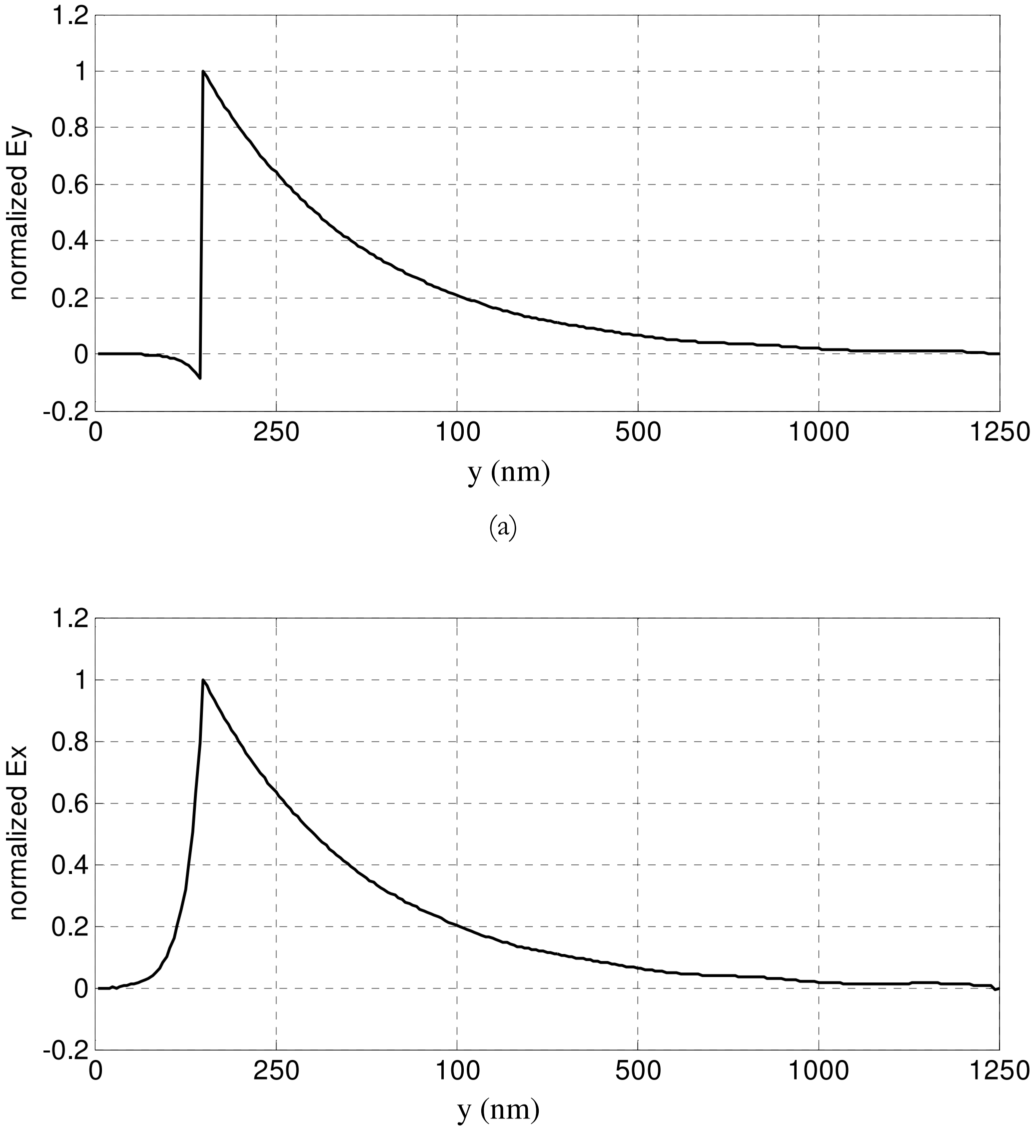

Figure 6-6: The field profile of propagating SPP (a) Ey profile (b) Ex profile.

Figure 6-5 shows a snap shot of SPP propagation through nonlinear As_2S_3 for Ex and Ey. The profiles in figure 6-6 are taken after SPP passes a distance of around 20 micrometer. To describe the non-linear effect more elaborately, we need to observe the temporal and spatial diagram of Ex or Ey at the interface for different inputs.

First of all the peak amplitude of Ey was set to 2×10^8 V/m at x=0 and t=0. The simulation results are shown in Figure 6-7 to 6-9.

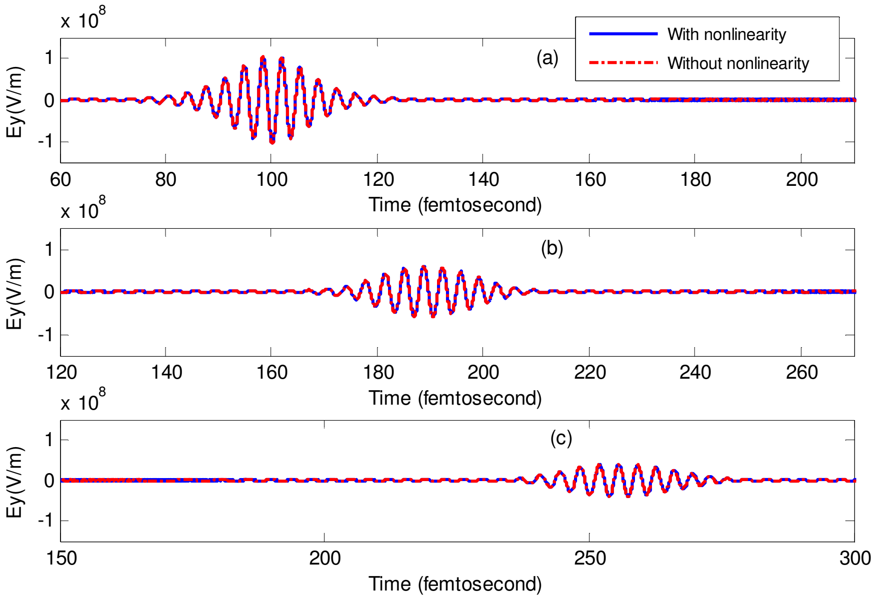

Figure 6-7: The simulated temporal evolution of the optical SPP pulse for peak Ey value of $\mathbf{2 \times 10^8}$ V/m at the distance of (a) 5μm, (b) 15μm and (c) 22.5μm.

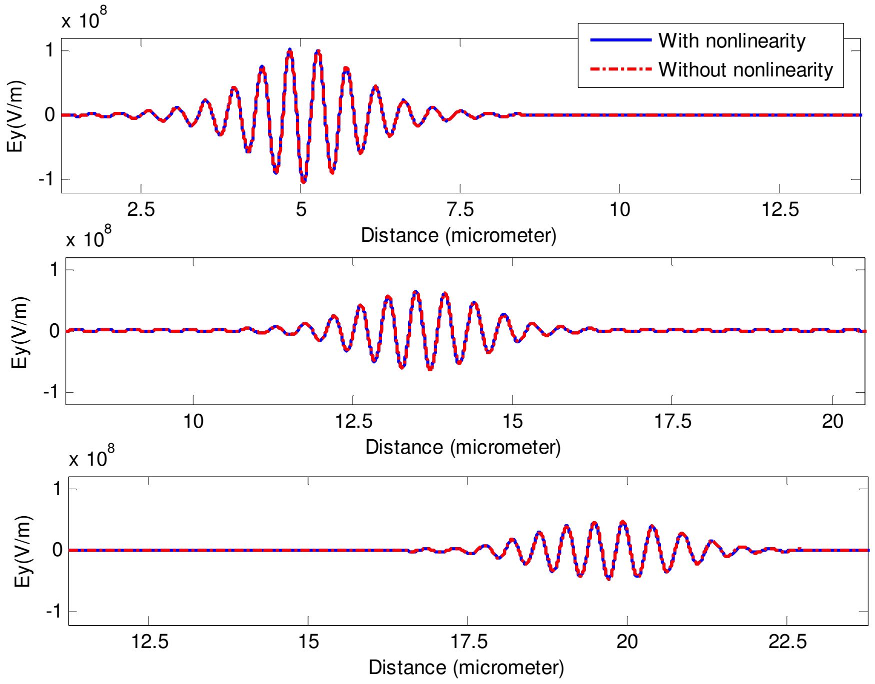

Figure 6-8: The simulated spatial evolution of optical SPP pulse for peak Ey value of $\mathbf{2 \times 10^8}$ V/m after (a) 100 fs, (b) 168 fs and (c) 232 fs.

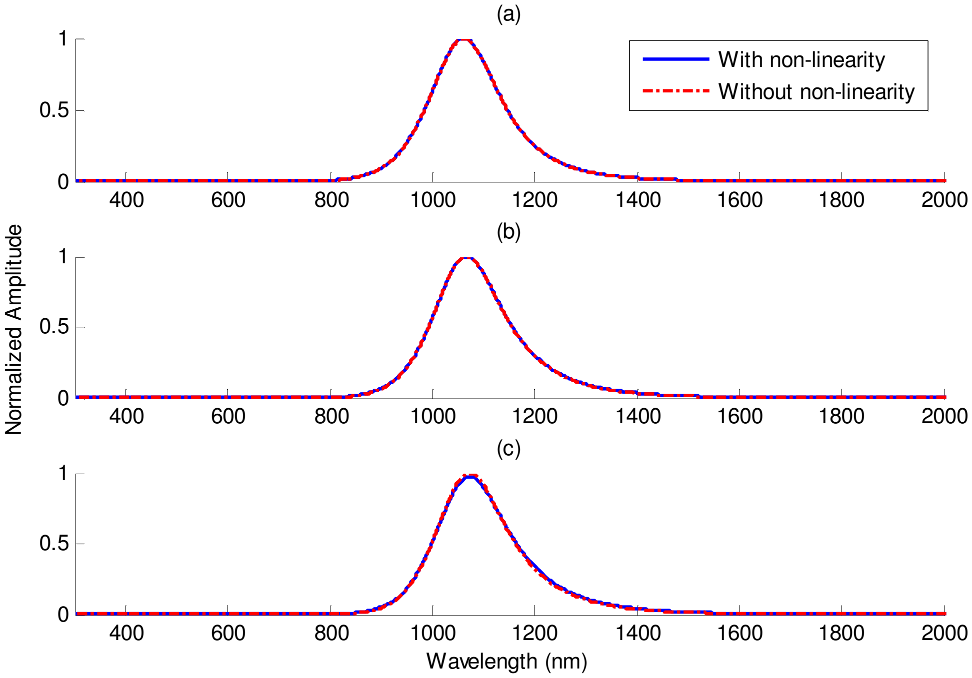

Figure 6- 9: The SPP pulse in the frequency domain without and with non-linear effect of As_2S_3 for peak Ey value of $\mathbf{2} \times \mathbf{10^8}$ V/m at the distance of (a) 5μm, (b) 15μm and (c) 22.5μm.

Figure 6-7 shows the temporal evolution of the SPP at different x distance. Figure 6-8 and 6-9 give the spatial field value and SPP pulse in frequency domain respectively. It is clear from figure 6-7 to 6-9 that the non-linearity has almost no effect on SPP along the metal-dielectric interface. In order to have the non-linear effect to appear we need to apply a higher intensity Ey field as input. But before that we will examine the amplitude of Ey for which the SPP starts to experience non-linearity. After doing a considerable number of simulations, it was found that for Ey having amplitude 6×10^8 V/m, the SPP just starts cause material non-linearity. In simulation results to be shown next, the pumped normalized mode was multiplied by 6×10^8. The resulting temporal, spatial and frequency domain output is calculated. The results are shown in Figure 6-10 to 6-12. For all cases, the solid lines represent the non-linearity of the material and the dashed line represents only linear dispersive material.

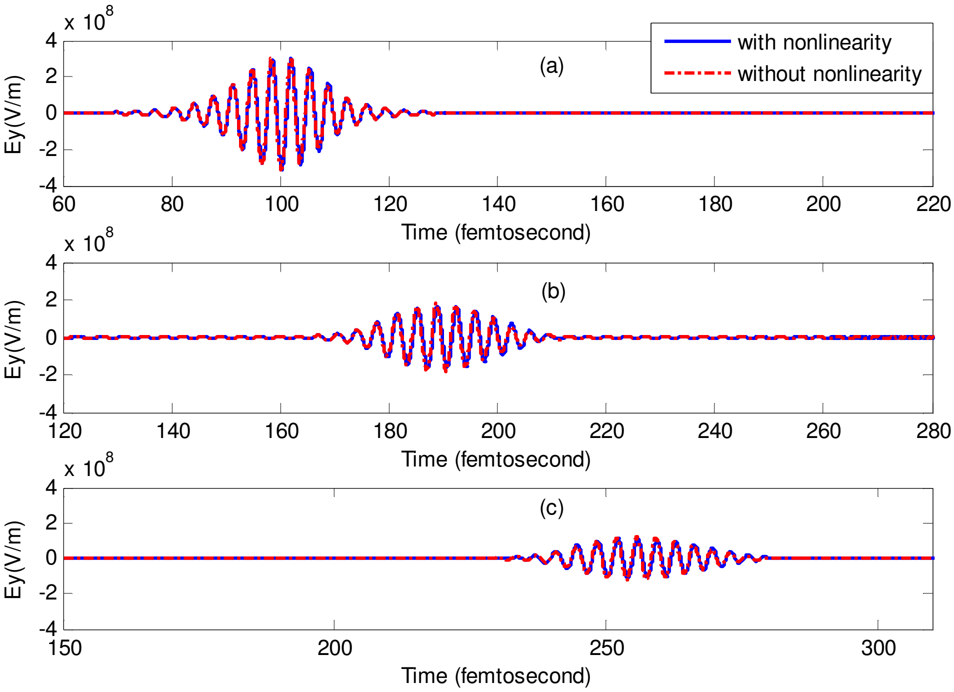

Figure 6-10: The simulated temporal evolution of the optical SPP pulse for peak Ey value of 6×10^8 V/m at the distance of (a) 5μm, (b) 15μm and (c) 22.5μm.

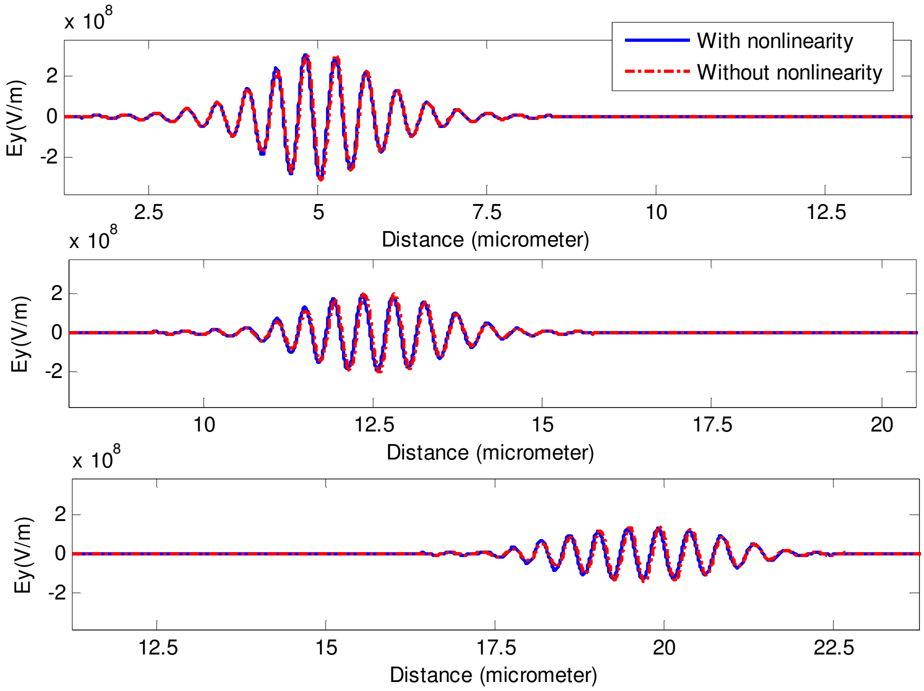

Figure 6-11: The simulated spatial evolution of optical SPP pulse for peak Ey value of 6×10^8 V/m after (a) 100 fs, (b) 168 fs and (c) 232 fs.

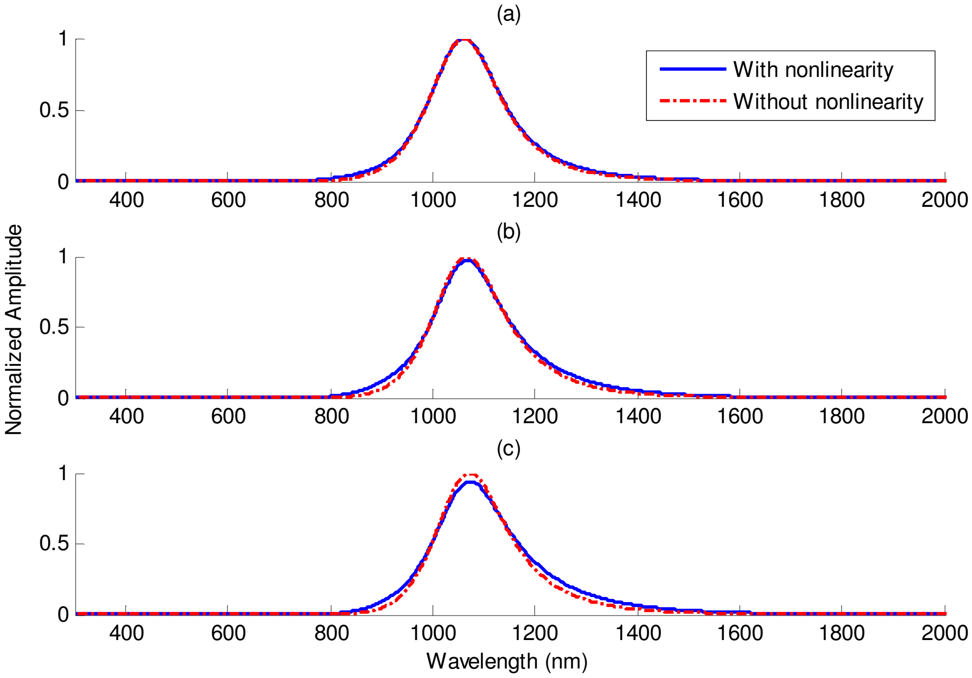

Figure 6-12: The SPP pulse in the frequency domain without and with non-linear effect of As_2S_3 for peak Ey value of $\mathbf{6 \times 10^8}$ V/m at the distance of (a) 5μm, (b) 15μm and (c) 22.5μm.

If we observe the frequency domain output (Figure 6-12), it is clear that the SPP is just becoming non-linear. The frequency spectrum expands in both sides. To observe the non-linear effect, in the next steps, we will increase the input Ey field drastically. The linear dispersive case does not have any significant effect on the frequency spectrum. However, in the nonlinear case, some interesting features have been observed which will be described later.

The next set of figures (Figure 6-13 to 6-15) show the calculated results for pumped Ey amplitude of $16 \times 10^8 \mathrm{V/m}$ at x=0 and t=0.

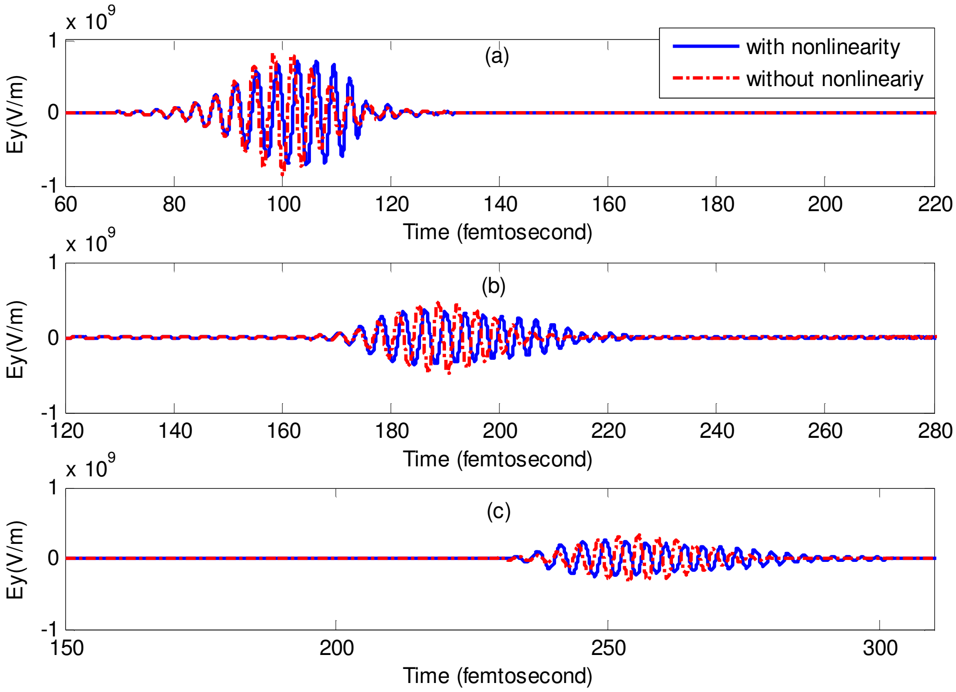

Figure 6-13: The simulated temporal evolution of the optical SPP pulse for peak Ey value of $\mathbf{16 \times 10^8}$ V/m at the distance of (a) 5μm, (b) 15μm and (c) 22.5μm.

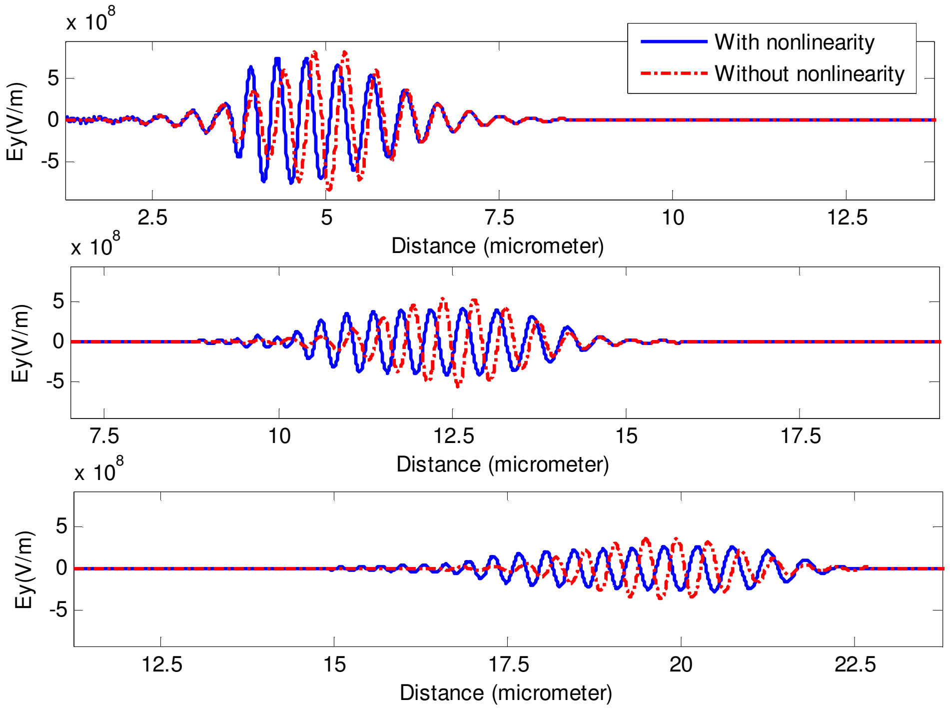

Figure 6-14: The simulated spatial evolution of optical SPP pulse for peak Ey value of $\mathbf{16 \times 10^8}$ V/m after (a) 100 fs, (b) 168 fs and (c) 232 fs.

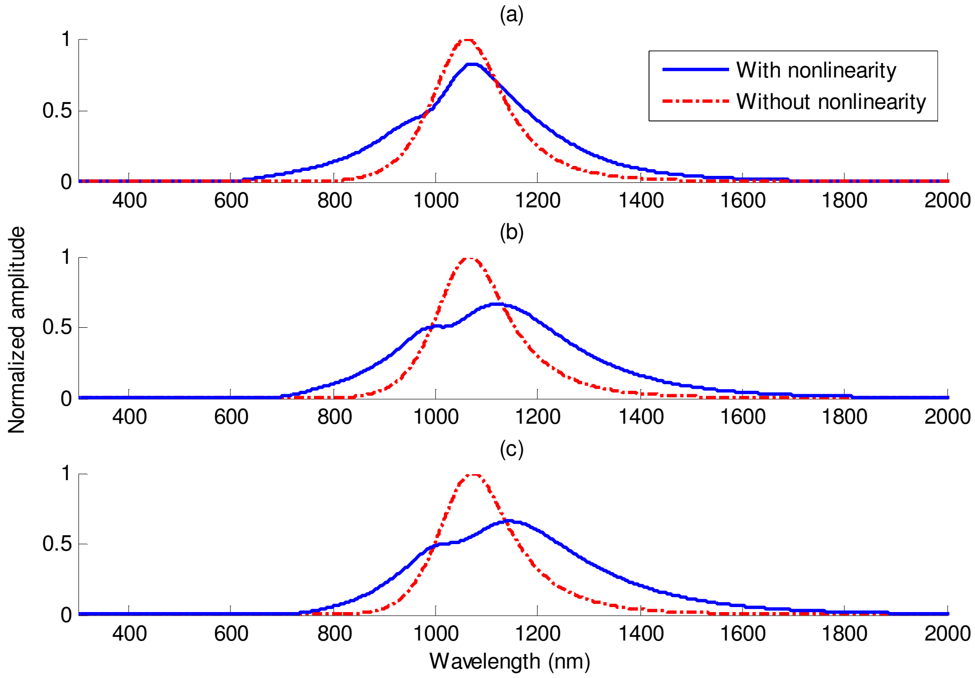

Figure 6-15: The SPP pulse in the frequency domain without and with non-linear effect of As_2S_3 for peak Ey value of $\mathbf{16\times 10^8}$ V/m at the distance of (a) 5μm, (b) 15μm and (c) 22.5μm.

For high intensity input, the non-linear effect starts acting on the SPP instantaneously as we considered only the Kerr instantaneous effect of non-linearity. If we analyze figures 6-13 to 6-15, we can observe that initially when the input has a very high intensity, the nonlinearity causes the signal to generate new frequencies which were not present in the input signal spectrum. As the signal propagates, those newly-generated frequencies start to become dominant. Due to losses, when the signal level goes below $6\times 10^8\mathrm{V/m}$, the material behaves as a linear dispersive media. Also, there is a creation of a third harmonic signal, which is considerably visible for larger inputs of Ey.

Next, The temporal, spatial and frequency domain response corresponding to an input field with Ey=$24\times 10^8\mathrm{V/m}$ at x=0 and t=0 are shown in figures 6-16 to 6-18.

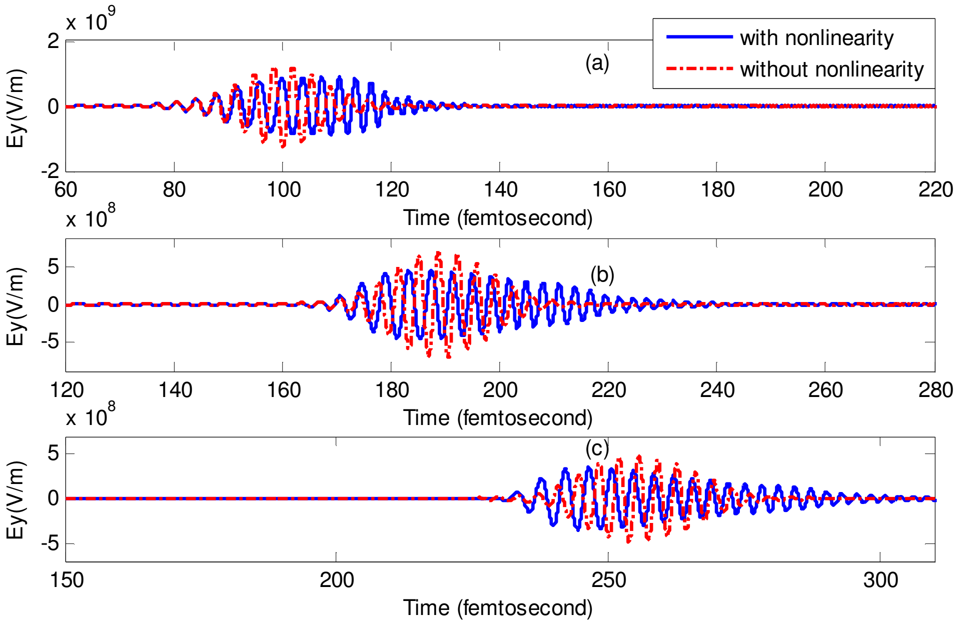

Figure 6-16: The simulated temporal evolution of the optical SPP pulse for peak Ey value of $\mathbf{24 \times 10^8}$ V/m at the distance of (a) 5µm, (b) 15µm and (c) 22.5µm.

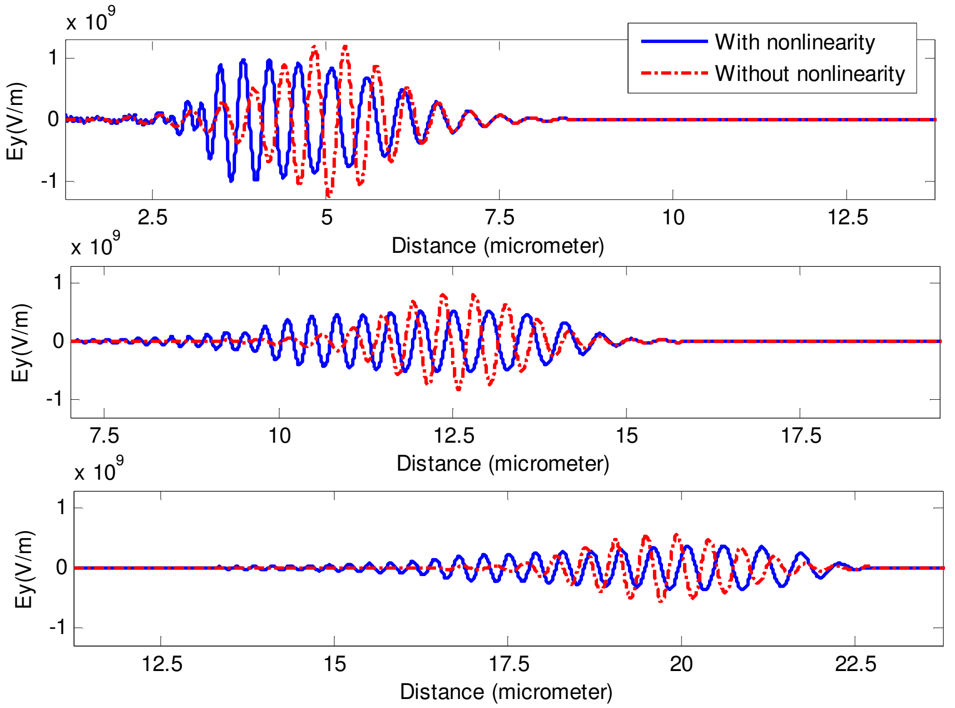

Figure 6-17: The simulated spatial evolution of optical SPP pulse for peak Ey value of $\mathbf{24 \times 10^8}$ V/m after (a) 100 fs, (b) 168 fs and (c) 232 fs.

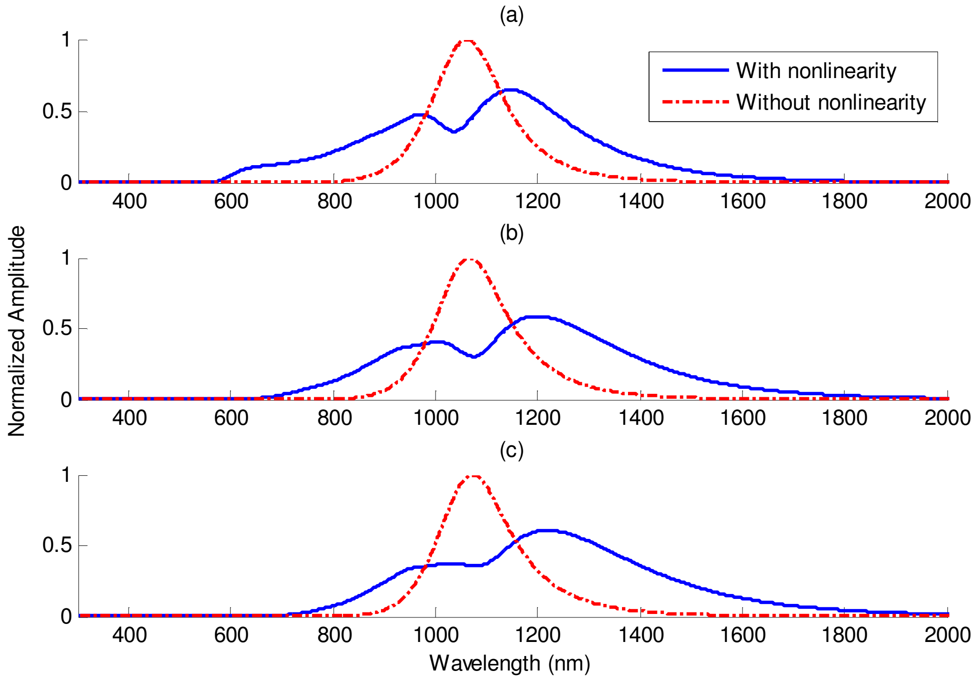

Figure 6-18: The SPP pulse in the frequency domain without and with non-linear effect of As_2S_3 for peak Ey value of $\mathbf{24 \times 10^8}$ V/m at the distance of (a) 5μm, (b) 15μm and (c) 22.5μm.

Again, the temporal, spatial and frequency domain output for Ey=32×10^8V/m pumped at x=0 and t=0 are shown in figures 6-19 to 6-21.

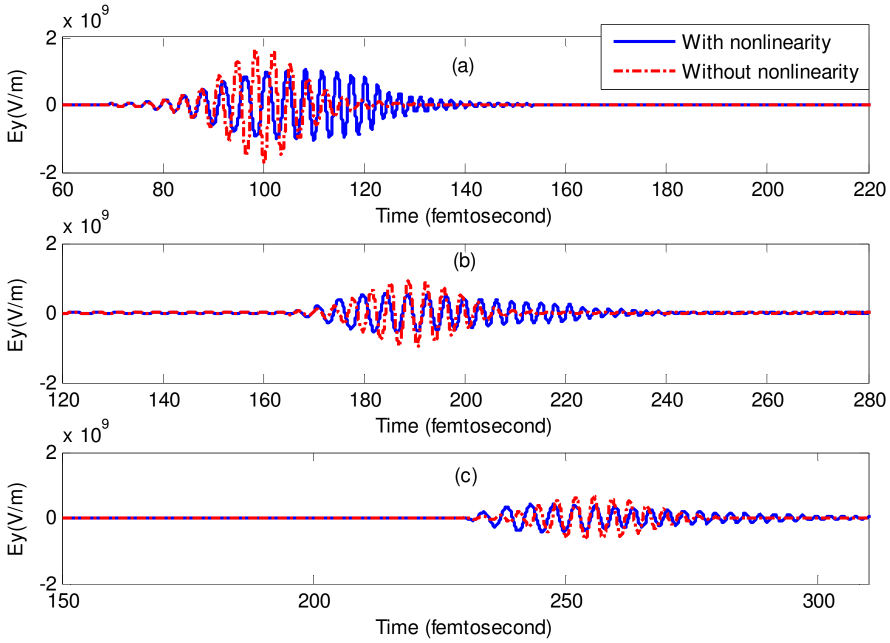

Figure 6-19: The simulated temporal evolution of the optical SPP pulse for peak Ey value of $\mathbf{32 \times 10^8}$ V/m at the distance of (a) 5μm, (b) 15μm and (c) 22.5μm.

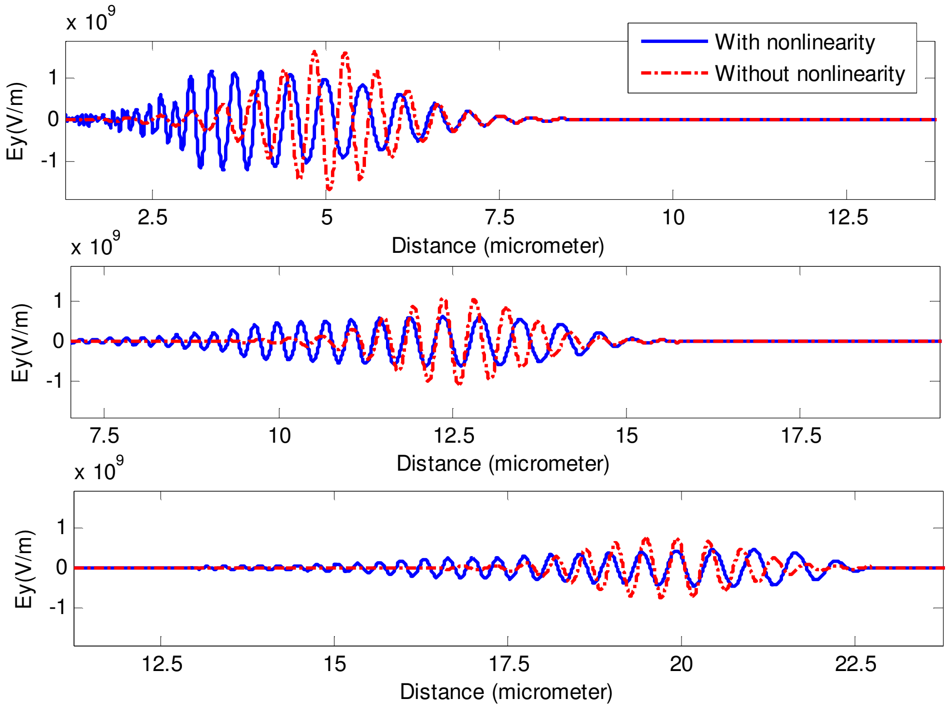

Figure 6-20: The simulated spatial evolution of optical SPP pulse for peak Ey value of $\mathbf{32 \times 10^8}$ V/m after (a) 100 fs, (b) 168 fs and (c) 232 fs.

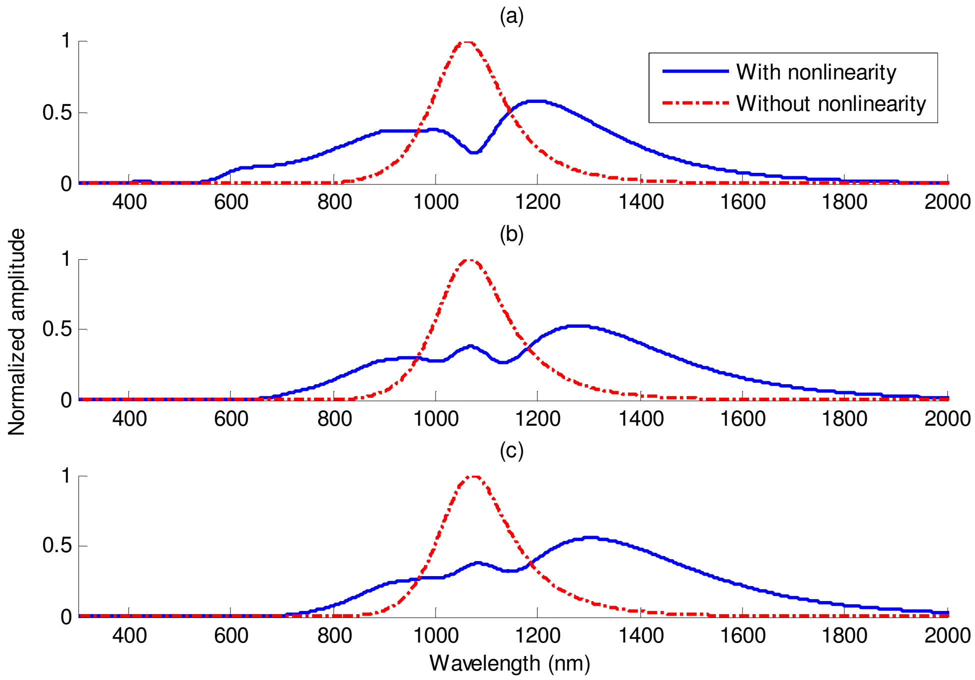

Figure 6-21: The SPP pulse in the frequency domain without and with non-linear effect for peak Ey value of $\mathbf{32 \times 10^8}$ V/m at the distance of (a) 5μm, (b) 15μm and (c) 22.5μm.

Finally, the temporal, spatial and frequency domain output for Ey=40×10^8V/m pumped at x=0 and t=0 are shown in figures 6-22 to 6-24.

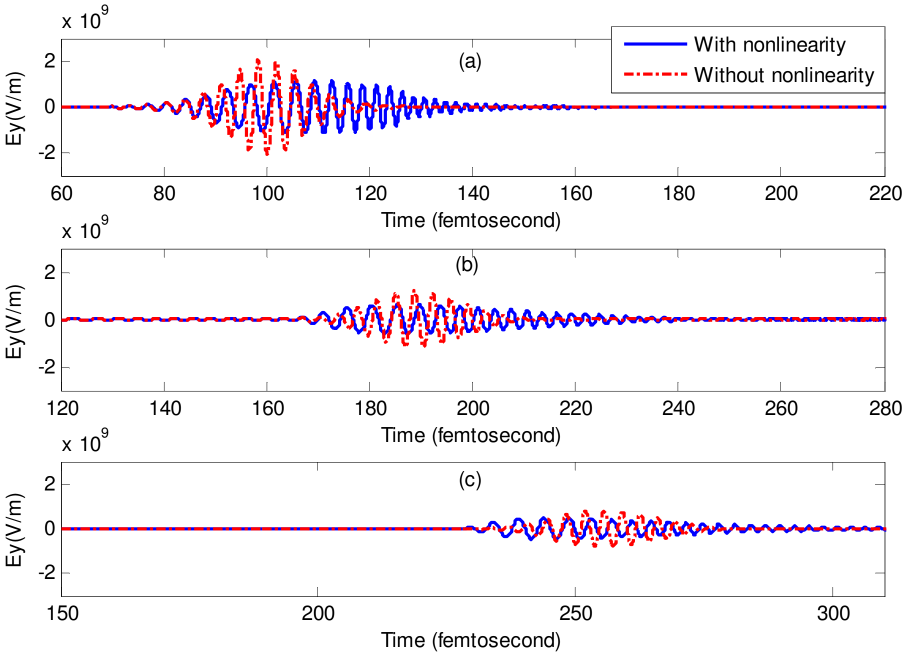

Figure 6-22: The simulated temporal evolution of the optical SPP pulse for peak Ey value of $\mathbf{40 \times 10^8}$ V/m at the distance of (a) 5µm, (b) 15µm and (c) 22.5µm.

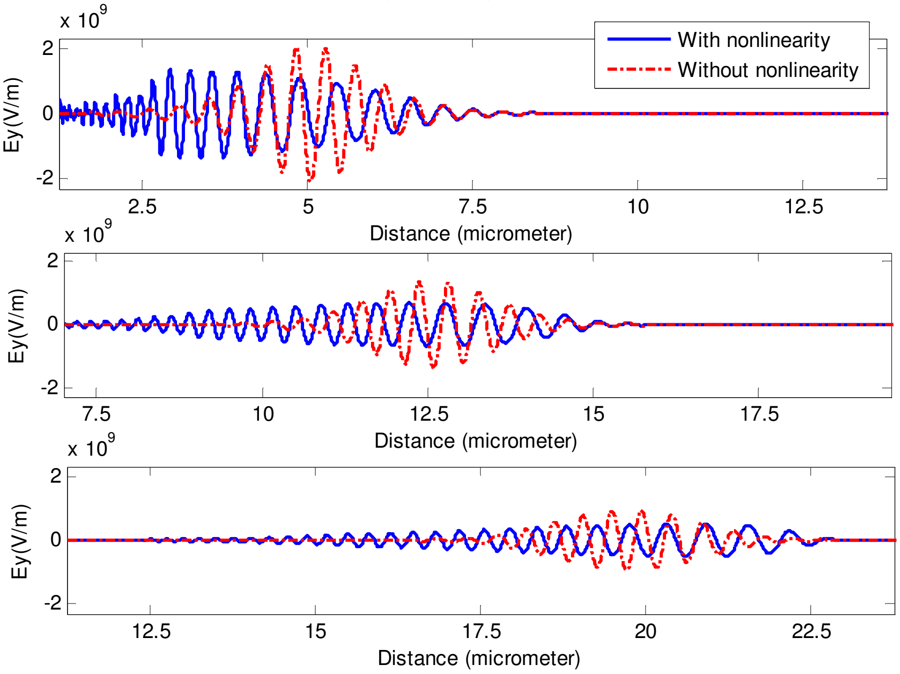

Figure 6-23: The simulated spatial evolution of optical SPP pulse for peak Ey value of $\mathbf{40 \times 10^8}$ V/m after (a) 100 fs, (b) 168 fs and (c) 232 fs.

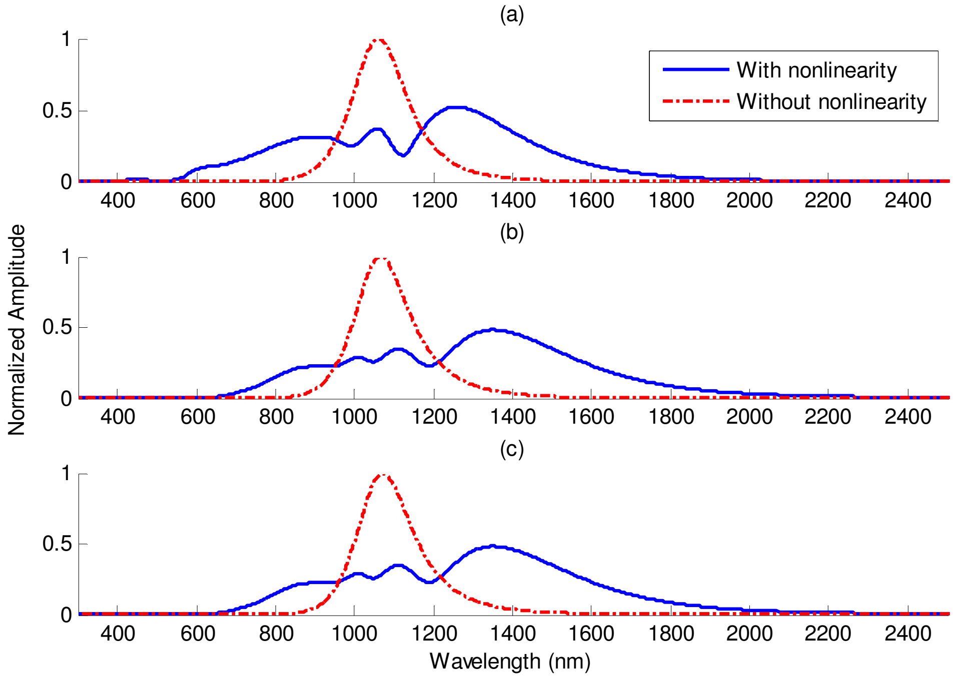

Figure 6-24: The SPP pulse in the frequency domain without and with non-linear effect for peak Ey value of $\mathbf{40 \times 10^8}$ V/m at the distance of (a) 5μm, (b) 15μm and (c) 22.5μm.

Figure 6-16 and figure 6-24 show very interesting behavior of SPP propagation through non-linear As_2S_3 chalcogenide glass. As we increase the amplitude of the input field, the Kerr instantaneous non-linear behavior becomes more apparent. However, by varying the peak amplitude of Ey pulse, we come to the conclusion that, for As_2S_3 glass, the non-linear behavior is significant at Ey having the pulse peak values of $6 \times 10^8 \mathrm{V/m}$ or more. So, approximately 6×10^8 V/m is the threshold level to have non-linear effect. For the temporal figure 6-16, 6-19 and 6-22 it is clearly visible that due to non-linear effect of chalcogenide glass, the SPPs starts deforming, and when the amplitude of Ey is reduced to around 6×10^8 V/m, the material starts acting as a linear dispersive media. That is why we do not see a significant deformation at distances between 15 μm and 22.5 μm in figure 6-16. The frequency domain results shown in figure 6-18 give more information. At the initial distance of 5 μm, due to non-linearity, there is a creation of new frequencies which remain in the propagation pulse. After propagating a distance of 15 μm, the fundamental wavelength becomes 1145 nm. At the same time we can see that there is a creation of new frequency peak whose wavelength is around 969 nm. When the peak amplitude of Ey goes below $6 \times 10^8 \mathrm{V/m}$ the material behaves as a linear dispersive media. The same behavior is seen in figure 6-21 and 6-24. One very important feature that is occurring here is the generation of third harmonic signals. If we closely observe figure 6-18(a), 6-21(a) and 6-24(a) then we can see those small third harmonic being generated due to nonlinearity. However, as the amplitudes of these third harmonics are very low, due to losses, the third harmonic signals die out as the signal propagates along the x direction.

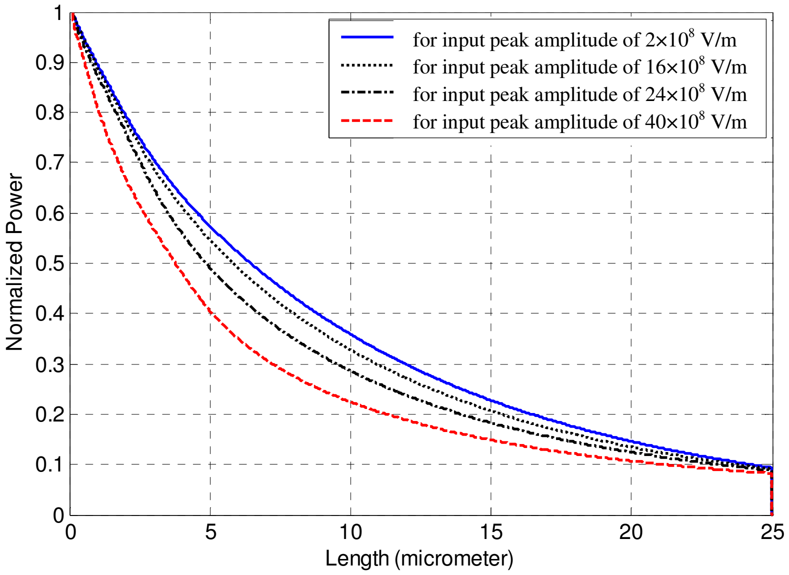

Figure 6-25: The Normalized power curve for nonlinear case having different level of input.

The propagated power curves along the structure gives further insight into nonlinear SPP behavior. Figure 6-25 shows the normalized power passing through each plane along the propagation direction. From the figure we can observe that, due to the non-linearity the signal produces some other frequencies which attenuate in this nonlinear media. We can see that for 2.5μm to around 15μm, the power measuring in the device is reduced for higher values of Ey. We also see that, for higher values of Ey, the non-linear effect of the medium is significant which causes the generation of new frequencies. The power curve shows that the newly generated frequencies are experience higher loss than the input frequencies.

6.4 The Raman Effect

Up to the previous section we considered only Kerr instantaneous nonlinear effect. Now the same behavior will be observed for Ey having maximum amplitude 24×10^8 V/m with the presence of Raman effect. We chose 24×10^8 V/m as our input value because from the previous results it has been found that for this Ey input both the nonlinear and linear dispersive properties can be observed for the SPP. In this case we will discuss only temporal and frequency domain results.

Figures 6-26 to 6-28 show the 30% Raman effect of nonlinearity on the SPP signal. As the Kerr effect is instantaneous, considering Kerr effect only, initially the signal experiences more nonlinear effect than the Kerr-Raman case. But after some time, Raman non-linearity also comes into action, which causes the signals to have almost similar frequency spectrum after some distances. The power curves in figure 6-28 are seen to give a better idea regarding this behavior. From the power curve we can see that the nonlinear effects for the case of Kerr effect causes creation of new frequencies signal which attenuates faster and causes loss of power.

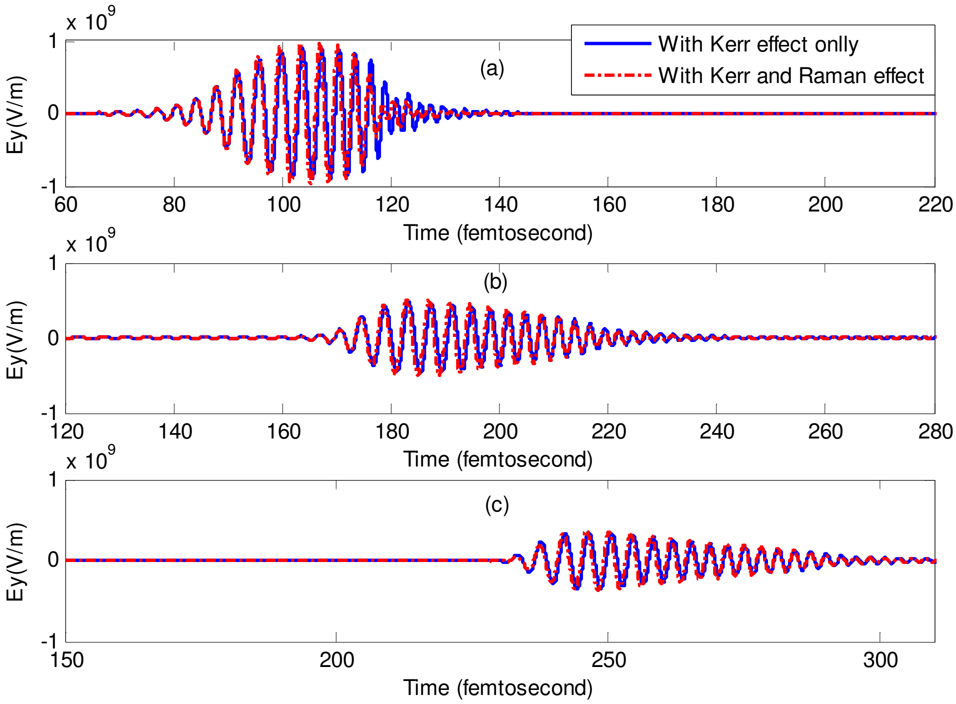

Figure 6-26: The The simulated temporal evolution of the optical SPP pulse for peak Ey value of $\mathbf{24 \times 10^8}$ V/m with 30% Raman effect at the distance of (a) 5μm, (b) 15μm and (c) 22.5μm.

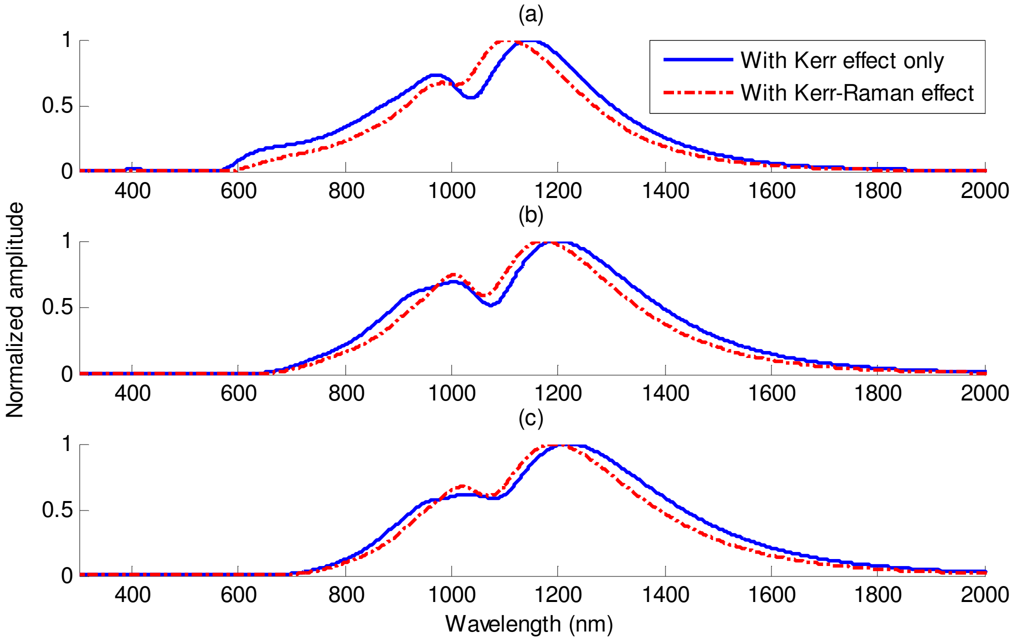

Figure 6-27: The SPP pulse in the frequency domain without and with non-linear effect for peak Ey value of $\mathbf{24 \times 10^8}$ V/m with 30% Raman effect at the distance of (a) 5μm, (b) 15μm and (c) 22.5μm.

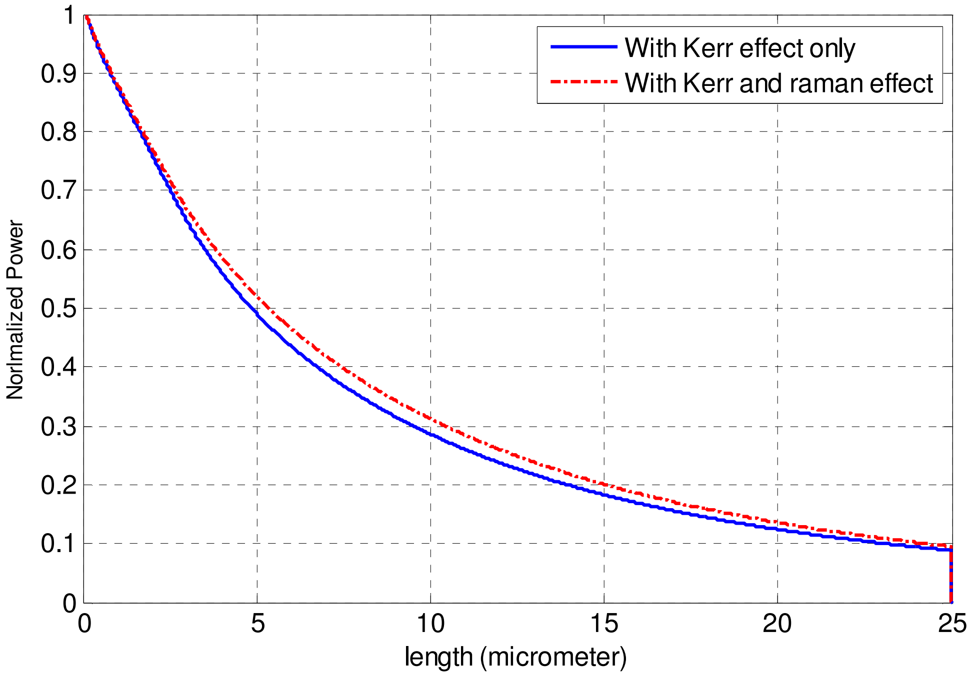

Figure 6-28: The Normalized power curve with and without considering Raman effect.

6.5 Inputs with Different Pulse Widths

Next, the effect of the pulse width on SPP propagation is considered. The analysis presented previously is repeated for a pulse having width of 34 fs. In this case, the wider pulse having width of 68 fs, is exposed to stronger nonlinearity effect as shown in figure 6-29. However the rate of power decay is almost the same for both pulse widths (see figure 6-30).

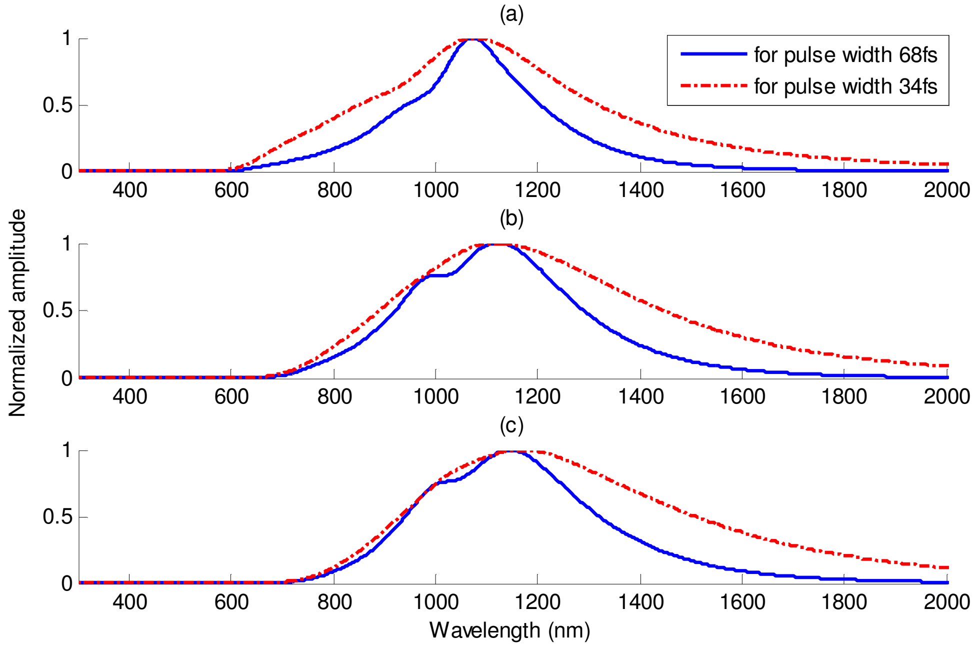

Figure 6-29: The SPP pulse in the frequency domain with non-linear effect for peak Ey value of $\mathbf{16 \times 10^8}$ V/m and for different pulse width at the distance of (a) 5µm, (b) 15µm and (c) 22.5µm.

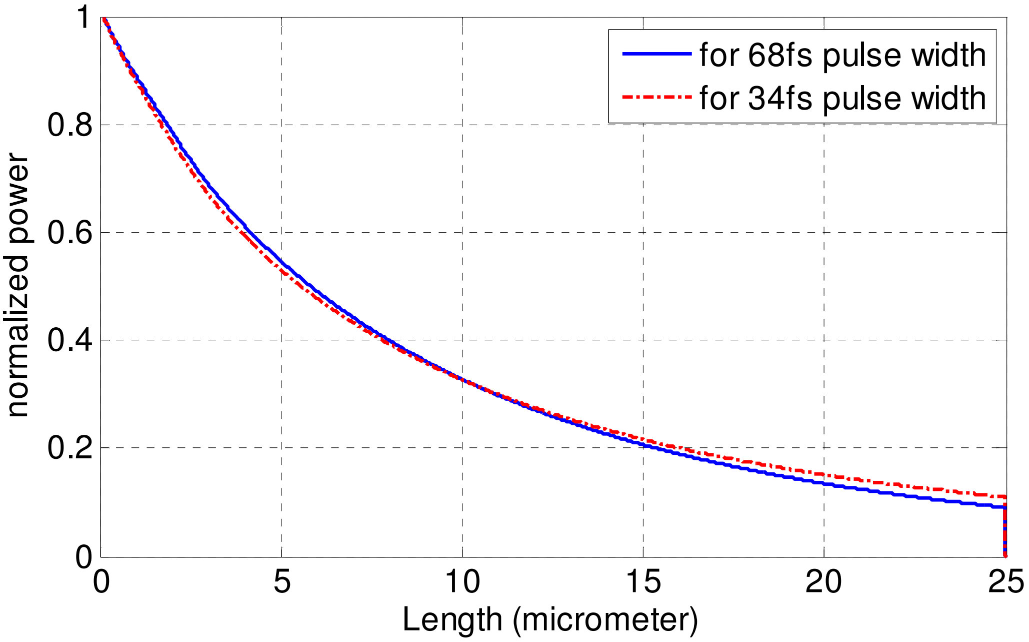

Figure 6-30: The Normalized power curve for input having different pulse width.

6.6 Inputs with Different Wavelengths

Next, the effect of carrier wavelength on SPP propagation is considered next. For this purpose we chose two additional carriers having wavelengths of 830 nm and 2190 nm. Figures 6-31 and 6-32 show the calculated frequency spectrum and power curves for each wavelength at different distances respectively. The peak value of Ey is set at 16×10^8 V/m for input. The thin solid lines represent the linear dispersive case spectrum for each corresponding dashed line which represents the non-linear dispersive case. First of all, the very interesting feature that we observe is that for wavelength of 2190 nm the non-linear effect is not that significant compared to the two shorter wavelengths. Shorter wavelengths induce stronger nonlinearity effects in glass.

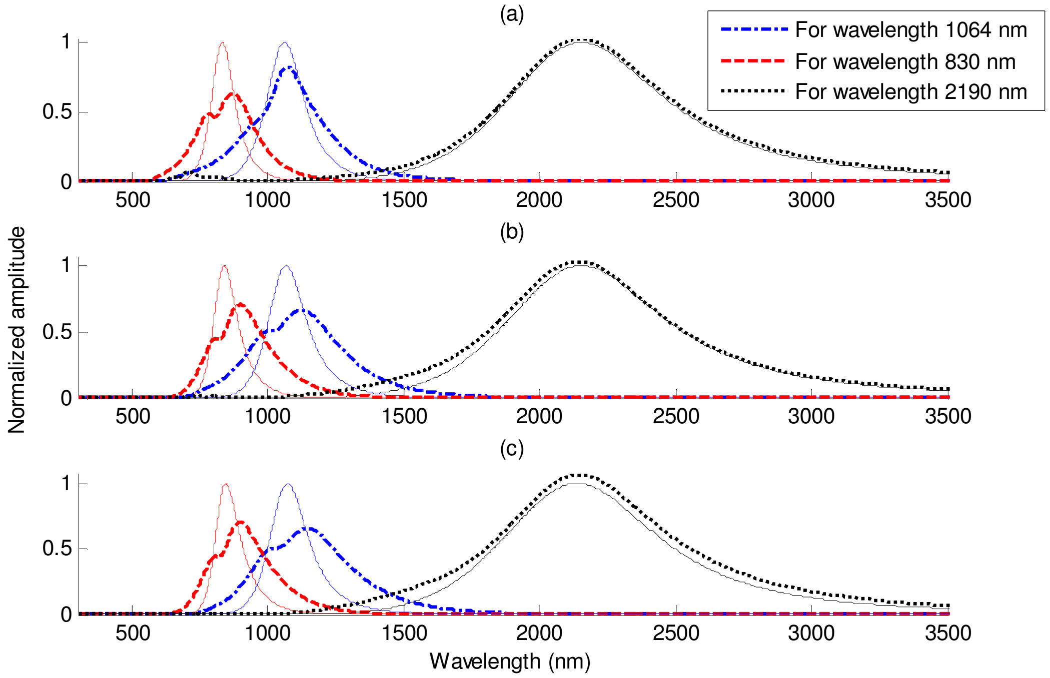

Figure 6-31: The SPP pulse in the frequency domain without and with non-linear effect for peak Ey value of 16×10^8 V/m and for different wavelength at the distance of (a) 5μm, (b) 15μm and (c) 22.5μm.

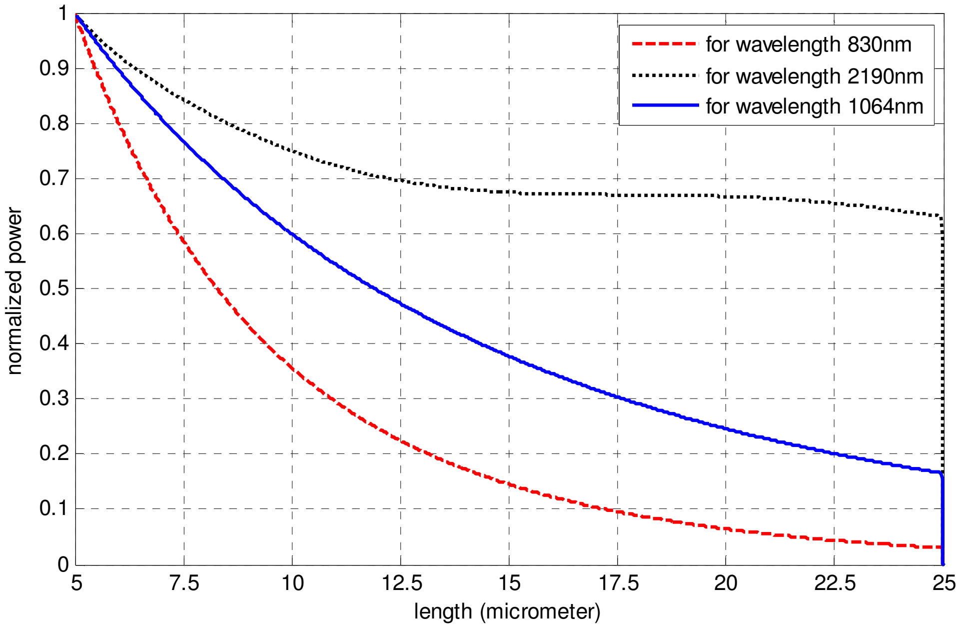

Figure 6-32: The Normalized power curve for linear and nonlinear case with different carrier wavelength.

The feature of having lower loss at 2190 nm can be due to the dispersion relation of chalcogenide glass in chapter 5. The strong frequency dependent loss of silver also causes the high loss at higher frequency.

CHAPTER 7

NON-LINEAR SPP PROPAGATION: MULTIPLE INTERFACE PLASMONIC STRUCTURES

In this chapter the nonlinear SPP propagation along multiple longitudinal interfaces will be analyzed. The multiple interfaces considered here are: 1. Metal-glass-metal structure and 2. Glass-thin-film-glass structure. The following subsections give the descriptions of the results for these multiple interface plasmonic structures.

7.1 Metal-Glass-Metal Structure

Figure 7-1 shows the basic structure for the Metal-glass-metal case. Here, the width of the glass is taken to be 100nm and the length is 25μm. The input field is pumped at x=0 and t=0 with carrier wavelength of 1064 nm. The normalized Ey input field is shown in figure 7-2.

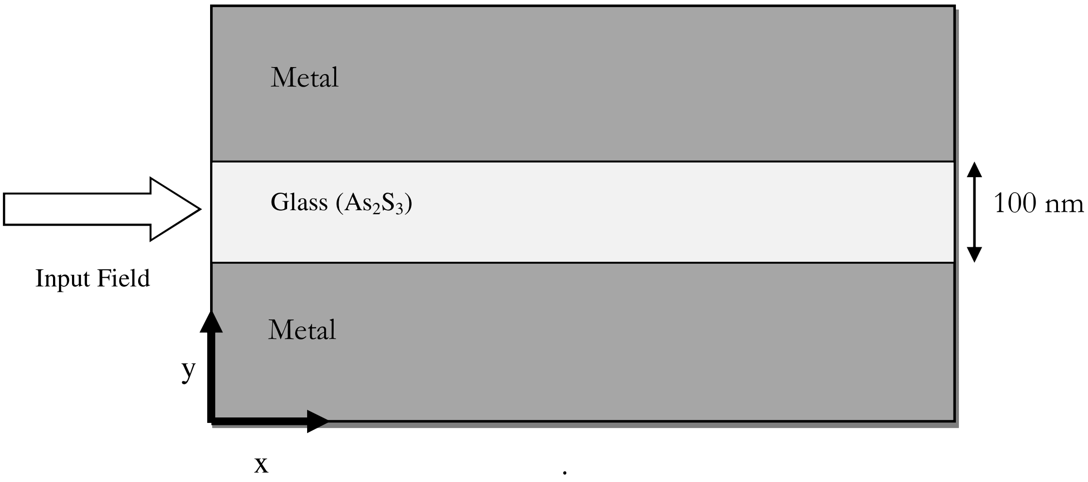

Figure 7-1: Basic diagram of the metal-glass-metal structure.

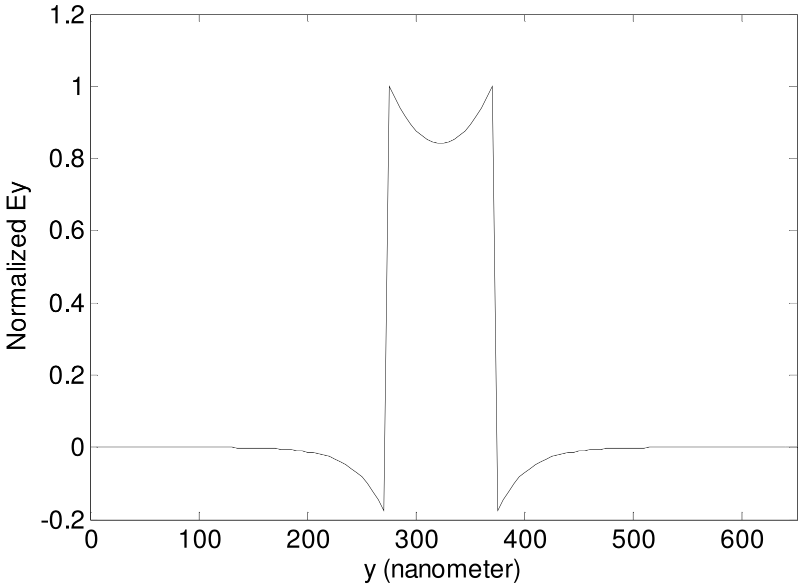

Figure 7-2: The normalized Ey field profile pumped in the device.

First of all, the input Ey field was taken having peak amplitude of 2×10^8 V/m. It is evident from the results in chapter 6 that, this input intensity is not sufficient to stimulate the nonlinearity in the glass. The snapshots in figure 7-3 show the propagation of SPPs along metal-glass-metal structure.

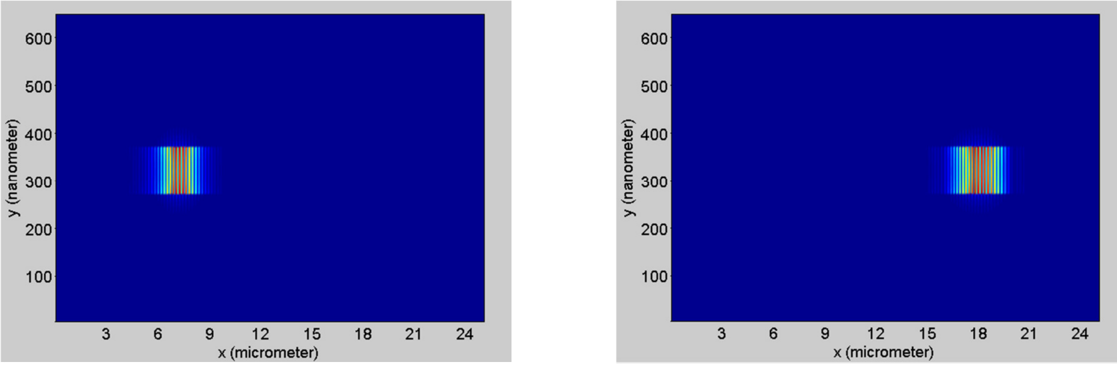

Figure 7-3: The snapshot of propagation of mode with peak input Ey=2×10^8 V/m for non-linear case after crossing different distance.

To observe the nonlinear effect of the glass, the input peak Ey field is increased to 16×10^8 V/m, which is sufficient enough to stimulate the nonlinearity of the glass. Due to nonlinear effect, a very interesting feature appeared. There is a creation of two different modes. The mode which was pumped into the device is comparatively faster than the newly generated mode. The snapshots in figure 7-4 show the SPPs propagation at different distances. The two different modes with different velocities are clearly visible from the snapshots. The Ey field profile is shown in figure 7-5. Figure 7-5 (a) and (b) show the field profiles of the slower mode and faster mode, respectively. The mode which is faster, keeps the original shape of the pumped mode.

The power curves of figure 7-6 show that, for the non-linear dispersive case, the signal experiences more losses due to reflection.

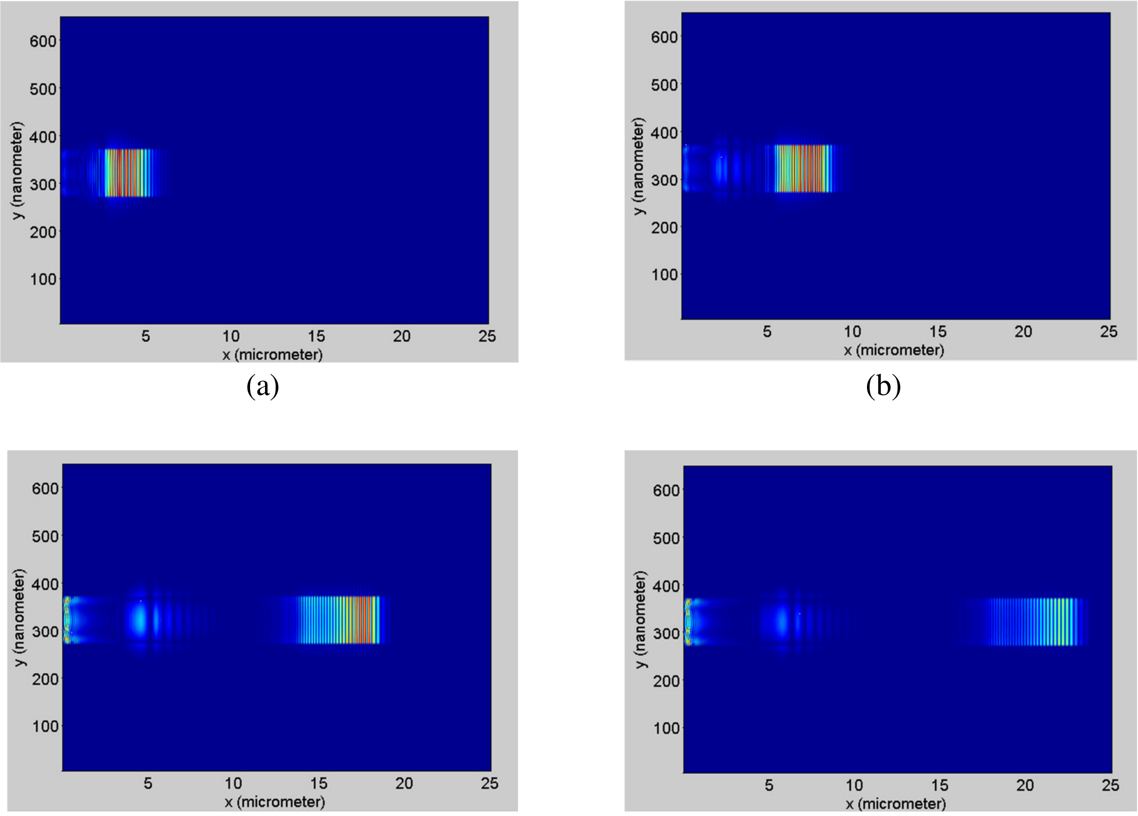

(a) (b)

(c) (d)

Figure 7-4: The snap shot of propagation of mode with peak input Ey=$\mathbf{16 \times 10^8}$ V/m for non-linear case after crossing different distances.

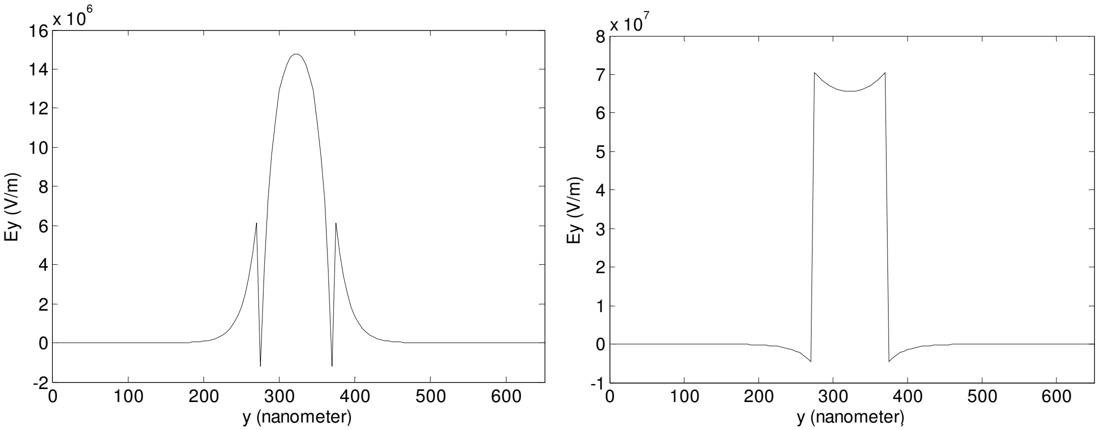

(a) (b)

Figure 7-5: The Ey field profile for metal-glass-metal structure (a) slower mode, (b) pumped faster mode.

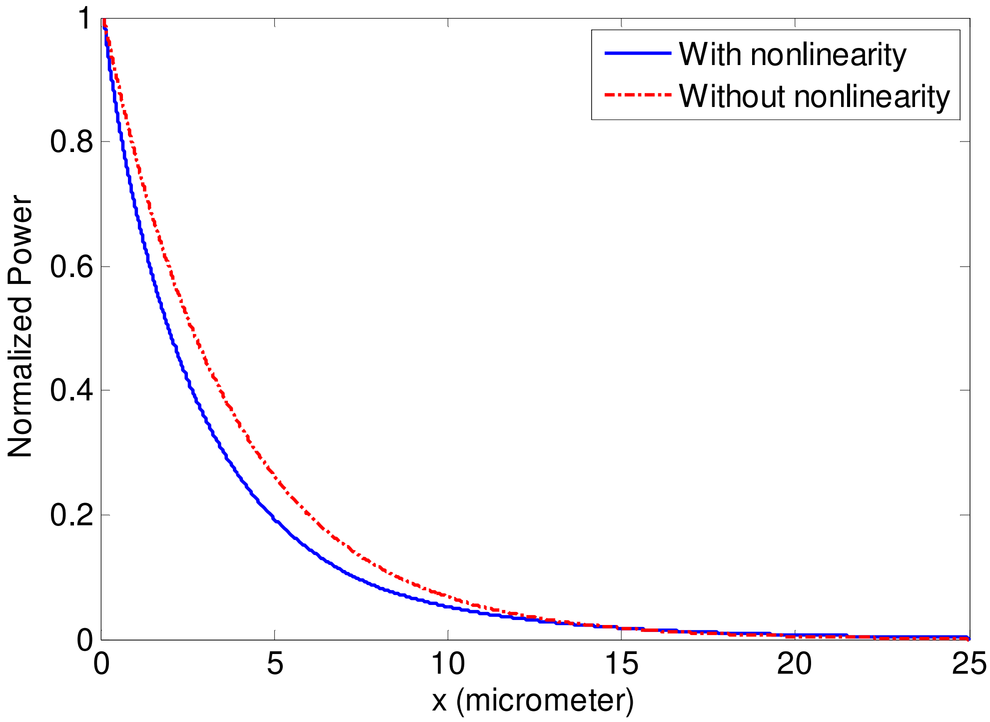

Figure 7-6: Normalized power curve for metal-glass-metal structure.

7.2 Silver Thin Film Coated with As_2S_3 Glass

Next, a structure having thin Ag film coated on both sides with As_2S_3 glass is considered. Figure 7-7 gives the basic structure diagram in this case. The thickness of the metal film is taken as 40 nm.

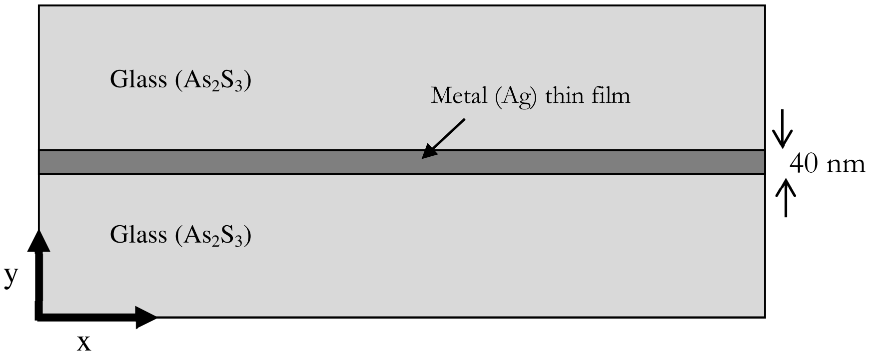

Figure 7-7: Basic structre of thin film coated with As2S3 glass.

Figure 7-8 shows a snapshot of the Ey field. Figure 7-9 shows the Ey profile which propagates along the Ag thin film.

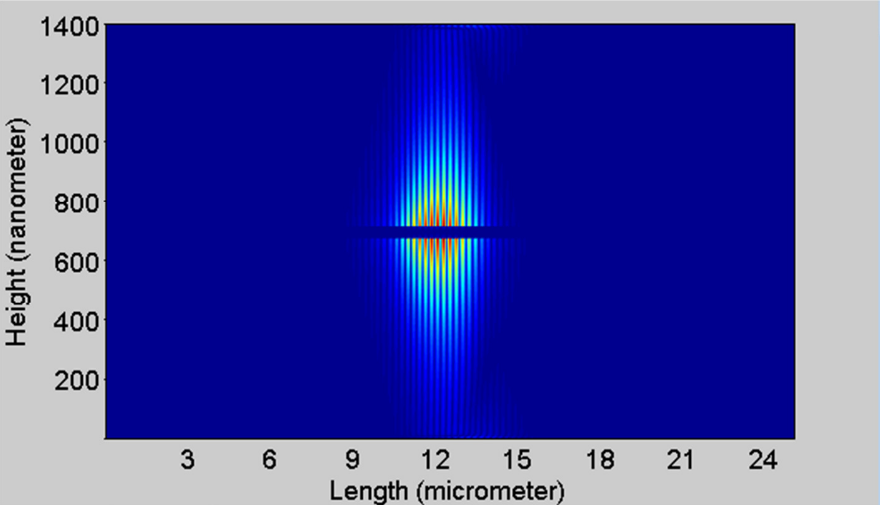

Figure 7-8: A snap shot of SPPs propagation in a glass-metal-glass structure.

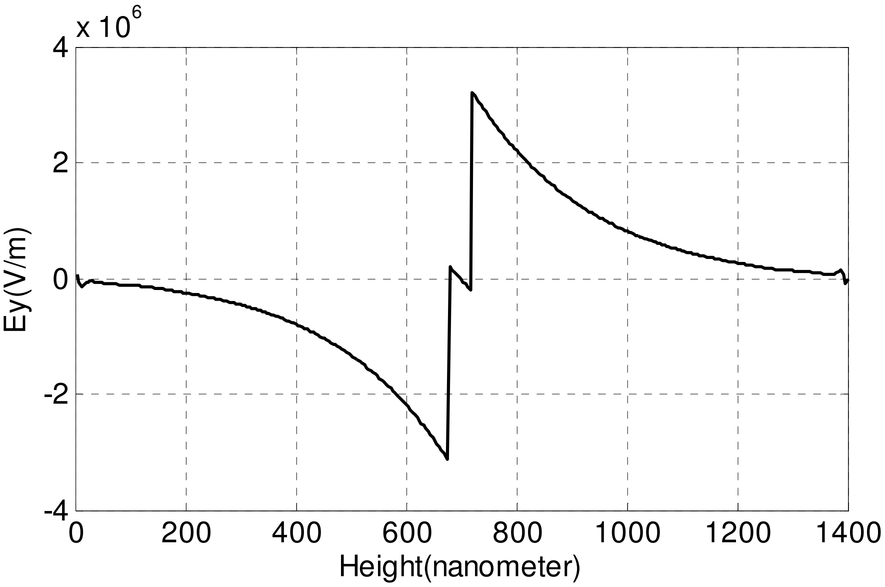

Figure 7-9: The Ey field profile corresponds to a linear medium.

The same previous analysis is repeated for this thin-film case. The time domain, frequency domain and power curves are shown in figures 7-10 to 7-12. From the figures it is clear that because of the high metal loss in this particular structure, the nonlinear effects do not appear at this input level of 16×10^8 V/m.

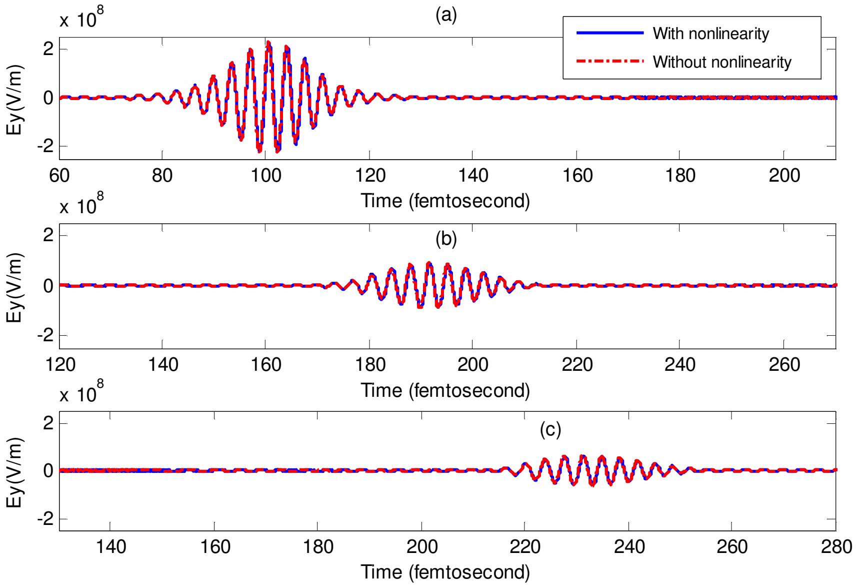

Figure 7-10: The simulated temporal evolution of the optical SPP pulse for peak Ey value of 16×10^8 V/m at the distance of (a) 5μm, (b) 15μm and (c) 22.5μm.

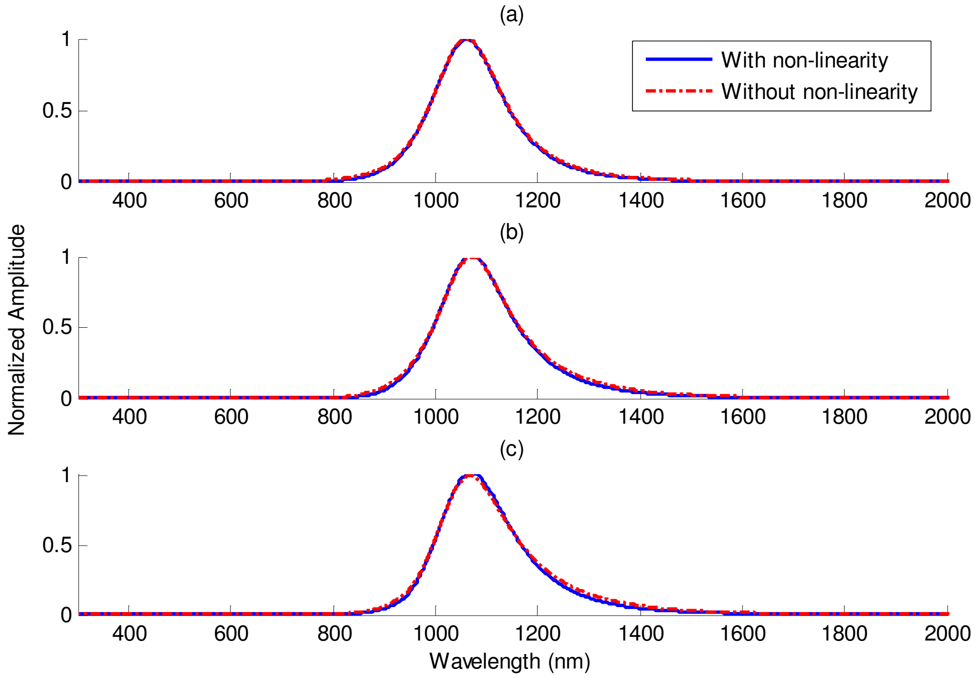

Figure 7-11: The SPP pulse in the frequency domain without and with non-linear effect for peak Ey value of $\mathbf{16 \times 10^8}$ V/m and for thin film structure at the distance of (a) 5µm, (b) 15µm and (c) 22.5µm.

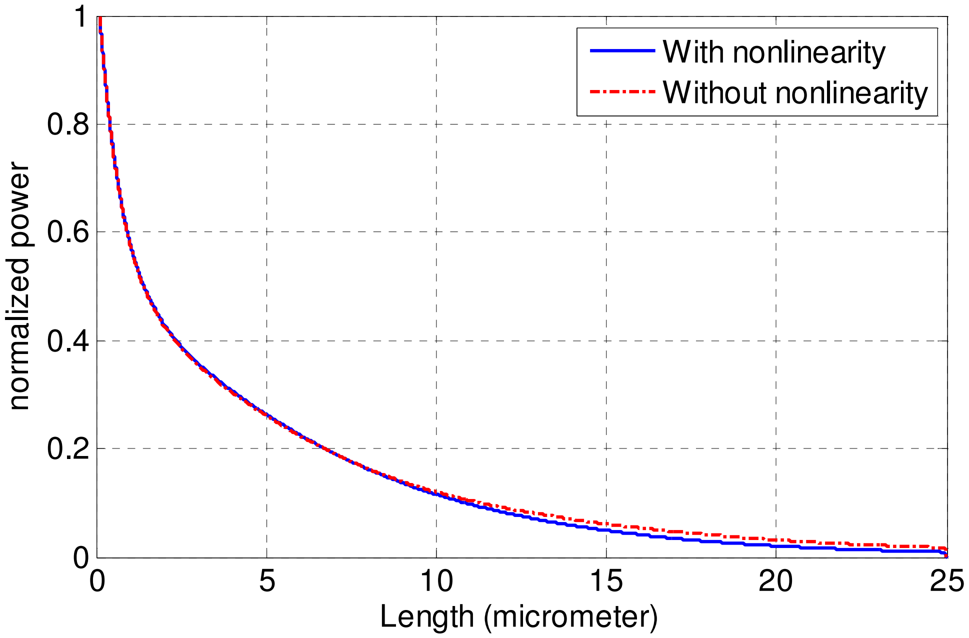

Figure 7-12: Normalized power curve for the thin film case considering linear and nonlinear dispersion.

CHAPTER 8

NUMERICAL CONSIDERATIONS

8.1 Numerical Stability Limit

We have seen in chapter 4 that the choice of space increment affects Δt, and thus the velocity of propagation of the numerical wave. The stability criterion of equation (4.21) was derived for a linear system. As, we used nonlinear model of As_2S_3, the simulator had to solve a cubic equation in every time cycle. The simulator becomes unstable under several conditions such as high input fields, higher value of $\chi^{(3)}$ and long propagation distances. So in order to ensure stability for the third order non-linear problem, we needed to reduce our time step by 5% below that predicted by equation (4.21). So the time step used in our simulator is

$$\Delta t = \frac{0.95}{c\sqrt{\frac{1}{\Delta x^2} + \frac{1}{\Delta y^2} + \frac{1}{\Delta z^2}}} \tag{8.1}$$

The derivation of the stability criterion of the nonlinear FDTD algorithm involves mathematical analysis beyond the scope of this thesis.

8.2 Numerical Dispersion

The step size for the spatial calculation should be taken such that we do not lose information. The numerical results should converge. This convergence depends on the relationship between the step size and wavelength λ. However, convergence is generally obtained by experience. For the microwave range of frequencies the step size should be $\leq \frac{\lambda}{40}$ in the direction of propagation. But this condition is not valid for optics or plasmonics. For optical frequencies the step size should be taken to less than or equal to $\frac{\lambda}{200}$. In our case, most of the time the Yag laser wavelength was used which has a value of 1064 nm. We therefore chose our step size to be $\Delta x = 5nm$; which meets the above mentioned condition. Moreover, many researchers reported that $\Delta x \leq \frac{\lambda}{200}$ to be a suitable condition.

8.3 Computational Time

The computational time for the FDTD simulation of the third-order nonlinear model was relatively high. In FDTD method, the field parameters are calculated in every loop and these are stored in the memory to calculate the field parameters in the next time cycle. There were several cubical equations in each time loop which took a very high computational time. For example, considering $\Delta x = \Delta y = 5nm$, to simulate a 2-D structure $30\mu m \times 1.25\mu m$, the computational time was almost 26 hours for Pentium core *i5* 2.67 GHz. One of the techniques to reduce the computational time is to use a moving computational window concept which is discussed in the following section. We had to analyze the propagation of SPP for longer distances as well. The main problem to calculate the field in long optical devices is limited memory. For Pentium Dual core system with 2 GB RAM, it was possible to simulate a 2-D structure of dimensions up to $50\mu m \times 1.25\mu m$. However, to simulate the propagation beyond $50\mu m$, we used another technique: where the boundaries at the two sides were rotated. Details of the rotating boundary method are given in section 8.5.

8.4 Moving Computational Window

If the total size of the computational window becomes very high, the computational time needed to complete the whole simulation becomes also very high. For more accuracy, Δx and Δy should be taken sufficiently small. But small step sizes results in a higher run time. The reduction of the computational time is one of the main concerns of today's researcher in the field of computational electromagnetics.

One of the efficient methods in term of computational time is called the moving window method[40]. In this method, instead of taking into account the whole problem dimension for computation, the computational dimension is taken only where the signal is present. For example, when the SPP propagates along the positive x direction, a computational window of a small dimension is used which covers only the SPP signal. This window also moves along with the SPPs. There are two factors which are to be considered in this case:

1. Size of the window.
2. Velocity of the window.

The window size should be large enough so that the signal does not reach the window's boundaries. Especially in the dispersive case, after some time, the signal waist becomes larger and the tail of the signal may hit the boundary which will cause unwanted reflection if the window size is not sufficiently large.

The velocity of the window should be equal to the velocity of the signal. Figure 8-1 describes the moving window concept more elaborately. The upper limit of the window should have a velocity of *V1* which should be equal or greater than the highest velocity of plasmonic signal *V* and the lower limit of the window should have a velocity of *V2* which must be equal or less than *V*. So the condition is $V2 \leq V \leq V1$.

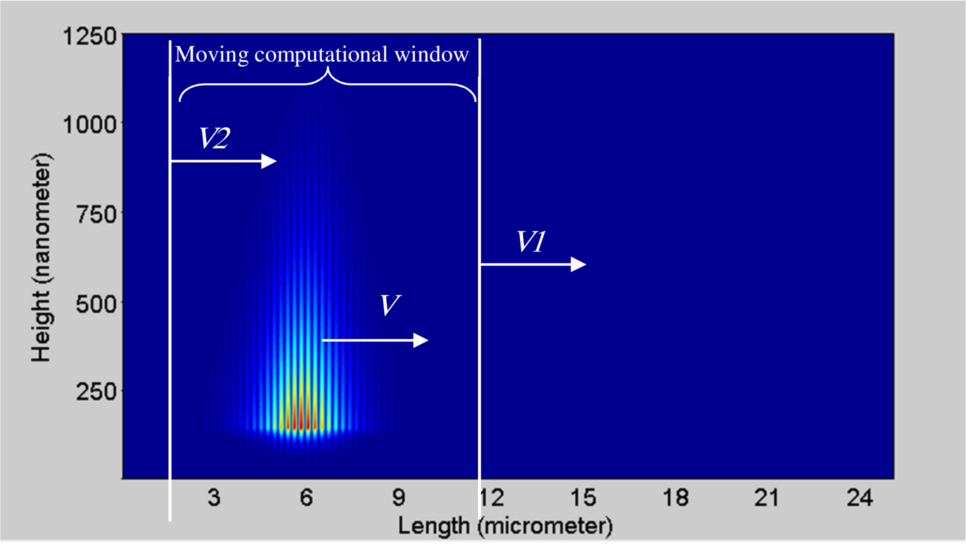

(a)

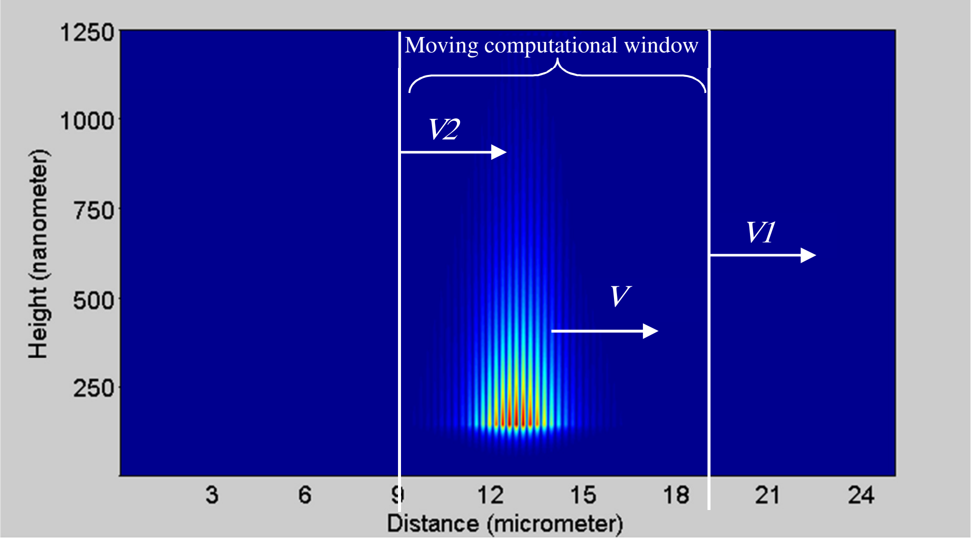

(b)

Figure 8-1: The concept of a moving window for efficient simulation.

In our case, to be on the safe side, we took the upper limit velocity a bit higher than the velocity of the signal, and velocity of lower limit a bit smaller than the velocity of the signal. So as the signal propagates the window size becomes larger. This causes the dispersed pulse to move freely without hitting the boundary. The lower limit of the window should start moving after the pulse enters completely in the computational domain.

8.5 Rotating Boundary Concept

To analyze SPP propagation for longer distances, for the 5 nm step size, the compiler becomes out of memory. To overcome this problem, we can increase the step size which will reduce accuracy. Another technique is to use a rotating boundary concept as illustrated in figure 8-2.

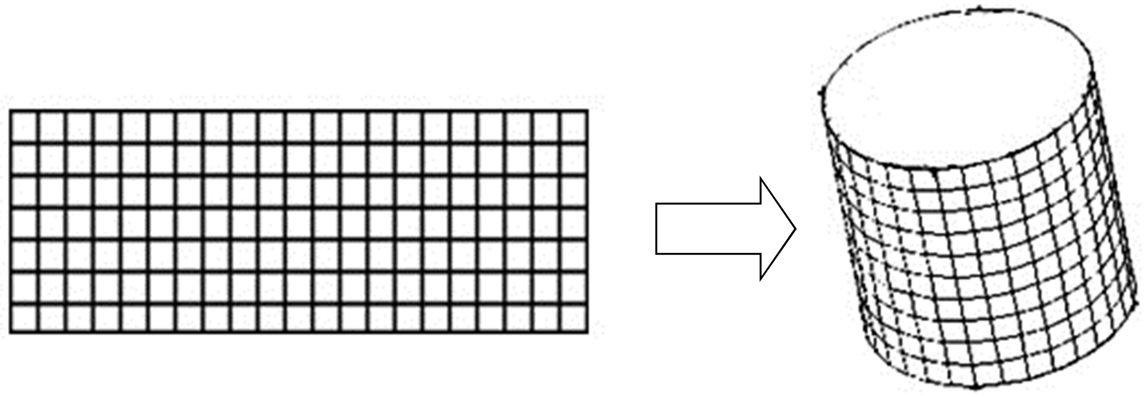

Figure 8-2: The concept of rotating boundary for efficient simulation.

Here, we take a small section and excite it with the input signal. Once the full signal has entered inside this domain, the boundaries in the x-direction are connected. So the domain takes a cylindrical shape (figure 8-2), where the total number of mesh points is the same as it was for the original rectangle shaped domain. Since the signal totally enters into the domain, if we run the simulation for a longer time, we can observe the signal's behavior after a long distance. The factor which should be kept in mind is that, the initial dimension needs to be sufficiently large so that the front of the signal does not hit the back. One of the main disadvantages of this concept is the calculation of the total power which may not be straightforward. However, to observe the field parameter for long distances, the rotating boundary concept is a better approach in terms of computational time and memory space requirements.

CHAPTER 9

CONCLUSIONS AND FUTURE WORK

9.1 Summary and Conclusions

The main contribution of this thesis work is to develop a flexible numerical simulator capable of simulating third order non-linear dispersion as well as linear-dispersion for plasmonic structures. Chalcogenide glass has been considered as the nonlinear material. The third-order nonlinear properties of chalcogenide glass were modeled and used in the simulator. The investigation of the propagation of the SPP has been carried out for several plasmonic structures. In particular, single as well as double longitudinal interface structures have been analyzed. The research work done in this thesis is summarized as follows:

- The theoretical derivation of the third-order non-linear material model was formulated. The third-order nonlinear model resulted in a FDTD algorithm that involved the solution of a cubic equation. Both Kerr and Raman nonlinear responses were considered. The material model equations were based on the linear susceptibility ($\chi^{(1)}$) and third order-nonlinear susceptibility ($\chi^{(3)}$).
- A frequency-dependent dispersion model for the linear response of As_2S_3 chalcogenide glass was developed, and the non-linear susceptibility value was

obtained from published experimental reports. The properties of As_2S_3 were assumed to follow the lorentzian third order non-linear material model.

- A time-domain two-dimensional simulator capable of calculating the propagation dynamics of SPP in Chalcogenide glass was developed. This simulator is based on the FDTD method and the general dispersive algorithm, where the PML was used as an absorbing boundary.
- The simulation results for single interface structures present the SPP propagation through non-linear As_2S_3, for different cases. It has been shown and discussed that the third-order non-linear behavior affects the SPP propagation when the input field intensity is sufficiently high. The non-linear properties cause the generation of new frequencies in SPPs, which is an interesting feature to draw attention to.
- It was observed that the input carrier wavelength and initial input pulse width both play an important role in the behavior of the propagated pulse.
- It has been observed that for a metal-glass-metal structure, new plasmonic field was generated for high input intensity of Ey field.
- For a thin metal film, the structure is very lossy making it difficult to observe nonlinear behavior.

9.2 Future Work

The numerical simulator developed in this work is powerful in the sense that it is capable of simulating an unlimited number of devices and structures containing linear dispersion and third-order nonlinearity. It can be used to examine the following future ideas.

- Investigation of novel nonlinear material structures with higher order nonlinearities. New and interesting features are expected in those cases.
- Generation and extraction of highly dominant frequencies which are created due to non-linear effect and using directional couplers or other coupling devices for the purpose of extraction.
- The highly dominant generated frequencies can be used for switching in optically controlled circuits.
- The current numerical simulator can be extended to 3-D structures in order to simulate the linear dispersion and the third order-nonlinearity for the more realistic 3-D structures.

References

[1] S. A. Maier, *Plasmonics: fundamentals and applications*: Springer Verlag, 2007.

[2] P. Franken*, et al.*, "Generation of optical harmonics," *Physical Review Letters,* vol. 7, pp. 118-119, 1961.

[3] P. P. Banerjee, *Nonlinear optics: theory, numerical modeling and applications* vol. 86: CRC Press, 2004.

[4] B. J. Eggleton, "Chalcogenide photonics: fabrication, devices and applications Introduction," *Optics Express,* vol. 18, pp. 26632-26634, 2010.

[5] A. K. Sharma and R. Jha, "Surface plasmon resonance-based gas sensor with chalcogenide glass and bimetallic alloy nanoparticle layer," *Journal of Applied Physics,* vol. 106, pp. 103101-103101-4, 2009.

[6] M. N. O. Sadiku, *Numerical techniques in electromagnetics*: CRC, 2000.

[7] J. Verwer and J. Sanz-Serna, "Convergence of method of lines approximations to partial differential equations," *Computing,* vol. 33, pp. 297-313, 1984.

[8] K. Yee, "Numerical solution of initial boundary value problems involving Maxwell's equations in isotropic media," *Antennas and Propagation, IEEE Transactions on,* vol. 14, pp. 302-307, 1966.

[9] A. Taflove and M. E. Brodwin, "Numerical solution of steady-state electromagnetic scattering problems using the time-dependent Maxwell's equations," *Microwave Theory and Techniques, IEEE Transactions on,* vol. 23, pp. 623-630, 1975.

[10] A. Taflove and S. C. Hagness, "Computational electrodynamics: the finite-difference time-domain method," 2000.

[11] P. M. Goorjian and A. Taflove, "Direct time integration of Maxwell's equations in nonlinear dispersive media for propagation and scattering of femtosecond electromagnetic solitons," *Optics letters,* vol. 17, pp. 180-182, 1992.

[12] J. P. Berenger, "A perfectly matched layer for the absorption of electromagnetic waves," *Journal of computational physics,* vol. 114, pp. 185-200, 1994.

[13] R. M. Joseph and A. Taflove, "FDTD Maxwell's equations models for nonlinear electrodynamics and optics," *Antennas and Propagation, IEEE Transactions on,* vol. 45, pp. 364-374, 1997.

[14] A. Zafarullah, "Application of the method of lines to parabolic partial differential equations with error estimates," *Journal of the ACM (JACM),* vol. 17, pp. 294-302, 1970.

[15] R. Ritchie, "Plasma losses by fast electrons in thin films," *Physical Review,* vol. 106, p. 874, 1957.

[16] A. Otto, "Excitation of nonradiative surface plasma waves in silver by the method of frustrated total reflection," *Zeitschrift für Physik A Hadrons and Nuclei,* vol. 216, pp. 398-410, 1968.

[17] E. Kretschmann and H. Raether, "Radiative decay of non radiative surface plasmons excited by light(Surface plasma waves excitation by light and decay into photons applied to nonradiative modes)," *ZEITSCHRIFT FUER NATURFORSCHUNG, TEIL A,* vol. 23, p. 2135, 1968.

[18] S. A. Maier, "Plasmonics: Metal nanostructures for subwavelength photonic devices," *Selected Topics in Quantum Electronics, IEEE Journal of,* vol. 12, pp. 1214-1220, 2006.

[19] W. Saj, "FDTD simulations of 2D plasmon waveguide on silver nanorods in hexagonal lattice," *Optics Express,* vol. 13, pp. 4818-4827, 2005.

[20] R. J. Blaikie and D. O. S. Melville, "Imaging through planar silver lenses in the optical near field," *Journal of Optics A: Pure and Applied Optics,* vol. 7, p. S176, 2005.

[21] D. O. S. Melville and R. J. Blaikie, "Super-resolution imaging through a planar silver layer," *Opt. Express,* vol. 13, pp. 2127–2134, 2005.

[22] B. Lamprecht*, et al.*, "Surface plasmon propagation in microscale metal stripes," *Applied physics letters,* vol. 79, p. 51, 2001.

[23] T. Onuki*, et al.*, "Propagation of surface plasmon polariton in nanometre sized metal clad optical waveguides," *Journal of microscopy,* vol. 210, pp. 284-287, 2003.

[24] A. Owen and J. Robertson, "Electronic properties of some simple chalcogenide glasses," *Journal of Non-Crystalline Solids,* vol. 2, pp. 40-51, 1970.

[25] W. Burckhardt, "Refractive index and dispersion of glasses with different degrees of linking," *Journal of Non-Crystalline Solids,* vol. 50, pp. 173-182, 1982.

[26] M. Asobe, "Nonlinear optical properties of chalcogenide glass fibers and their application to all-optical switching," *Optical Fiber Technology,* vol. 3, pp. 142-148, 1997.

[27] K. Cerqua-Richardson*, et al.*, "Comparison of nonlinear optical properties of sulfide glasses in bulk and thin film form," *Optical Materials,* vol. 10, pp. 155-159, 1998.

[28] A. Zakery and S. Elliott, "Optical properties and applications of chalcogenide glasses: a review," *Journal of Non-Crystalline Solids,* vol. 330, pp. 1-12, 2003.

[29] J. Sanghera*, et al.*, "Nonlinear properties of chalcogenide glass fibers," *Journal of optoelectronics and adavnced materials,* vol. 8, pp. 2148-2155, 2006.

[30] X. Gai*, et al.*, "Progress in optical waveguides fabricated from chalcogenide glasses," *Optics Express,* vol. 18, pp. 26635-26646, 2010.

[31] K. Suzuki and T. Baba, "Nonlinear light propagation in chalcogenide photonic crystal slow light waveguides," *Optics Express,* vol. 18, pp. 26675-26685, 2010.

[32] P. Drude, "Zur elektronentheorie der metalle," *Annalen der Physik,* vol. 306, pp. 566-613, 1900.

[33] P. Drude, "Zur elektronentheorie der metalle; II. Teil. galvanomagnetische und thermomagnetische effecte," *Annalen der Physik,* vol. 308, pp. 369-402, 1900.

[34] A. D. Rakic*, et al.*, "Optical properties of metallic films for vertical-cavity optoelectronic devices," *Applied Optics,* vol. 37, pp. 5271-5283, 1998.

[35] M. Fujii*, et al.*, "High-order FDTD and auxiliary differential equation formulation of optical pulse propagation in 2-D Kerr and Raman nonlinear dispersive media," *Quantum Electronics, IEEE Journal of,* vol. 40, pp. 175-182, 2004.

[36] Y. Hao*, et al.*, *FDTD modeling of metamaterials: theory and applications*: Artech House, 2009.

[37] M. A. Alsunaidi and A. A. Al-Jabr, "A general ADE-FDTD algorithm for the simulation of dispersive structures," *Photonics Technology Letters, IEEE,* vol. 21, pp. 817-819, 2009.

[38] Z. L. Sámson*, et al.*, "Chalcogenide glasses in active plasmonics," *physica status solidi (RRL)–Rapid Research Letters.*

[39] W. L. Barnes, "Surface plasmon–polariton length scales: a route to sub-wavelength optics," *Journal of Optics A: Pure and Applied Optics,* vol. 8, p. S87, 2006.

[40] M. A. Alsunaidi and H. M. Al-Mudhaffar, "A New Carrier-Free Nonlinear FDTD Algorithm Suitable for the Moving Computational Window Technique," *Photonics Technology Letters, IEEE,* vol. 21, pp. 878-880, 2009.

VITAE

Name : Rakibul Hasan Sagor.

Nationality : Bangladeshi.

Date of Birth : December 31, 1984.

Permanent Address : Section-1, Block-D, Road no-3, House no-30,

Mirpur, Dhaka-1216, Bangladesh.

Present Address : Room#811/314, KFUPM, Dhahran, K.S.A.

Email : sagor1883@gmail.com

Phone : +88-02-9007253
+966535440562

Degrees :

Bachelor of Science in Electrical & Electronic Engineering from Islamic University of Technology (IUT) (OIC) (Jan. 2004 – Oct. 2007).

Experiences :

Research Assistant in Electrical Engineering Department of King Fahd University of Petroleum & Minerals (KFUPM) (Oct. 2009 – Jul. 2011).

Lecturer in Electrical and Electronic Engineering Department of Stamford University Bangladesh (SUB) (Apr. 2008 – Sept. 2009).